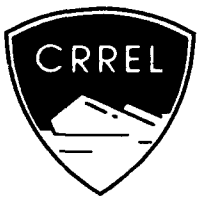

MONOGRAPH 91-1

Physical and Dynamic Properties of Sea Ice in the Polar Oceans

Anthony J. Gow and Walter B. Tucker III

September 1991

For conversion of SI metric units to U.S./British customary units of measurement consult ASTM Standard E380, Metric Practice Guide, *published by the American Society for Testing and Materials, 1916 Race St., Philadelphia, Pa. 19103.*

Cover: Setting up ice coring site on multiyear floe with aid of helicopter. F.S. Polarstern *in background (W.B. Tucker, photograph).*

Monograph 91-1

U.S. Army Corps
of Engineers
Cold Regions Research &
Engineering Laboratory

Physical and Dynamic Properties of Sea Ice in the Polar Oceans

Anthony J. Gow and Walter B. Tucker III

September 1991

Prepared for
OFFICE OF NAVAL RESEARCH
and
OFFICE OF THE CHIEF OF ENGINEERS

PREFACE

This report was written by Dr. Anthony J. Gow, Geologist, and Walter B. Tucker III, Geologist, USA Cold Regions Research and Engineering Laboratory (CRREL). The report was funded by the Office of Naval Research under contract numbers N0001488WM24013 and N0001489WM24004 and by the U.S. Army Corps of Engineers as part of DA Project 4A161102AT24, *Research in Snow, Ice, and Frozen Ground*, Program Element 6.11.02A, Work Units SS/001, *Sea Ice Geophysics*, and SS/006, *Structural Relationships in Snow and Ice*.

The authors gratefully acknowledge the extensive reviews and revisions suggested by Dr. Gary A. Maykut, Dr. Donald K. Perovich, and Stephen F. Ackley.

CONTENTS

	Page
Preface	ii
Introduction	1
Small-scale ice properties	2
Ice growth and structure	2
Salinity of sea ice	9
Bipolar comparisons of sea-ice salinity	11
Crystalline structure of polar sea ice	14
Large-scale ice properties	24
Ice growth and decay	24
Ice dynamics and drift	29
Morphological ice features	33
Ice thickness distribution	36
Ice extent and zonation	37
Summary	41
Literature cited	42
Abstract	47

ILLUSTRATIONS

Figure

1. Major sea ice types encountered in the polar oceans 2
2. Temperature of the density maximum and of the freezing point for seawater of different salinities 4
3. Initial stage of ice crystal formation in calm seawater 4
4. Pancake ice from the Fram Strait 4
5. Horizontal cross-section of a thin section of sea ice showing the multiplate/brine layer substructure of individual crystals 5
6. Dendrite and groove structure of two columnar sea-ice crystals 6
7. Thin section of a crystal of sea ice showing individual brine pockets interspersed between the ice plates 6
8. Major structural, crystal texture and c-axis fabric elements in a 2-m-thick first-year sea-ice sheet 7
9. Thin sections photographed between crossed polarizers 8
10. Idealized salinity profiles in Arctic sea ice of various thicknesses 10
11. Best-fit salinity trend lines 11
12. Bulk salinity values of ice cores as a function of floe thickness in the Fram Strait 12
13. Mean salinity profiles from the Fram Strait for all multiyear and first-year ice cores analyzed during June and July 1984 12
14. Bulk salinities of Weddell Sea ice floes plotted as a function of thickness 13
15. Bulk salinities of first-year and multiyear sea ice in McMurdo Sound plotted as a function of thickness 13
16. Equal-area horizontal projection plots of individual c-axis orientations from three sites in Kotzebue Sound, Alaska 14
17. C-axis orientations as determined by Cherepanov in sea ice in the Kara Sea region of the U.S.S.R. 15

Figure Page
18. Percentages of columnar and granular ice as a function of thickness for various ice floe types in the Fram Strait 16
19. Salinity–temperature–structure profiles from an undeformed first-year ice floe in the Fram Strait 17
20. Salinity–temperature–structure profiles from an undeformed multiyear ice floe in the Fram Strait 17
21. Salinity–temperature–structure profiles from a ponded multiyear ice floe in the Fram Strait 18
22. Salinity–temperature–structure profiles through old ridged ice from a multiyear floe in the Fram Strait 19
23. Horizontal thin-section photographs demonstrating retexturing of ice in the upper layers of an Arctic multiyear floe 20
24. Locations of primary sampling sites visited in 1980 during summertime investigations of the physical and structural properties of pack ice in the Weddell Sea 21
25. Abundances of congelation and granular ice vs ice thickness in Weddell Sea floes 21
26. Salinity and structure profiles of a 4.18-m-thick multiyear floe from the Weddell Sea ... 21
27. Salinity and structure profiles of a 2.92-m-thick multiyear floe from the Weddell Sea ... 22
28. Salinity and structure profiles of a 1.57-m-thick first-year floe from the Weddell Sea 22
29. Salinity and structure profiles of a 1.92-m-thick first-year floe from the Weddell Sea 24
30. Average monthly values of radiative heat fluxes 25
31. Average monthly values of net radiative heat flux and sensible and latent heat fluxes observed over perennial ice 25
32. Equilibrium thickness of arctic sea ice as a function of average annual oceanic heat flux 26
33. Average equilibrium thickness of perennial Arctic sea ice as a function of annual snow depth 27
34. Estimate of the force balance on sea ice for winter conditions based on wind and water stress measurements 30
35. Mean field of ice interpolated spatially and temporally from manned ice stations and automatic data buoys 31
36. Surface circulation and published trajectories of icebergs around Antarctica 32
37. Drift tracks of automatic data buoys in the Weddell Sea during 1979 and 1980 32
38. Contours of ridge sail frequency for the four seasons 34
39. Distribution of mean ridge keel depths for the four seasons and various Arctic Ocean subregions 35
40. Probability density function of ice draft from 400 km of submarine track in the Beaufort Sea 37
41. Mean ice draft derived from submarine tracks 38
42. Probability density function of ice thickness derived from 4400 drill-hole measurements made during winter in the Weddell Sea 39
43. Mean sea ice extents in the Arctic for the months of February and September averaged for the years 1973–1976 39
44. Mean sea ice extents in the Antarctic for the months of February and September averaged for the years 1973–1976 40

TABLE

Table
1. Ridging parameters from the Ross Sea compared with data from Arctic locations for winter and early spring 36

Physical and Dynamic Properties of Sea Ice in the Polar Oceans

ANTHONY J. GOW AND WALTER B. TUCKER III

INTRODUCTION

This monograph addresses the physical and dynamic characteristics of the sea ice covering the polar oceans. It is this ice cover that gives rise to many unique conditions in the polar oceans and atmospheres. Volumetrically, the sea ice cover is almost negligible when compared to the ice contained in the earth's glacial ice masses. It covers an area, however, that encompasses about two-thirds of the total permanent ice cover. Because sea ice is such a thin layer in contrast to the large area that it covers, small changes within the atmosphere or the ocean can cause major changes in the areal extent and thickness of the ice. Such changes, in turn, will have pronounced effects on the ocean and atmosphere through modification of the albedo, the ocean–atmosphere heat and momentum exchanges, and the oceanic salt flux.

Although sea ice in the polar oceans has been under scientific scrutiny for many years, research efforts in the past two decades have become considerably more focused toward understanding specific aspects of sea ice. These studies have been stimulated by several factors. The identification of the floating ice covers as key elements in the ocean and climate systems, brought about by large-scale computer simulations, has prompted efforts to develop numerical models of sea-ice behavior. Interest by several nations in exploring and developing mineral resources in ice-covered waters has encouraged much research dealing with the mechanical behavior of sea ice. The development of airborne and satellite-borne remote sensing instruments capable of all-weather day and night surveillance of the ice cover has also stimulated many studies dealing with the electromagnetic properties of ice. Finally, the desire for commercial and strategic transportation on the surface and beneath the ice cover has resulted in research addressing the morphology and seasonal variations of sea ice extent and thickness. Significant progress into these areas of research has been made possible with the advent of efficient computer systems, state-of-the-art instrumentation, satellite technology, modern icebreakers, and improvements in logistics that enhance field studies.

In this monograph, we review our current understanding of sea ice primarily as it pertains to the creation and subsequent dynamic behavior of sea ice in the polar oceans. We have purposely omitted any detailed discussions of the mechanical and electromagnetic properties of sea ice. This review was undertaken largely because evidence accrued over the past decade has shown that

- The physical and dynamic properties of sea ice in the Arctic differ appreciably from those observed in the Antarctic, and
- Such differences are linked closely to differences in land/sea relationships in the two hemispheres and their effects on ocean/ atmosphere interaction and oceanic circulation.

First we deal with small-scale properties, beginning with the freezing characteristics of sea water and progressing to the crystalline structure and salinity characteristics of sea ice. Specific features of the small-scale properties of the Arctic and Antarctic sea ice are then compared to demonstrate the significant bipolar contrasts.

The next section deals with the large-scale aspects of floating ice covers, from thermodynamic and dynamic characteristics to specific ice features. The characteristics of Arctic and Antarctic sea ice are again contrasted.

A standard taxonomy for the classification of sea ice based on its stage of growth has been developed by the World Meteorological Organization (WMO 1956). While much of this terminology deals with very young ice, it is a more common practice among sea ice specialists to refer to thicker ice (> 50 cm) as simply first- or

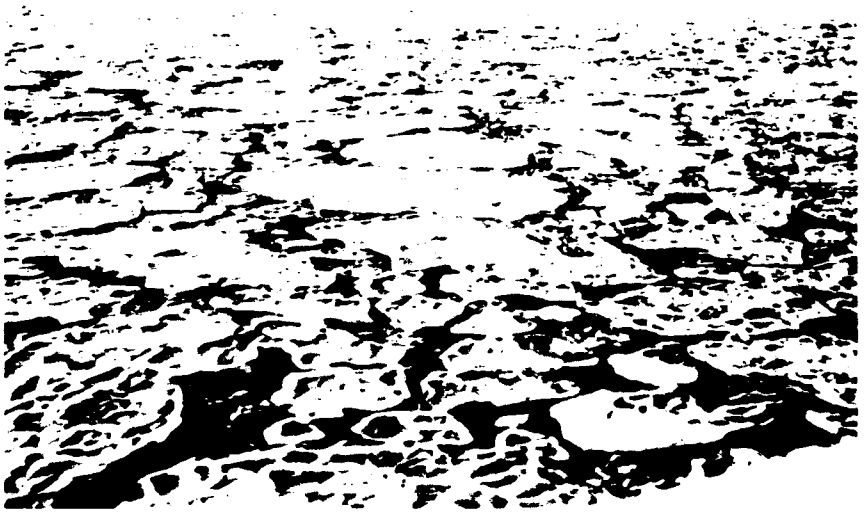

a. Pancake ice. Individual pans measure 2–3 m across.

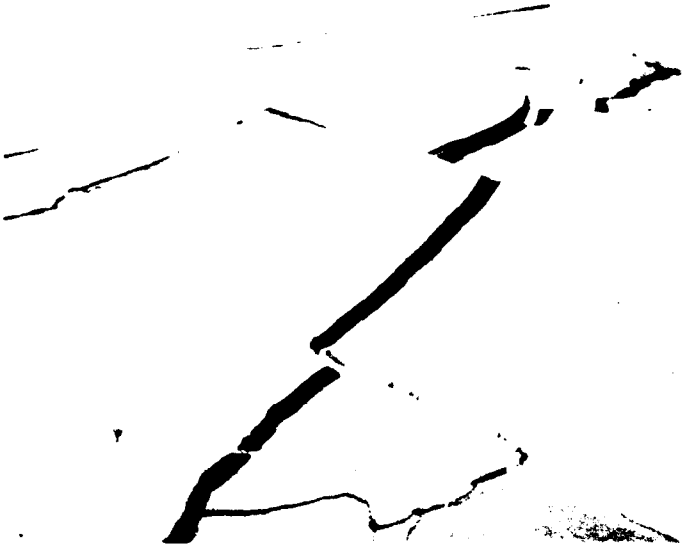

b. First-year ice floes. The lead separating floes in the center of the photo measures 20–25 m in width.

Figure 1. Major sea ice types encountered in the polar oceans.

multiyear. The WMO definition of multiyear ice requires that it have survived two summers. However, the distinction between multiyear ice and second-year ice (ice that has survived only one summer) is subtle, because, in the Arctic at least, one melt season is often sufficient to give the ice a characteristic surface relief appearance of alternating hummocks and melt ponds. Here, unless otherwise noted, we will make only the distinction between first-year ice and other ice that has survived one or more summers, which we will call multiyear ice. Examples of the major ice types encountered in the polar oceans are shown in Figure 1.

SMALL-SCALE ICE PROPERTIES

Ice growth and structure

The addition of salt to water depresses the freezing point, T_f, of the seawater according to the approximation $T_f = -0.055S_w$ (Maykut 1985) where S_w is the salinity per mil (‰) of the seawater. Because the great bulk of polar ocean water has a salinity greater than 24.7‰, its freezing point is always higher than its temperature of maximum density (Fig. 2); surface cooling of this seawater yields an unstable vertical density distribution leading to convective mixing, which con-

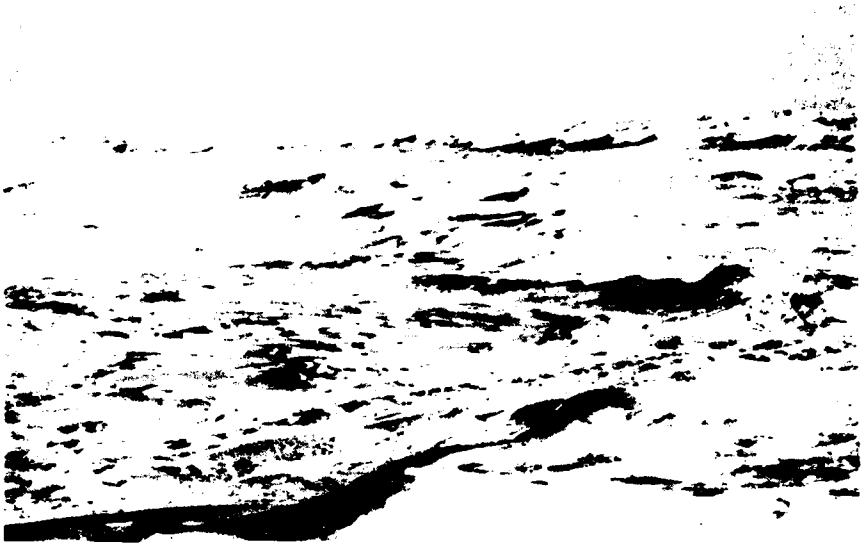

c. Multiyear ice. Maximum relief of surface features is about 2 m.

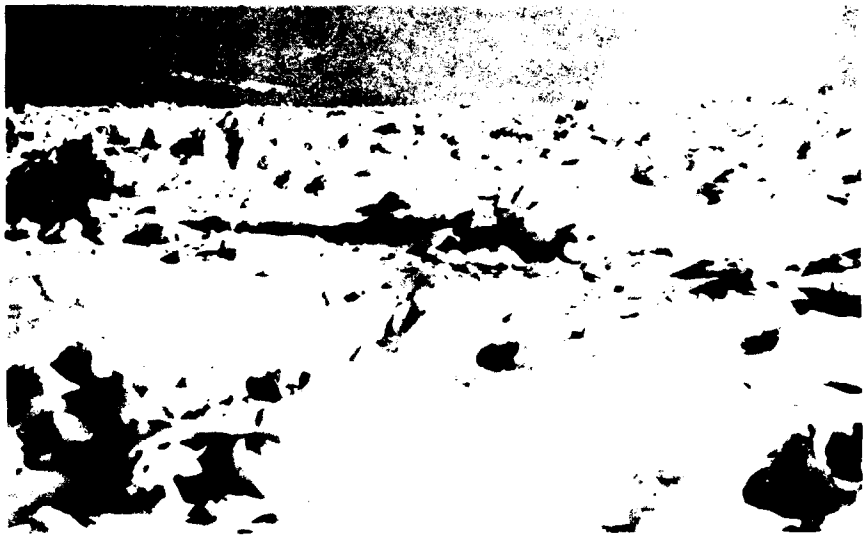

d. Ridged first-year ice. Maximum height of ridges is 2 m.

Figure 1 (cont'd).

tinues un.il the water reaches the freezing point (Weeks and Ackley 1982). Density gradients in the upper ocean usually limit the depth to which seawater must be cooled before freezing can begin. Therefore, the density structure of the ocean is a major factor in determining the onset of freezing (Maykut 1985). Once the entire mixed layer in the upper ocean reaches the freezing point, additional heat loss produces slight supercooling of the water, and ice formation begins. The amount of supercooling necessary to initiate ice growth is small, although observations near Greenland have shown a supercooling of as much as 0.2–0.4°C to depths of tens of meters (Maykut 1985).

Sea ice generally contains much less salt than the water from which it freezes. Most of the salt is rejected back to the ocean during the freezing process. Further loss of salt occurs during continued growth and aging of the ice by vertical drainage of brine from the ice to the underlying ocean. Normal seawater contains about 34‰ of salt, and salinities as high as 20‰ may be found in ice formed during the earliest stages of freezing. By the end of winter, however, the bulk salinity of the ice (1–2 m thick) rarely exceeds 6‰, which is less than 20% of the salinity of the original seawater.

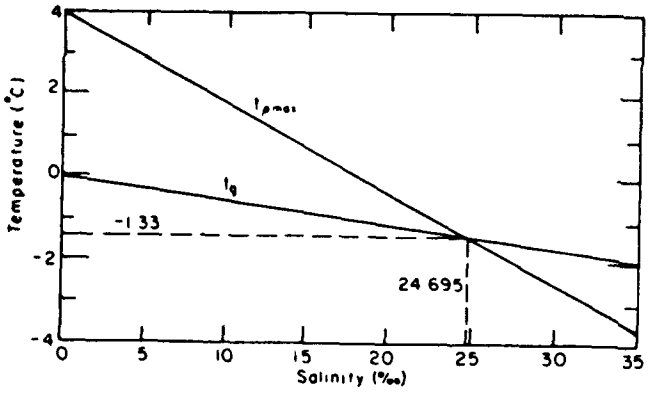

Figure 2. Temperature of the density maximum $t_{\rho max}$ and of the freezing point t_g for seawater of different salinities. In normal seawater (salinity > 24.4‰), a several-meter-thick layer of surface water must be lowered to its freezing point, or slightly below it, before freezing can begin (after Weeks and Ackley 1982).

Figure 3. Initial stage of ice crystal formation in calm seawater (after Weeks and Ackley 1982).

Figure 4. Pancake ice from the Fram Strait. In this instance a sheet of pancake ice was fragmented by wave action to form second-generation pancakes measuring 2 to 3 m across.

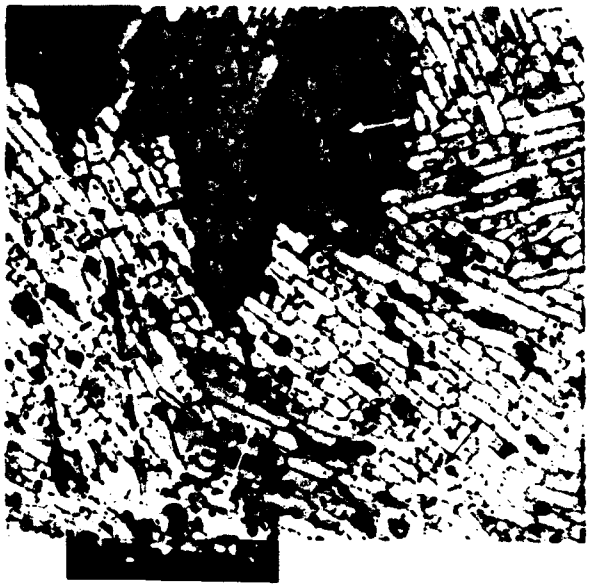

Figure 5. Horizontal cross-section of a thin section of sea ice showing the multiplate/brine layer substructure of individual crystals (photographed between crossed polarizers). Arrows indicate c-axis orientations in three of the crystals. Scale subdivisions measure 1 mm.

Initial ice formation occurs at or near the surface of the seawater in the form of small platelets and needles called frazil (Fig. 3). Continued freezing results in the production of grease ice, a soupy mixture of seawater and unconsolidated frazil crystals. Under quiescent conditions the frazil crystals quickly freeze together to form a solid, continuous ice cover with thicknesses between 1 and 10 cm. More often, however, wind-induced turbulence in the water inhibits immediate development of a solid cover. Wind and wave action in leads (linear openings in the ice) and polynyas (pools of open water) drive frazil crystals downwind, where accumulations up to 1 m thick may occur. In the presence of a sustained wave field, pancakes usually form (Fig. 4). These circular masses of semiconsolidated frazil, ranging from 0.3 to 3.0 m in diameter, often display irregular raised rims due to constant bumping and pushing up of frazil crystals around their perimeters. Eventually, the pancakes consolidate by freezing together to form a continuous sheet of ice.

Once a continuous ice sheet has formed, the underlying ocean is isolated from the cold air, so latent heat is extracted through the ice sheet by thermal conduction; the growth rate is now determined by the temperature gradient in the ice and its effective thermal conductivity. In addition, once a continuous sheet has formed, ice crystals lose a degree of growth freedom. Further crystal growth can proceed, without one grain interfering with the growth of another, only if the grain boundaries are perpendicular to the freezing interface. Direct freezing of seawater to the underside of the ice sheet is called congelation growth, typically yielding columnar-shaped crystals. In the transition zone between the granular frazil and the onset of columnar congelation ice growth, a process of geometric selection occurs in which crystals in the favored growth direction eliminate crystals in the unfavored orientation. This transition layer is usually 5 to 10 cm thick (Weeks and Ackley 1982), and below it congelation ice is found in which there exists a strong vertical crystal elongation parallel to the direction of heat flow. With the onset and full development of congelation growth, those crystals with c-axes* parallel to the ice/water interface quickly begin to eliminate crystals with a less-favored orientation. The elimination of the slower-growing crystals proceeds until only those crystals with c-axes substantially parallel to the freezing interface remain.

Within the columnar ice zone a crystal substructure is developed consisting of pure ice plates interspersed with parallel layers of brine inclusions. The overall nature of this substructure, which is best observed in cross-section (Fig. 5), is the direct result of constitutional supercooling,† the process by which sea ice incorporates residual brine at the ice/water interface as freezing progresses. Residual brine is that brine that cannot be rejected from the freezing interface; since brine cannot be incorporated within the ice crystal lattice, it is segregated instead as inclusions between the plates. These plates originate as pure ice dendrites, with their tips protruding downward into the seawater beneath the residual brine layer (Fig. 6) and it is in the grooves between these dendrites that brine is systematically trapped. Continuation of this process leads to the formation of columnar-shaped crystals, each crystal consisting of a

* The c-axis is the principal hexagonal axis of the ice crystal; it also corresponds to the optic axis and is widely used as the reference axis for describing crystal structure and for measuring crystal orientation.

† Constitutional supercooling is simply compositional supercooling. The process whereby the liquid near the freezing interface can become constitutionally supercooled is due to the different diffusivities of heat and salt in the liquid. Essentially, the heat can be extracted from the liquid faster than the salt can diffuse away, resulting in a supercooled layer at that composition. Such a process has been well documented in connection with solidification from the melt of alloys and impure metals (Tiller et al. 1953). It was subsequently extended to the freezing of salt water by Harrison and Tiller (1963) and Lofgren and Weeks (1967). In the freezing of seawater, constitutional supercooling allows for systematic entrapment of brine via the formation of a stable dendritic ice growth interface.

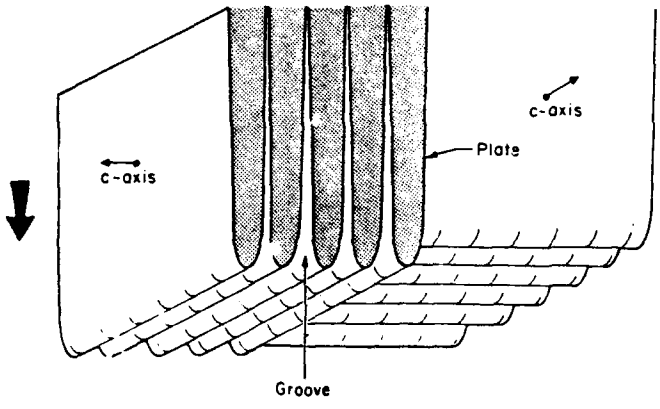

Figure 6. Dendrite and groove structure of two columnar sea-ice crystals. Residual brine is trapped in grooves between dendrites (plates), which remain essentially salt-free. Large vertical arrow at left indicates direction of ice growth.

number of platelike dendrites between which are sandwiched layers of brine pockets (Fig. 7). The spacing of these plates (or brine layer separation distance) varies from a few tenths of a millimeter to about 1 mm, depending mainly on the rate of freezing. Upon more rapid freezing, the plate spacing becomes narrower and the salinity greater. A schematic to demonstrate the major changes in the structure of a typical sea-ice sheet as outlined above is given in Figure 8. A more detailed and exhaustive account of the overall growth process in sea ice is given in Weeks and Ackley (1982).

Changes with time in the overall structure of sea ice occur mainly in response to temperature changes in the ice. Brine inclusions are particularly sensitive in this regard; even small changes in thermal regime resulting from daily variations in surface air temperature can cause significant changes in the size, shape, and distribution patterns of the inclusions and the concentration of the entrapped brine. In the case of sea ice subjected to protracted warming, originally disconnected brine inclusions will tend to coalesce into vertical channels that promote migration of the brine. Such a process can

Figure 7. Thin section of a crystal of sea ice showing individual brine pockets interspersed between the ice plates. The spacing between successive layers of brine pockets (also called plate spacing) is about 0.6 mm. The c-axis direction (arrow) is normal to the platy substructure.

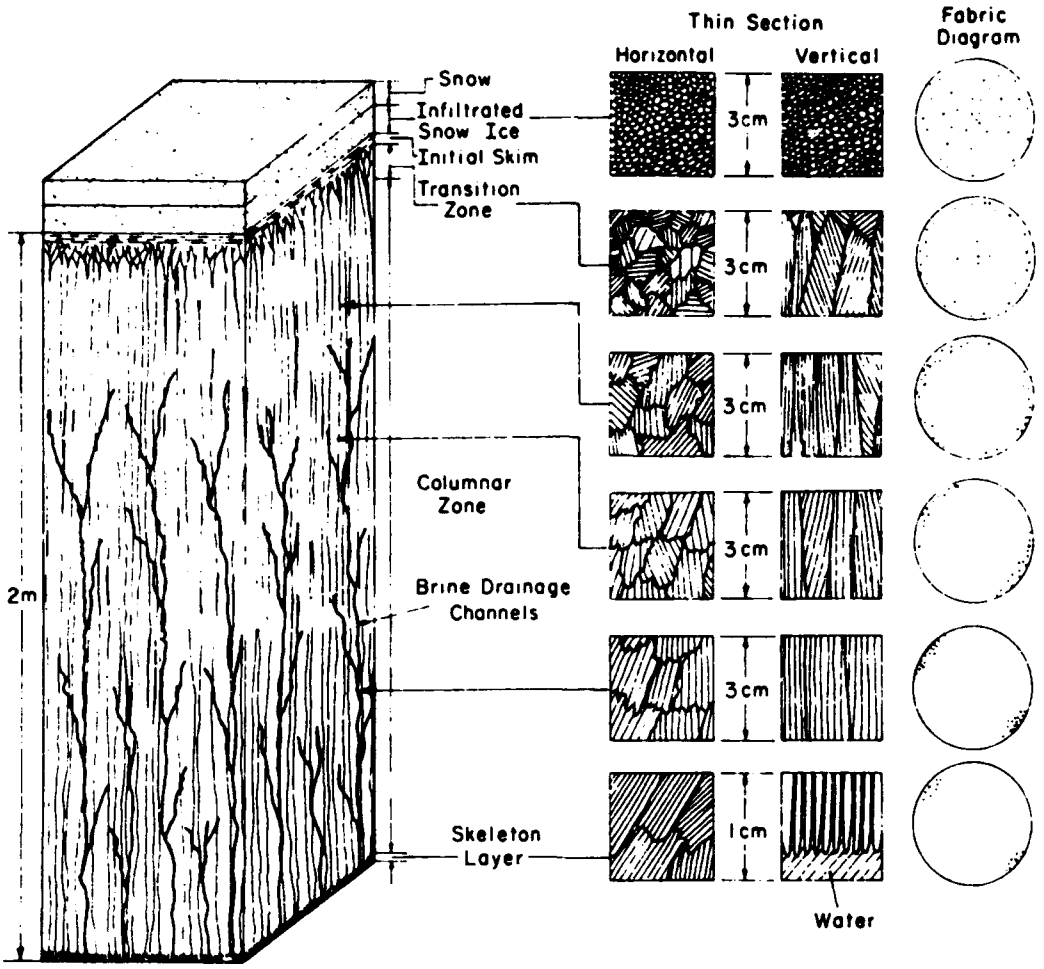

Figure 8. Major structural, crystal texture, and c-axis fabric elements in a 2-m-thick first-year sea-ice sheet. In this schematic the initial skim of frazil ice is overlain in succession by snow ice and snow. The skeleton layer at the bottom of the sheet corresponds to the region of dendritic ice growth (adapted from Schwarz and Weeks 1977).

lead to substantial redistribution of the brine and eventual drainage and desalination of the ice. Furthermore, desalination and changes in the distribution of the brine are often accompanied by changes in the mechanical properties, e.g. hardness and strength of the ice. The effects of extreme desalination and the resultant increased hardness have been used successfully in the Arctic to differentiate between the two principal ice types—multi- and first-year sea ice. Physical property changes, particularly those affecting the salinity profile of the ice and the free-water content of the overlying snow, are also responsible for major changes in the electrical properties of the ice, which in turn can have a critical bearing on remote sensing signatures and how they are interpreted.

As noted earlier, congelation ice growth invariably leads to the formation of vertically elongated (columnar) crystals with their c-axes oriented in the horizontal plane. This planar distribution of c-axes often is transformed into one in which the c-axes become aligned in a given direction. Such alignments of c-axes are commonplace in shorefast sea ice (often extending over areas of many square kilometers), and the direction of the alignment can usually be correlated with the measured or implied direction of current motion at the ice/water interface (Weeks and Gow 1978, 1980).

In addition to frazil ice, occurring by consolidation of frazil at the top of a sea ice sheet, another type of granular* ice is snow ice, which is formed from the freezing of interstitial water in snow that had been

* Frazil ice and snow ice are both forms of granular ice originating via different growth mechanisms. The term granular is used to describe the textural characteristics of these two kinds of ice. Similarly, the term congelation ice is simply descriptive of the growth mechanism giving rise to columnar-textured crystals. Textural and growth mechanism terms are often used interchangeably.

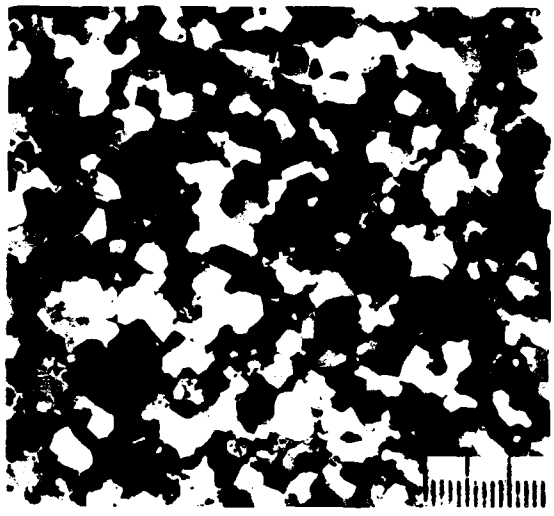

a. Snow ice from the top of an Arctic floe; note the polyhedral shapes of the grains and air bubbles located at the intersection of the grains.

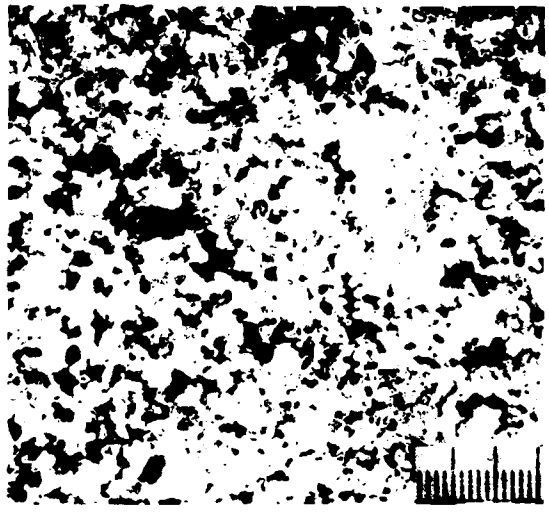

b. Shapeless grains of frazil ice from a depth of 10 cm in Arctic sea ice.

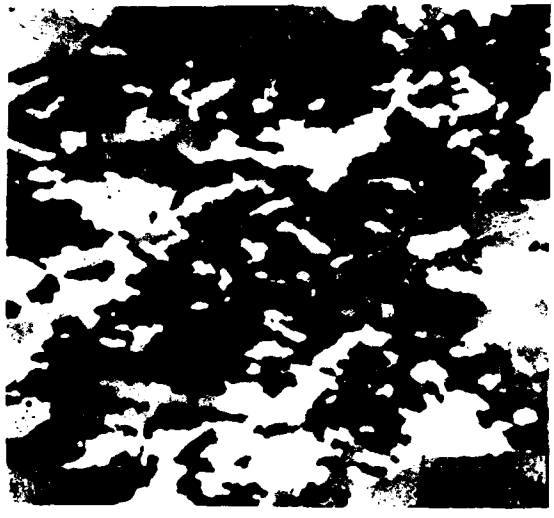

c. Fine-grained congelation ice showing traces of brine layer/plate structure within individual crystals.

Figure 9. Thin sections photographed between crossed polarizers. Smallest scale subdivisions measure 1 mm.

soaked by rain, snow meltwater, or seawater. Naturally, such ice would be restricted to the top of the ice sheet (Fig. 8). However, it is often necessary to be able to differentiate snow ice from frazil ice and, occasionally, frazil ice from fine-grained congelation ice (Fig. 9). As noted earlier, the formation of sea ice usually begins with the growth of frazil crystals at the surface, but frazil can also form at some depth in the water column beneath a sea-ice sheet. By floating upward either as crystals or clumps of crystals, frazil is able to adhere directly to the bottom of an existing ice sheet. Such a process is believed responsible, at least in part, for the widespread occurrence of frazil in pack ice in the Weddell Sea (Gow et al. 1982, 1987a). In the Arctic, however, frazil is thought to be mainly the product of turbulent water conditions and thus confined to ice margins, leads, and polynyas. According to Martin (1981), frazil ice accounts for less than 10% of Arctic sea ice, an estimate in general agreement with extensive observations by Weeks and Gow (1978, 1980) of shorefast ice along the

coasts of the Chukchi and Beaufort Seas and with observations of the structure of ice exiting the Arctic Basin through the Fram Strait (Tucker et al. 1987, Gow et al. 1987b). In addition, granular ice has been observed in substantial amounts in ridges, where it is thought to originate either by crushing or by growth of frazil in water-filled voids between blocks of ice.

The various forms of granular ice can usually all be distinguished from fine-grained columnar ice on the basis of the ice plate–brine layer substructure that characterizes the latter, and differences in texture usually suffice to allow the various granular types to be differentiated. Snow ice, for example, is generally much more coarse-grained and bubbly than frazil ice.

Principal inclusions occurring in sea ice are brine, salt, and air, with the amounts of each depending on the thermal state of the ice and its age. In addition, varying amounts of lithogenic and biological material may be incorporated into sea ice. A variety of mechanisms have been invoked to explain entrainment of sediment into both the top and bottom of sea-ice sheets. These include turbulent freezing of sediment-laden water leading to the formation of sediment-rich frazil ice up to 1 m thick, adfreezing of sea bed deposits to the bottom of grounded ice sheets, and the uplift of sea-floor debris to the underside of sea ice by anchor ice crystals. Recent reviews of the subject are to be found in Osterkamp and Gosink (1984) and Reimnitz et al. (1987). Incorporation of biological material, especially of algae into the bottom of sea ice, has been widely documented for both polar regions (Horner 1985). Differing environmental conditions leading to the formation of different ice types (e.g. frazil and congelation ice) may help to explain differences among ice algal communities. Dieckmann et al. (1986) have also reported on the significance of uprise of platelet ice from depth on biological processes in sea ice forming along the edges of Antarctic ice shelves.

Salinity of sea ice

The incorporation of salt into sea ice is the singular characteristic feature that distinguishes sea ice from all other forms of floating ice. It is also the single most important parameter in determining the mechanical, electromagnetic and thermal properties of sea ice (see, for example, Weeks and Ackley 1982). The salt content of sea ice is usually described in terms of a bulk salinity, S, where

$$S\ (‰) = \frac{\text{mass of salt}}{\text{mass of ice + mass of brine}} \times 10^3. \quad (1)$$

If ice temperatures are measured simultaneously with salinity, then a property known as the brine volume can be calculated (Frankenstein and Garner 1967, Cox and Weeks 1983). Brine volume was a commonly used parameter against which temperature-dependent properties of sea ice (such as strength) were usually evaluated. However, porosity, which includes air as well as brine volume, is now more widely used. Estimates of the entrapped air volume require accurate measurements of bulk density, which in the case of freshly formed congelation ice can reach values of 0.92–0.93 Mg m^{-3}. However, in ice that has undergone significant desalination with aging, densities can fall to 0.8 Mg m^{-3} or lower.

The mass of salt initially trapped as brine in the ice depends on both the rate of freezing of the seawater and its salinity. Subsequent changes in the distribution and concentration of salt in sea ice are controlled by phase equilibrium requirements that dictate that any change in the temperature of the ice must be accompanied by freezing or melting on the walls of brine pockets, leading to reductions or enlargements of the brine pockets and corresponding increases or decreases in the brine volume and brine concentration. With increased warming, as occurs with the onset of summer, individual brine inclusions will enlarge and ultimately coalesce. In the event of extreme or protracted warming, further coalescence will cause channelization of the brine and result in drainage and desalination of the ice. Some idea of the nature of the changes occurring in sea ice as it ages is given in Figure 10, which shows idealized salinity profiles based on data from several different sources for both first- and multiyear ice in the Arctic. Important features of these profiles include

- High salinities at the top and bottom of thinner ice sheets, leading to strongly c-shaped salinity profiles,
- General weakening of the c-shaped profile accompanied by progressive decrease in bulk salinity with increasing thickness and age of the ice sheet, indicative of downward migration of brine through the ice and its return to the underlying ocean,
- Virtual desalination of the upper levels of first-year ice during and after its transformation to multiyear ice.

To explain the observed profiles, Untersteiner (1968) described four mechanisms by which brine can be removed from the ice:

1. Migration of brine pockets through ice crystals,
2. Brine expulsion,
3. Brine drainage, and
4. Flushing.

The mechanisms are summarized below.

Migration of brine pockets

Temperature gradients in sea ice lead to the forma-

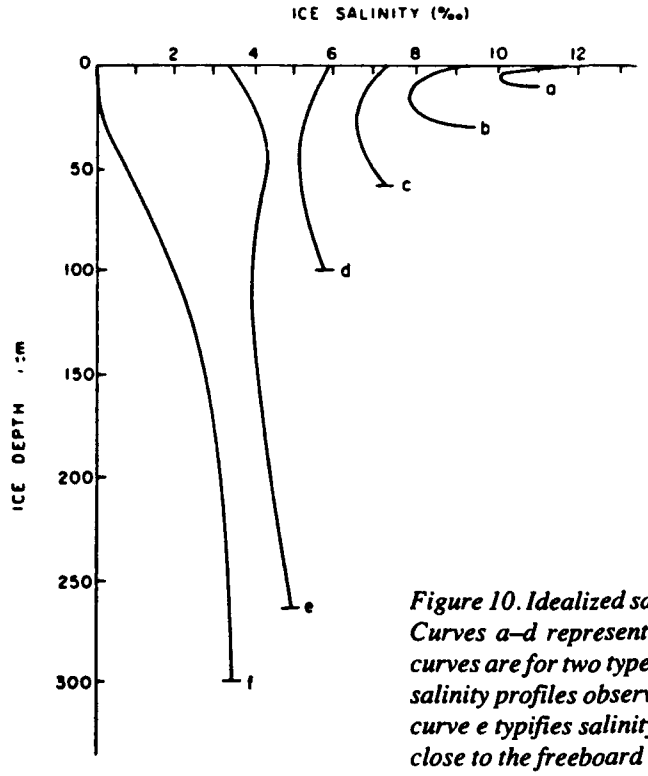

Figure 10. Idealized salinity profiles in Arctic sea ice of various thicknesses. Curves a–d represent changes observed in first-year ice. The remaining curves are for two types of profile found in multiyear ice: curve f is typical of salinity profiles observed beneath hummocks and other elevated areas, and curve e typifies salinity distribution beneath low areas where the surface is close to the freeboard level (after Maykut 1985).

tion of concentration gradients in the brine pockets. Because of phase equilibrium requirements, the ice at the warm end of a brine pocket dissolves while freezing occurs at the cold end, resulting in the migration of the brine pocket toward the warm side of the ice. This mechanism is not generally considered to be a significant cause of brine loss.

Brine expulsion

Brine expulsion occurs when a pressure buildup in the brine pocket causes the liquid portion of the inclusion to separate from the vapor bubble. This pressure may become sufficient to cause the surrounding ice to fail along the basal planes of crystals, allowing brine to escape. Brine expulsion upward to the surface is most effective in thin ice when the ice sheet is undergoing rapid cooling. Generally, however, brine expulsion accounts for only a minor amount of the desalination of first-year ice.

Brine drainage

Gravity drainage is the process whereby brine, under the influence of gravity, drains out of the ice sheet into the underlying seawater. As the ice thickens, its surface gradually rises above sea level to maintain isostatic equilibrium, producing a pressure head in the interconnected brine channels that drives the underlying brine out of the ice. Because the density of the brine in equilibrium with the ice is determined by the temperature distribution during the time when the temperature within the ice increases downward, an unstable vertical density distribution exists within the brine channels. This produces convective overturning of the brine within the ice as well as an exchange between the denser brine within the sea ice and the underlying seawater. Cox and Weeks (1975) consider this one of the dominant desalination mechanisms in first-year sea ice, leading to gross weakening of the c-shaped profile that characterizes thinner ice and progressive reduction of the bulk salinity. Actual drainage of brine into the underlying sea water occurs via drainage channels, of the order of 5 mm in diameter, and streamers of brine discharging in this manner can lead to the formation of hollow tubes of ice called "ice stalactites," which can reach lengths of up to 6 m in the Antarctic (Dayton and Martin 1971).

Flushing

Flushing is a type of gravity drainage that occurs in spring and summer due to the hydrostatic head produced by surface meltwater. This is particularly true of sea ice in the Arctic, where it is believed that flushing is the most effective mechanism of summertime desalination because the time when flushing starts corresponds to the time during the spring and early summer when major changes in the salinity of the ice, especially in the top 50–100 cm, are observed (Weeks and Ackley 1982).

The salt rejected initially during the freezing process, and later through drainage of brine from the ice, passes into the oceanic mixed layer. This is especially important beneath midwinter leads where rapid ice growth may cause brine plumes to descend into the ocean, giving rise to intense local circulations. Because most of the salt is rejected during growth, the concept of a distribution coefficient becomes important. The distribution coefficient (K_{eff}), which expresses the amount of salt retained by the ice during freezing, is given by

$$K_{eff} = \frac{S_i}{S_w} \quad (2)$$

where S_i is the salinity of the ice and S_w is the salinity of the seawater. Cox and Weeks (1975), using radioactive tracers to examine the brine rejection process, were able to determine expressions for K_{eff} as a function of the ice growth velocity. These expressions have been recently slightly modified (Cox and Weeks 1988) for use in a time-dependent numerical model that calculates the salinity profile of a growing ice sheet.

The distribution coefficient can be used to estimate the amount of salt rejected into the oceanic mixed layer. Following Maykut (1982), the flux of salt rejected during growth is given by

$$F = \rho_i f(h) (1 - K_{eff}) S_w , \quad (3)$$

where ρ_i is the ice density and $f(h)$ is the growth rate. Assuming an ice density of 0.92 Mg m^{-3}, and determining K_{eff} from the expressions given by Cox and Weeks (1988), we calculate that, for an ocean salinity of 33‰, fluxes of salt into the mixed layer for growth rates of 10, 5, and 2 cm day^{-1} are 50.3, 29.7, and 13.0 kg m^{-2} mo^{-1}, respectively. Because the growth rate will decrease as ice thickness increases, a sustained growth rate of 10 cm day^{-1} is unlikely unless the new ice cover were being continuously advected away. Growth rates of 2 to 5 cm day^{-1} can be maintained for extended periods, however. These numbers provide for interesting speculation in cases of individual leads. However, when considering salt fluxes over an area or region, the role of ice dynamics must be addressed. Maykut (1982) presents model results in which salt fluxes over a large area of the Arctic are calculated using measured ice dynamics and the estimated ice thickness distribution. His results indicate that area-averaged salt fluxes are from 1 to 5 kg m^{-2} mo^{-1} during the ice growth season. The results also indicate that melting during the summer months causes a freshwater input to the mixed layer that is equivalent to extracting 12 to 13 kg m^{-2} of salt.

Bipolar comparisons of sea-ice salinity

Functional relationships between the average or bulk salinity of Arctic sea ice and its thickness and age were first examined by Cox and Weeks (1974), who found a strong negative correlation between bulk salinity and increasing ice-sheet thickness (and age) for cold winter ice and a very weak positive correlation with warm multiyear summer ice (Fig. 11). The abrupt change in slope at about 0.4 m for cold ice is consistent with a shift in the dominant desalination mechanism from brine expulsion to gravity drainage. The relationship between salinity (S_i) and thickness (h) in meters of cold ice can be represented by the two best-fit regression lines: $S_i = 14.24 - 19.39h$ ($h < 0.4$ m) and $S_i = 7.88 - 1.59h$ ($h > 0.4$ m). The plot of S_i vs h values for warm ice (Fig. 11) shows that the average salinity of warm multiyear ice is lower than that observed for cold ice up to about 3.5 m thick. A linear regression line for the warm multiyear ice data gives $S_i = 1.57 + 0.18h$. Although a wide range of growth conditions was represented, salinity as a function of thickness (and age) displayed relatively little scatter.

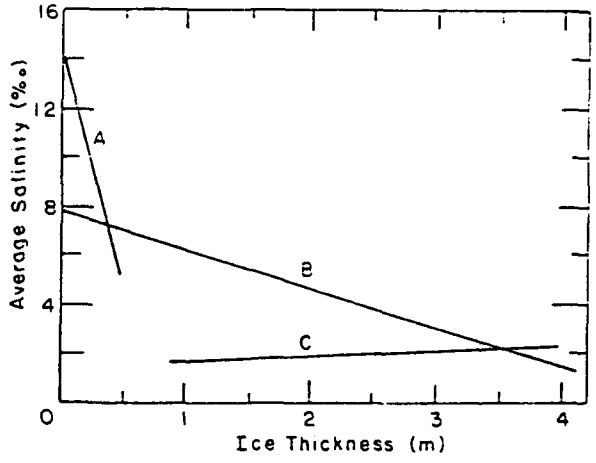

Figure 11. Best-fit salinity trend lines for data obtained by Cox and Weeks (1974) for cold ice sampled during the growth season (A and B) and for warm multiyear ice sampled during or at the end of the melt season (C).

From results of the 1984 Marginal Ice Zone Experiment (MIZEX-84), Tucker et al. (1987) and Gow et al. (1987b) found a sharp distinction between the bulk salinities of warm first-year and multiyear ice discharging through the Fram Strait from the Arctic Basin (Fig. 12). For warm multiyear ice the linear regression between salinity S_i and thickness h is $S_i = 1.58 + 0.18h$. Despite some scatter in the data, this least-squares fit is in close agreement with that found by Cox and Weeks (1974) for warm multiyear ice in the Beaufort Sea. On the YMER-80 expedition, however, where samples were collected in the Greenland and Barents Seas, Overgaard et al. (1983) found the regression between salinity and thickness to be $S_i = 1.59 + 0.47h$. The slope is more than

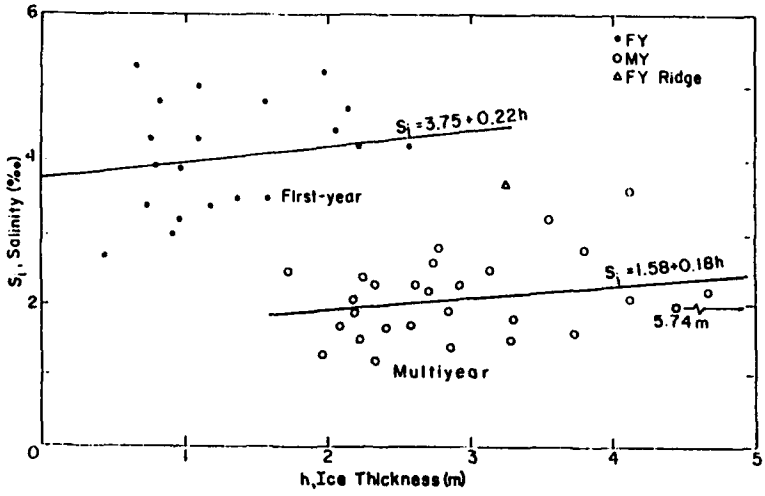

Figure 12. Bulk salinity values of ice cores as a function of floe thickness in the Fram Strait (after Tucker et al. 1987).

twice that found by Tucker et al. (1987) or Cox and Weeks (1974) and indicates that thicker ice sampled during the YMER-80 cruise was more saline (= 0.8‰ more saline for 3.0-m ice). However, the differences may not be significant because of the large scatter in the bulk salinities, particularly in the thicker ice categories.

For first-year ice (Fig. 12), Tucker et al. (1987) obtained $S_i = 3.75 + 0.22h$, while that found by Overgaard et al. (1983) was $S_i = 2.15 + 0.19h$. The YMER-80 sampling took place later in the summer than MIZEX-84, and the lower salinities observed are in keeping with the trend for salinities to decrease during summer warming. Again, desalination is explained in terms of the very active brine drainage occurring in the ice as it warms.

Tucker et al. (1987) also calculated mean salinity profiles of the multiyear and first-year ice cores collected during MIZEX. Separate profiles were calculated for first-year ice cores obtained from 15–28 June and 1–9 July 1984 to examine any possible effects of ongoing brine drainage. Results show that the first-year ice was losing brine for the duration of the field program (Fig. 13). The July profile is much less saline (by nearly 2.0‰ at some levels) than the June profile to a depth of 1.5 m, where the profiles begin to converge. All first-year cores had relatively low near-surface salinities, in contrast to normal winter first-year ice, which exhibits a typically c-shaped salinity profile with higher salinities at the top and bottom of the growing ice sheet (Nakawo and Sinha 1981, Maykut 1985). The low upper-level salinities are attributed (Tucker et al. 1987) to drainage resulting from warming of the ice prior to sampling. Multiyear ice salinities showed no such temporal dependence when individual mean profiles were calculated for June and July. Extensive desalination during previous summers left the ice nearly free of brine and

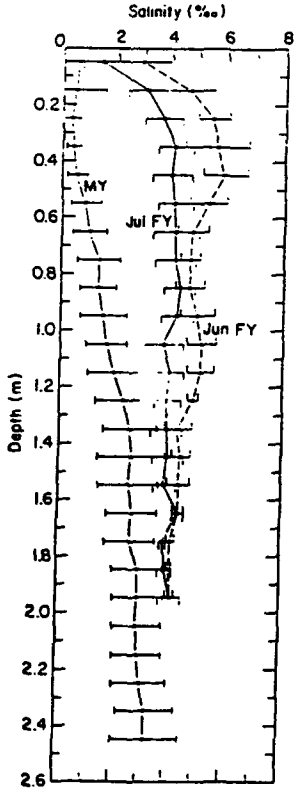

Figure 13. Mean salinity profiles from the Fram Strait for all multiyear and first-year ice cores analyzed during June and July 1984 (after Tucker et al. 1987).

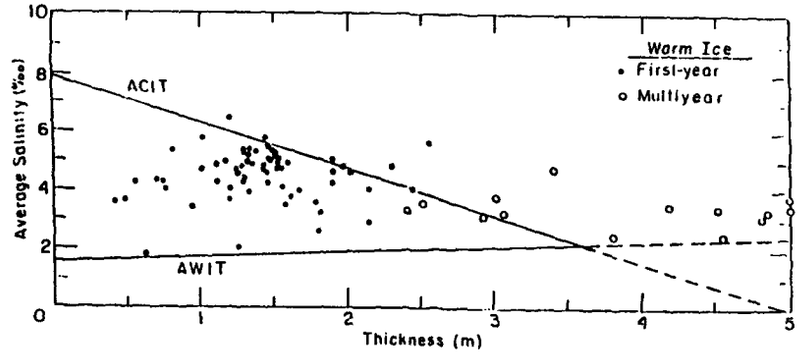

Figure 14. Bulk salinities of Weddell Sea ice floes plotted as a function of thickness. Trend lines for Arctic cold ice (ACIT) and Arctic warm ice (AWIT), after data taken from Cox and Weeks (1974), are included to illustrate the enhanced salinity of warm Antarctic sea ice relative to its Arctic counterpart (after Gow et al. 1987a).

solid salts, especially in the upper 1.0 m, making further changes difficult to detect.

A comparison of Arctic warm ice data with Antarctic summer sea ice salinity measurements indicates significant differences in their bulk salinities, especially for multiyear sea ice. In the only comparable studies made so far in the Antarctic (Ackley et al. 1980; Gow et al. 1982, 1987a), an average bulk salinity relationship of $S_i = 3.83 + 0.11h$ was obtained for multiyear ice in the Weddell Sea (Fig. 14). This relationship yields substantially higher salinities than those found, for example, in the Fram Strait ($S_i \approx 1.58 + 0.18h$). These salinity differences can be attributed mainly to the virtual absence of top surface melting in the Weddell Sea pack (Andreas and Ackley 1982). This greatly diminishes loss of brine through flushing, a major cause of desalination of sea ice in the Arctic during summer (Untersteiner 1968). Differences between first-year ice were not as great, with salinities averaging about 0.3 to 0.5‰ higher in Weddell Sea ice.

Salinity measurements on cold winter-type ice in Antarctica also indicate small but significant departures from those observed in the Arctic (Gow et al. 1982). An example from McMurdo Sound (Fig. 15) shows both first-year and multiyear ice to be more saline than their Arctic counterparts. The average salinity of 26 first-year sites was 6‰ compared to 4 to 5‰ for ice of the same age and thickness in the Arctic. Salinity at the one

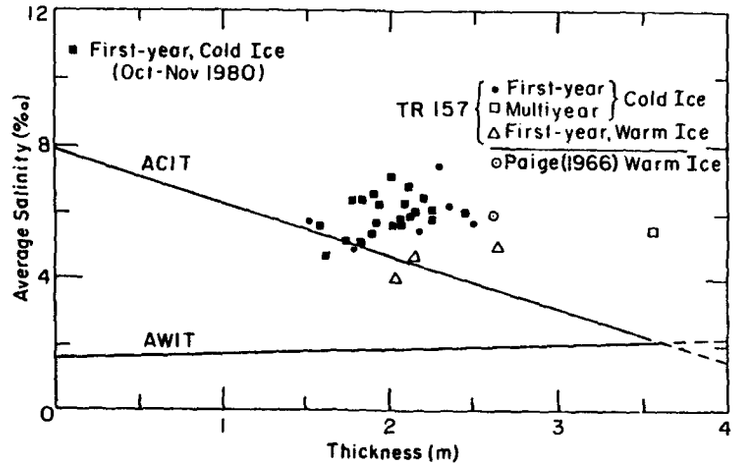

Figure 15. Bulk salinities of first-year and multiyear sea ice in McMurdo Sound plotted as a function of thickness. Trend lines for Arctic cold ice (ACIT) and Arctic warm ice (AWIT) are included for comparison. Data indicated by TR157 were taken from earlier measurements by Hendrickson and Rowland (1965).

multiyear site (not plotted in Fig. 15) averaged 4.2‰, which is more than double the value to be expected in ice of comparable age and thickness (5 m) in the Arctic (Cox and Weeks 1974). In the case of first-year ice, the higher average salinity observed in McMurdo Sound can probably be attributed to faster freezing rates related to colder winter temperatures than generally prevail at a comparable latitude (78°) in the Arctic.

Salinity variations in sea ice are not limited to changes in the vertical dimension. Tucker et al. (1984a), studying small-scale horizontal variations of salinity in a first-year ice sheet in Prudhoe Bay, Alaska, found that substantial horizontal variations also occur over relatively short distances. For 6 cores spaced from 38 to 76 cm apart, the bulk deviations ranged from 0.2 to 0.8‰; an average deviation of 0.4‰ was found between salinities from the same depth levels. The maximum salinity difference at a given level was 2.0‰. These variations in horizontal salinity, which confirmed preliminary observations made earlier by Untersteiner (1968), are attributed by Tucker et al. (1984a) to differential drainage of brine related to the irregular distribution of brine drainage channels in the ice.

Crystalline structure of polar sea ice

As described earlier under Ice Growth and Structure, sea ice characteristically possesses a polycrystalline structure that can occur in several different textures (e.g., granular and columnar), depending on the nature of freezing of the water. These textural variations and the changes associated with thermally activated modification of the ice as it ages have furnished a basis for distinguishing between different ice types, such as first-year and multiyear ice. Differences in crystalline texture and the nature and distribution of brine inclusions are of additional importance in that they exert a major effect on the mechanical, optical, and electrical properties of sea ice.

The past 10 to 15 years has seen a marked resurgence of interest in sea ice research that can be attributed in part to the discovery of vast oil reserves on the Arctic continental shelf and in part to the increased application of satellite and airborne remote sensing to studies of the polar ocean ice cover. During this period a number of important findings have been made concerning the crystalline structure of sea ice, including

- The discovery of widespread crystalline c-axis alignments in shorefast ice and their likely correlation with the direction of the oceanic current at the ice/water interface.
- The first detailed examination of the crystalline structure of first-year and multiyear ice floes exiting the Arctic Basin via the Fram Strait, including the assessment of new approaches for distinguishing between first-year and multiyear floes.
- The discovery that granular frazil ice is an important, if not major, component of Antarctic pack ice, as opposed to columnar congelation ice, which dominates the structure of Arctic pack ice.

C-axis orientations in sea ice

Field observations of the growth fabrics of fast and near-fast ice along the coasts of the Beaufort and Chukchi seas show that at depths of more than 60 cm below the upper ice surface, congelation sea-ice crystals frequently display striking alignments within the horizon-

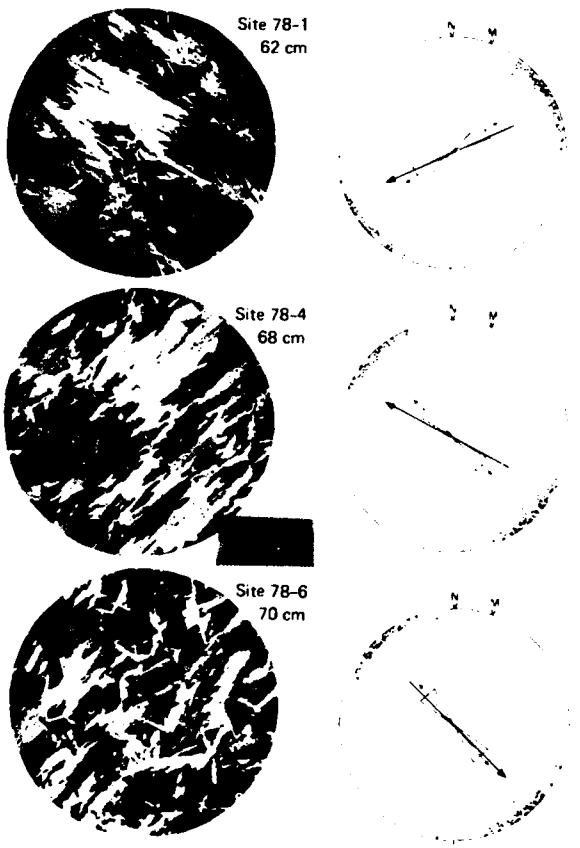

Figure 16. Equal-area horizontal projection plots of individual c-axis orientations (dots) from three sites in Kotzebue Sound, Alaska, showing strong c-axis alignments. The mean direction of c-axis alignment at each site is indicated by the double-arrowed line; simultaneously measured current directions beneath the ice are indicated by the single-arrowed lines. Current speeds ranged from 0.06 m s^{-1} at sites 78-1 and 78-4 to 0.02 m s^{-1} at site 78-6. Smallest scale subdivisions beside photos measure 1 mm.

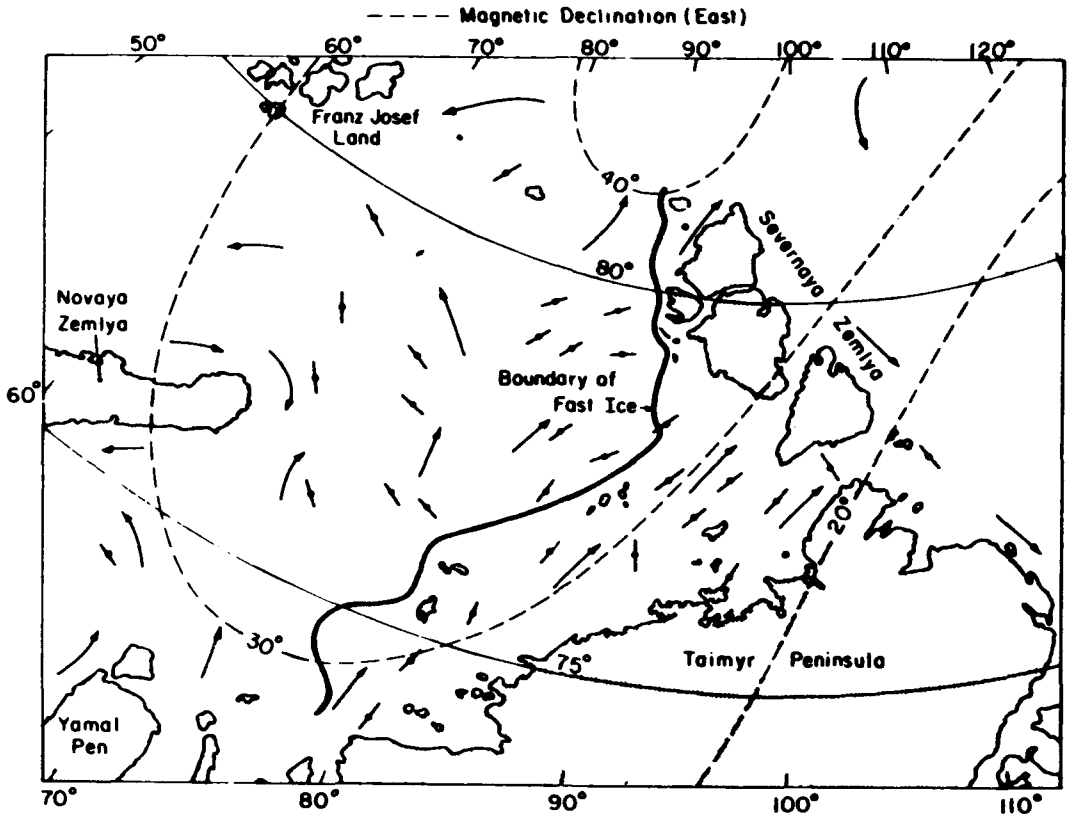

Figure 17. C-axis orientations as determined by Cherepanov (1971) in sea ice in the Kara Sea region of the U.S.S.R. The arrows indicate the estimated direction of the surface currents obtained from U.S. Navy sources (after Weeks and Gow 1980).

tal plane (Gow and Weeks 1977; Weeks and Gow 1978, 1980). Such alignments are frequently maintained to the bottom of thick first-year ice sheets. It had been known (see Weeks and Ackley 1982) that in congelation-type sea ice a dominant horizontal c-axis crystal orientation develops rapidly after an initial ice skim has formed. What was not as well known was that the c-axes often became strongly aligned within the horizontal plane. A few isolated observations, mainly on sea ice incorporated into ice islands (Cherepanov 1964, Smith 1964) and a single measurement on first-year ice by Peyton (1966), indicated the existence of strong azimuthal alignments of the c-axes. However, apart from later work by Cherepanov (1971) in the Kara Sea, the regional extent of such alignments and the probable explanation of their origin did not become apparent until the work of Weeks and Gow (1978, 1980), which indicated that the direction of the current at the growing ice/water interface controlled the direction of c-axis alignments.

Working along a 1200-km stretch of the north coast of Alaska between the Bering Strait and Barter Island, Weeks and Gow (1980) obtained excellent correlation between c-axis alignment directions and current measurements (Fig. 16). A similar situation was apparent in a reexamination of Cherepanov's (1971) results from the Kara Sea. Cherepanov did not include current data in his diagram of c-axis alignments, but when such information, based on summaries of ocean current data from U.S. Navy sources, is included, remarkable agreement between the direction of c-axis alignments and current direction is obtained (Fig. 17). This correlation extends beyond the boundary of the fast ice into the pack ice, indicating that at the time Cherepanov made his observations (March–April 1969) the pack ice was "frozen in" and undergoing little, if any, drift or rotation. More recent laboratory work by Langhorne (1983), Langhorne and Robinson (1986), and Stander and Michel (1989) confirms this general relationship between the direction of c-axis alignment and the direction of the prevailing current. Stander and Gidney (1980) have proposed an alternative mechanism based on stress-activated recrystallization to explain c-axis alignments, but convincing evidence supporting such a mechanism is lacking.

Weeks and Gow (1978, 1980) postulate that aligned c-axes are ultimately caused by the current affecting the transfer of impurities (salt) at the growing interface,

with crystals with their c-axes aligned parallel to the current gaining a slight growth advantage. Crystals whose c-axes are oriented closest to this favored direction (parallel to the current) eventually eliminate less-favored neighbors, a situation ultimately leading to the strong c-axis alignments observed. As such, c-axis alignments can be used to infer the principal current direction at a given location in shorefast ice. The development of strong crystal alignments also results in pronounced anistropy in the mechanical (Richter-Menge and Cox 1985a) and electrical (Campbell and Orange 1974, Kovacs and Morey 1978) properties of shorefast ice.

Arctic sea ice structure

Observations over the past 10 to 15 years of shorefast and near-shore fast ice along the coasts of the Arctic Ocean show that the great bulk of the ice (90% or more) is composed of congelation columnar-textured ice (Weeks and Gow 1978, 1980; Martin 1981). During the past few years concerted efforts have been made to evaluate the composition and structure of ice originating in the Arctic Basin, and the first detailed examination of the structural and physical properties of sea ice exiting the Arctic Basin via the Fram Strait was made in conjunction with MIZEX. The importance of the Fram Strait is that it is the major outflow region for Arctic Basin ice; according to Maykut (1985), approximately 10% of the ice in the basin is discharged annually through this relatively narrow strait located between Spitzbergen and the northeast coast of Greenland.

Prior to MIZEX very little was known of the structural characteristics of sea ice exiting the Arctic Basin; the discussion that follows is taken largely from results obtained by Tucker et al. (1987) and Gow et al. (1987b) on a large number of floes in the Fram Strait. Analyses were based mainly on examinations of cores drilled through the entire thickness of each floe. A major objective was to distinguish between first-year and multiyear ice, the identification of which was based largely on differences in their crystalline condition and salinity. Crystalline structure was assessed mainly on the basis of optical thin section studies using techniques described by Weeks and Gow (1978, 1980). Salinity was determined on the basis of conductometric analyses of melted samples (see Gow et al. [1987b] for details of the technique).

Identification of multiyear ice from measurements of freeboard or drilled thickness is not always reliable because of thickness overlaps between the thinnest multiyear ice (1.7 to 1.8 m) and the thickest undeformed first-year ice (2.3 m). However, positive identification of multiyear ice can generally be made from observations of the appearance and mechanical condition of the core drilled in the top meter of a floe. Because of the nature of its transformation (by thermal modification of first-year ice during the summer), approximately the top half-meter of multiyear ice becomes very much harder (more resistant to drilling and sawing) and appreciably less opaque than the upper half-meter of first-year ice. The opaque appearance and relative softness of first-year ice are closely linked to an abundance of brine pockets that enlarge, coalesce, and drain during the summer to yield ice with the hardness and transparency characteristics observed in the upper levels of multiyear ice.

Analyses of the crystalline structure of Arctic ice floes have shown that ice textures are predominantly of columnar (congelation) origin in both multiyear and first-year floes. Small amounts of granular ice, mainly frazil ice but including some snow ice, were found in nearly every floe (Fig. 18). This is not surprising since

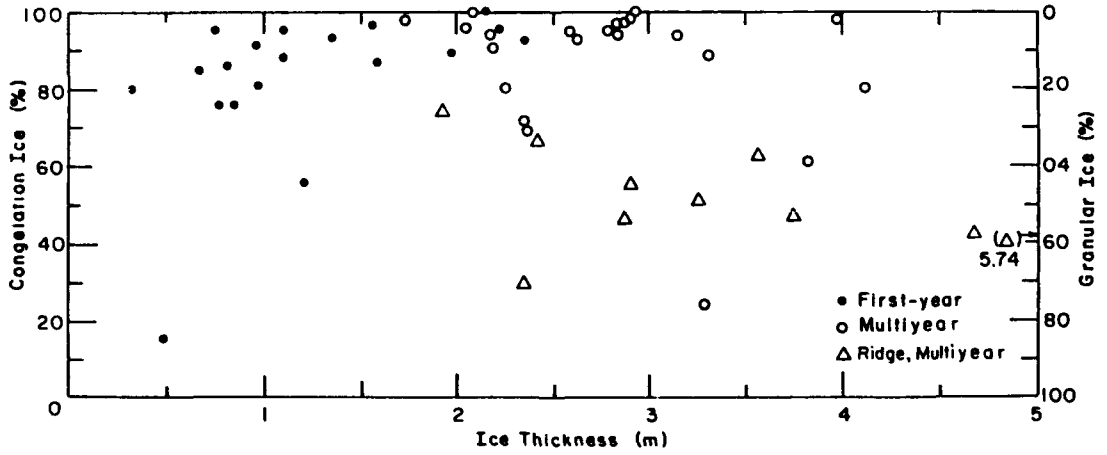

Figure 18. Percentages of columnar and granular ice as a function of thickness for various ice floe types in the Fram Strait (after Gow et al. 1987b).

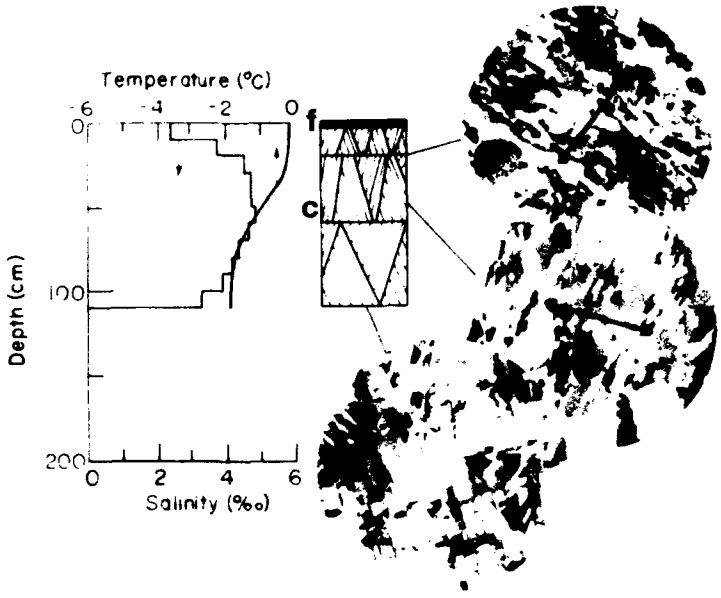

Figure 19. Salinity–temperature–structure profiles from an undeformed first-year ice floe in the Fram Strait. In the vertical structure diagram the symbols f and c designate freshwater ice and columnar ice, respectively. Arrows in the horizontal thin-section photographs indicate the direction of crystal c-axis alignment (after Gow et al. 1987b). Smallest scale subdivisions measure 1 mm.

the freezing of seawater generally begins with the formation of grease or slush ice. If ridged ice is excluded from the ice composition estimate, then the congelation component would amount to 85% of total ice thickness in undeformed floes. While the granular ice content of undeformed floes is somewhat higher (15%) than the 5 to 10% that Martin (1981) reports for Arctic nearshore conditions, it should be noted that Martin restricted his study to thick first-year ice, whereas the Fram Strait (MIZEX-84) investigations spanned a large range of ice thicknesses dominated by multiyear floes. It was also observed that one-third of multiyear ice floes examined for structure in the Fram Strait contained previously deformed ice, indicating that multiyear floes may be composed of substantial amounts of deformed ice (often occurring as worn-down ridge remnants).

A typical example of first-year ice encountered in the Fram Strait is shown in Figure 19. The floe consisted primarily of columnar ice exhibiting a moderate to strong c-axis alignment overlain by a thin (< 10 cm) layer of snow. An approximate 60° change in c-axis alignment at ca. 50 cm depth, suggesting a significant change in the direction of the prevailing current at the ice/water interface, is most probably linked to repositioning of the winter pack in which this piece of ice was growing. The top of the floe featured a thin (2–3 cm) layer of ice derived either from freezing rain or by refreezing of early spring snowmelt. Either process would be consistent with both the desalinated nature of the ice and the elevated temperatures measured at the top of the floe. The bulk salinity of the floe was 4.4‰.

A fairly typical example of undeformed multiyear Arctic ice (Fig. 20) was found to consist mostly of aligned crystals of columnar ice overlain successively by 7 cm of pond ice, 11 cm of snow ice, and a 25-cm-

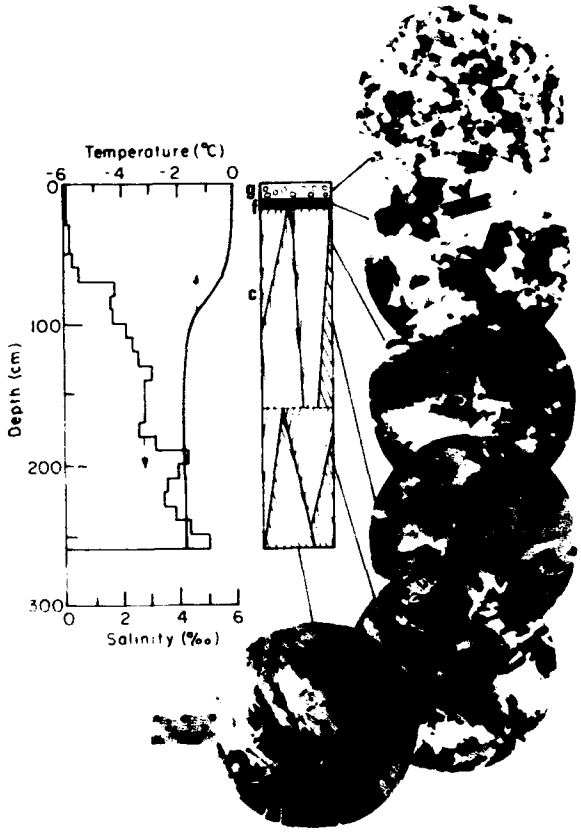

Figure 20. Salinity–temperature–structure profiles from an undeformed multiyear ice floe in the Fram Strait. The symbols g, f, and c beside the vertical structure diagram designate granular ice, freshwater pond ice, and columnar ice, respectively. Arrows in the horizontal thin-section photographs indicate directions of c-axis alignments (after Gow et al. 1987b). Smallest scale subdivisions measure 1 mm.

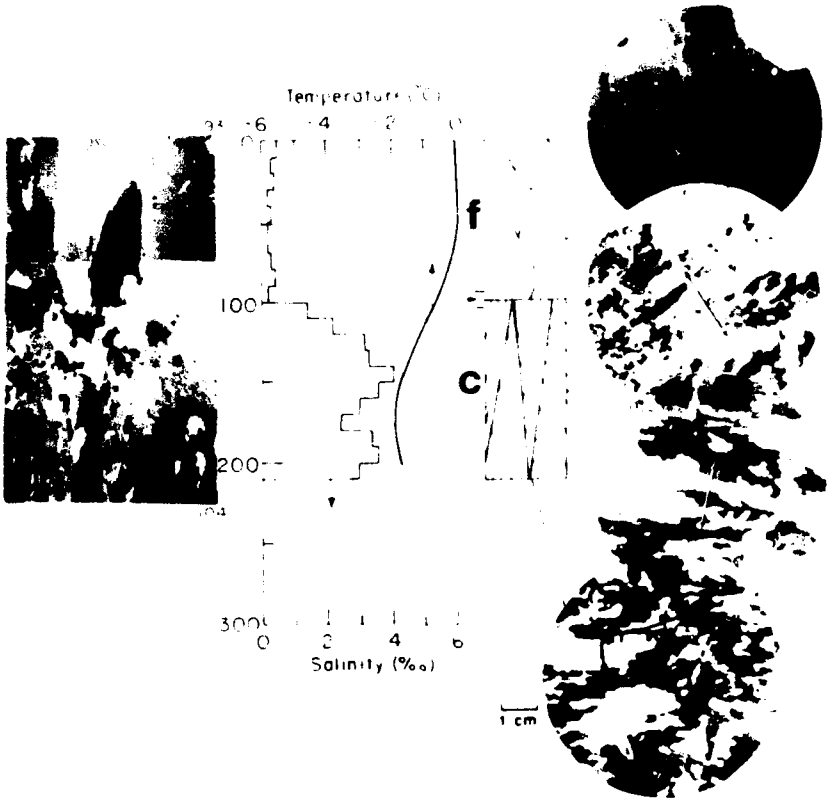

Figure 21. Salinity–temperature–structure profiles from a ponded multiyear ice floe in the Fram Strait. The symbols f and c designate freshwater pond ice and columnar ice, respectively. The vertical thin-section photograph shows the transition between the ponded and columnar ice at around 100 cm depth. C-axis alignments in horizontal thin-section photographs are also indicated (after Gow et al. 1987b).

thick layer of snow. Structure and salinity characteristics indicate a two-year old floe that underwent appreciable desalination in the top 70 cm during the summer of 1983. This desalination was accompanied by ponding and subsequent refreezing of the surface water, and by very substantial retexturing of the columnar ice to a depth of at least 100 cm. Individual salinities in the top 70 cm did not exceed 0.5‰; the overall salinity averaged 2.3‰ or only about half of that measured in the first-year floe (Fig. 19). A significant salinity surge, beginning at 180 cm depth and yielding salinities in excess of 4‰, corresponds closely with the onset of the second winter's ice growth.

Figure 21 features a multiyear floe from the Fram Strait in which very thick, coarse-grained freshwater pond ice, representing 47% of the floe thickness, is underlain by columnar sea ice. The sharp textural transition from pond ice to columnar ice was also accompanied by a sharp increase in salinity. A very large (80°) change in c-axis alignment between 1.0 and 1.5 m would imply that the melt pond was underlain by only a thin layer of sea ice at the end of the summer and that the bottom 0.5 to 1.0 m of ice represented growth during the ensuing winter.

Most of the granular ice observed by Tucker et al. (1987) in floes in the Fram Strait was associated with frazil crystal formation in old ridges. Such frazil occurred both in the voids between blocks of ice and near the bottoms and on the flanks of ridges. That found on the flanks of keels most likely originates when the frazil present in the water column is accumulated by the sweeping action of the keel as it moves relative to the water column. Only limited amounts of granular ice appear to have been generated by crushing of coarser-grained ice during the ridging process. On average, the multiyear ridges consisted of 40 to 60% frazil ice. Similar findings of high granular ice contents in multiyear ridges have been reported by Richter-Menge and Cox (1985b). The top 1 m of ice in the old ridge fragment featured in Figure 22 consisted of a mixture of tilted blocks of columnar ice with granular ice between them, whereas the lower part of the ridge contained more

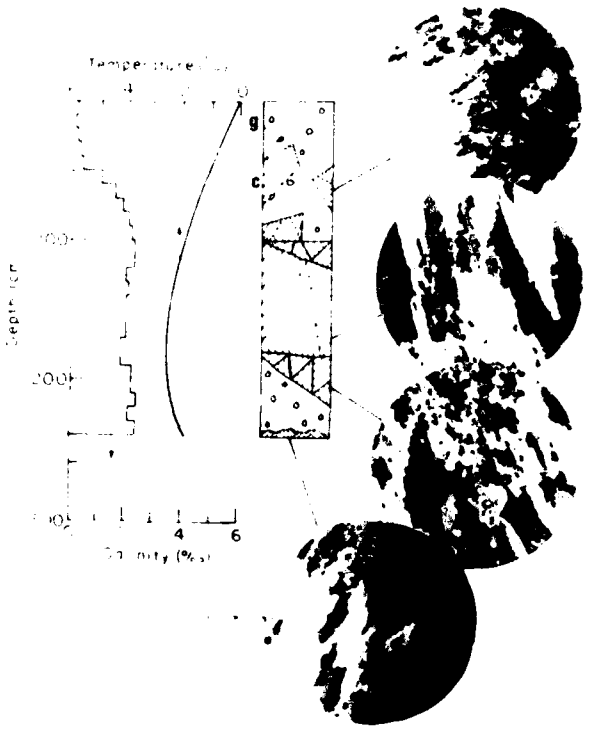

Figure 22. Salinity–temperature–structure profiles through old ridged ice from a multiyear floe in the Fram Strait. The symbols g and c beside the vertical structure diagram designate granular ice and columnar ice, respectively (after Gow et al. 1987b).

granular (principally frazil) ice underlain by columnar ice representing recent growth on the flank of the ridge.

Another structure-related feature observed by Tucker et al. (1987) in the uppermost layers of Arctic multiyear sea ice is the retextured condition of the ice crystals. This retexturing process is related to the elimination of brine pockets and the rounding off of crystal boundaries induced by elevated air temperatures and increased solar radiation during summer. The depth of retexturing may exceed 100 cm, and the glacial-like, brine-poor ice that results from thermally activated retexturing bears little resemblance to the original columnar-textured sea ice. The extent of the process is illustrated in thin sections of ice from a multiyear floe (Fig. 23).

Most floes examined during MIZEX exhibited evidence of c-axis alignments related to growth of ice under the direct influence of oceanic currents. Changes in the direction of alignment at two or more levels in the ice were observed in a number of floes. Such changes have been attributed to alternating episodes of movement and immobilization of a floe and thus constitute a record of a floe's orientation relative to the direction of the current beneath the ice. Assuming that the c-axes align on an annually repeating basis consistent with wintertime growth, such changes in alignment direction, together with crystal texture changes and surges in the salinity profile (which often coincide with change of crystal alignment) have been used to estimate the ages of multiyear floes (Gow et al. 1987b).

A winter marginal ice zone experiment was conducted in March and April 1987. Results of sea-ice observations (Perovich et al. 1988) essentially duplicated those obtained in MIZEX.

Antarctic sea ice structure

Current knowledge of the dynamics, structure, and related physical properties of Antarctic pack ice stems largely from studies initiated by Ackley in the Weddell Sea (Ackley 1979a,b, 1981; Ackley et al. 1978, 1980; Gow et al. 1981, 1982, 1987a; Lange et al. 1988). The open, broad-fronted nature of the marginal ice zone in the Weddell Sea contrasts drastically with the largely landlocked situation prevailing in the Arctic Basin. This and the fact that the Weddell Sea embayment is backed by a large floating ice shelf, the Filchner-Ronne, appear to exert a sufficiently strong impact on near-surface oceanic circulation in the Weddell Sea to cause significant differences in the formational processes and structure of sea ice compared to those of the Arctic Basin.

During February and March 1980 a total of 52 first-year and 14 multiyear floes were investigated by Ackley et al. (1980) along a 600-nautical-mile transect of the ice edge in the Weddell Sea (Fig. 24). In the absence of surface melt features, the higher freeboards of multiyear floes proved the only reliable criterion by which to distinguish these floes from first-year ice in the Weddell Sea.

The most significant result concerning the crystalline structure of Weddell Sea pack ice was the discovery of granular ice, principally frazil, in amounts not previously observed. In many of the ice floes examined structurally in 1980, frazil ice was the dominant component, averaging 72% of the ice thickness of 13 multiyear floes and 37% of 49 first-year floes. The overall average composition, based on the total length of first- and multiyear cores examined for structure, yielded 54% frazil ice, 39% congelation ice, and 7% admixtures of the two plus snow ice. In general, a higher percentage of congelation ice was found in floes up to 2 m thick (Fig. 25). However, every floe thicker than 2 m, except one first-year floe, contained more frazil than congelation ice. Much of this frazil appeared to have been generated during the second year of growth (Fig. 26). However, there were cases where multiyear floes were composed entirely of frazil ice (Fig. 27).

Interspersed layering of frazil and congelation ice (Fig. 28) in many floes shows that frazil formation is episodic. Such structure, especially in thinner floes (<

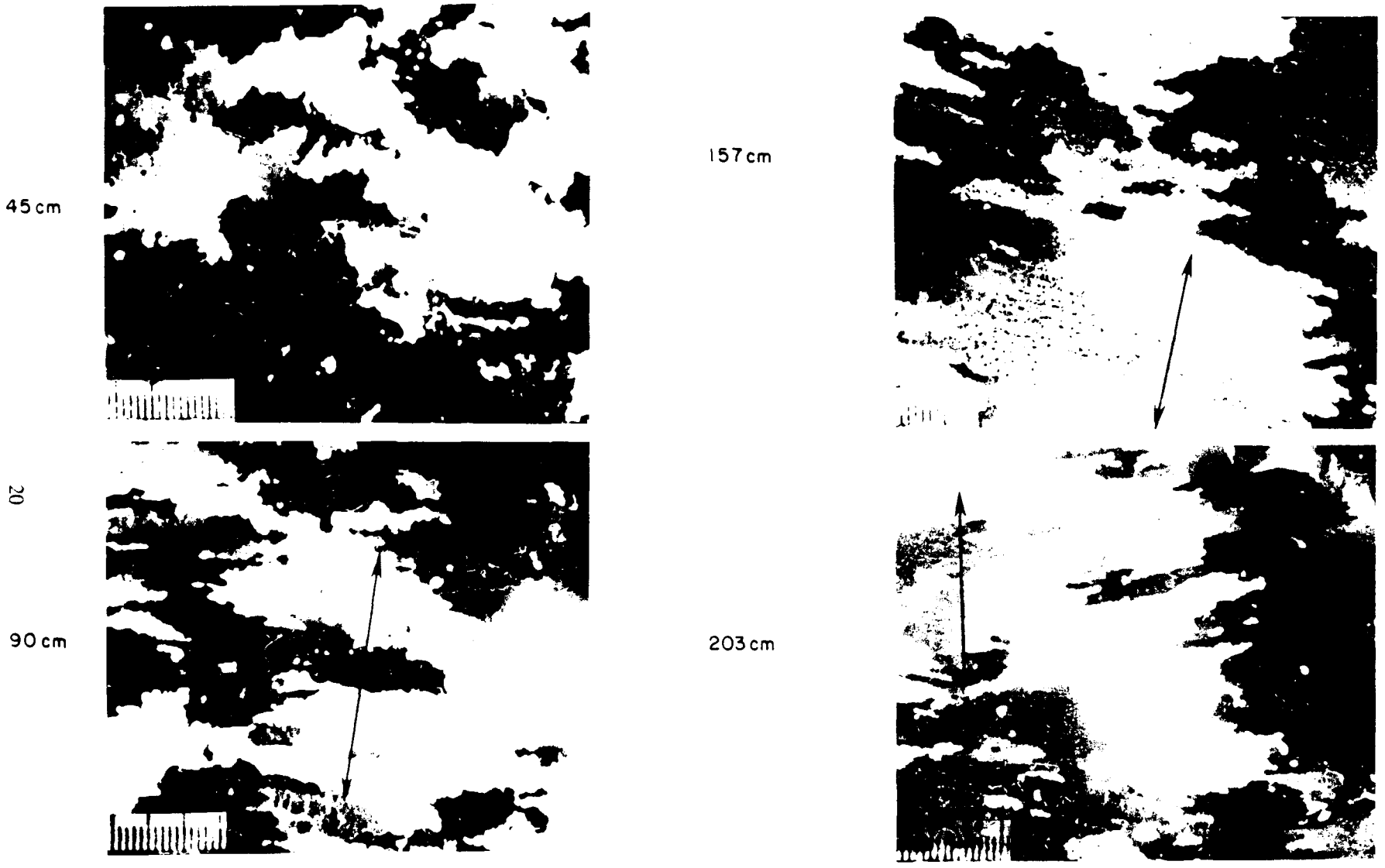

Figure 23. Horizontal thin-section photographs demonstrating retexturing of ice in the upper layers of an Arctic multiyear floe. Note in the section from 90 cm that the original c-axis alignment (arrow) is maintained despite nearly complete loss of brine pocket substructures, in contrast to substructures preserved in deeper unretextured ice (after Gow et al. 1987b). Smallest scale subdivision measures 1 mm.

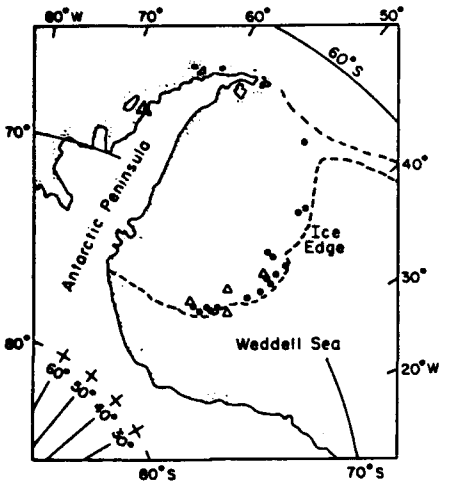

Figure 24. Locations of primary sampling sites (dots) visited in 1980 during summertime investigations of the physical and structural properties of pack ice in the Weddell Sea, Antarctica. Triangles mark the positions of data buoys used for satellite monitoring of drift and deformation of the pack in the Weddell Sea (after Gow et al. 1987a).

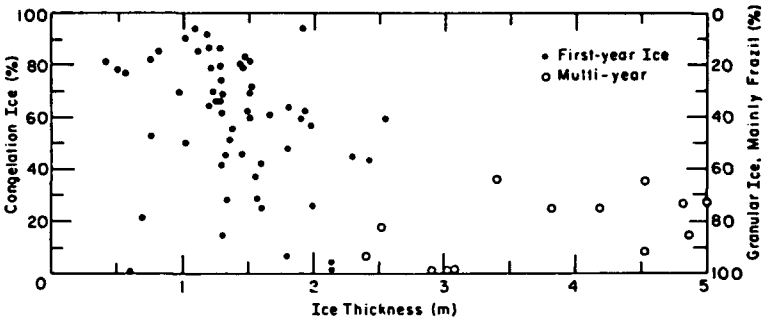

Figure 25. Abundances of congelation and granular (principally frazil) ice vs ice thickness in Weddell Sea floes (after Gow et al. 1987a).

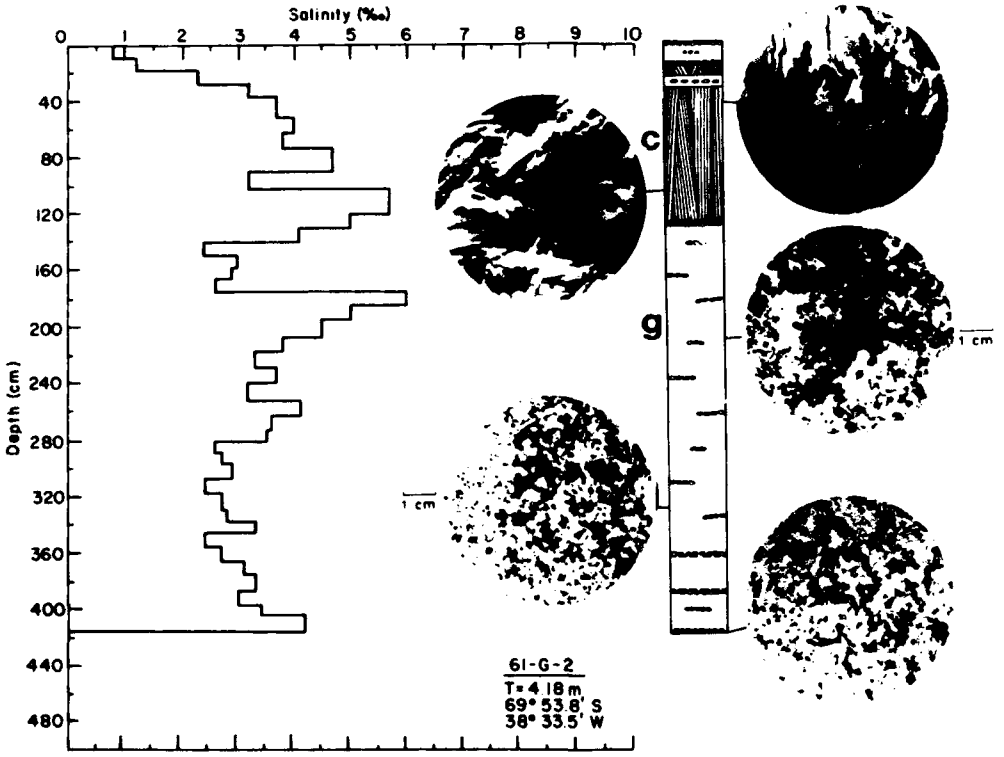

Figure 26. Salinity and structure profiles of a 4.18-m-thick multiyear floe from the Weddell Sea. Congelation ice (c) is limited to the top 1.3 m; the underlying frazil ice (g) represents 75% of the total ice thickness. Salinity averaged 3.59‰. The first year's growth is interpreted as having ended at the bottom of the congelation ice layer (after Gow et al. 1987a).

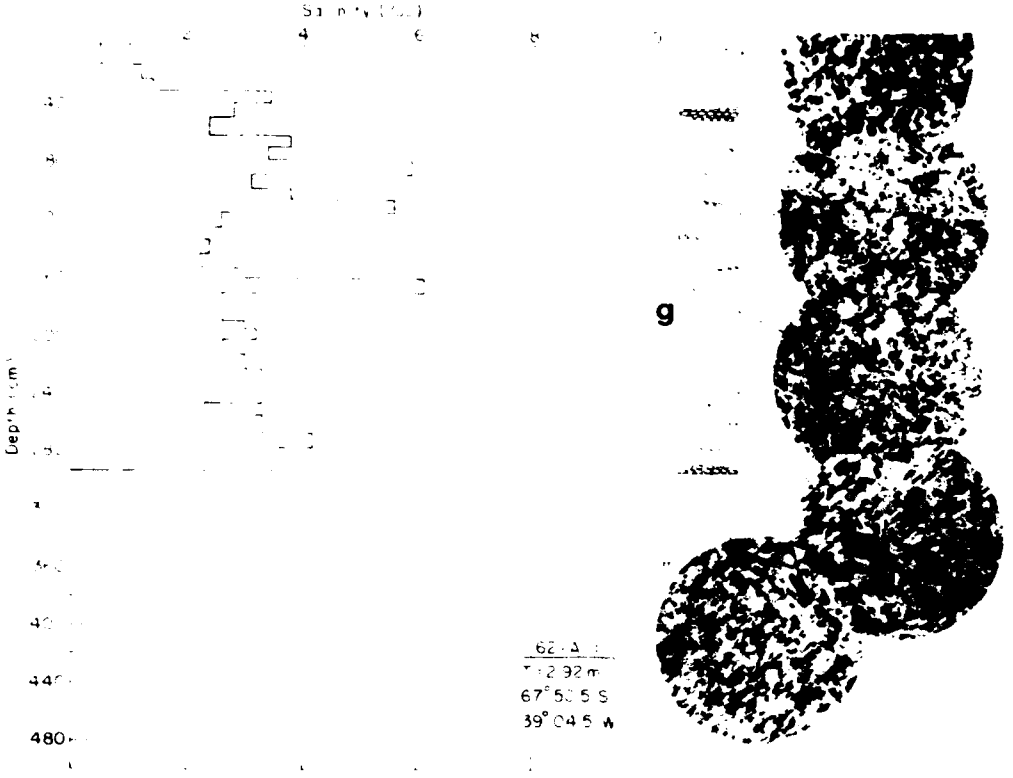

Figure 27. Salinity and structure profiles of a 2.92-m-thick multiyear floe from the Weddell Sea. As shown in the vertical structure section, this floe was composed entirely of granular ice, which, apart from a 40-cm-thick layer of frazil ice possibly mixed with snow ice in the top 10 cm of the floe, consisted completely of frazil ice of variable grain size and an average salinity of 3.1‰ (after Gow et al. 1987a).

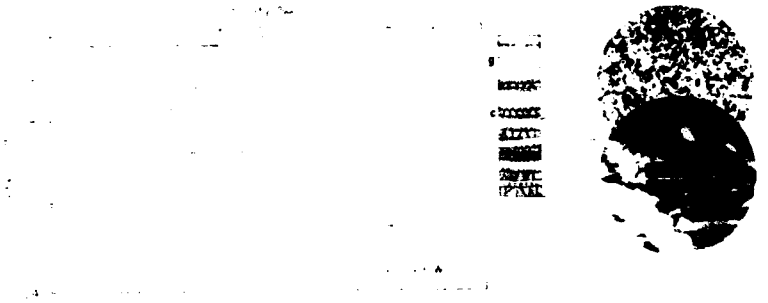

Figure 28. Salinity and structure profiles of a 1.57-m-thick first-year floe from the Weddell Sea. As shown in the vertical structure section, there were seven layers of columnar ice (c) interspersed with frazil ice (g), indicating that this floe probably formed by repeated rafting of thin ice. The average salinity of the floe was 3.4‰ (after Gow et al. 1987a).

1.0 m) is entirely consistent with multiple rafting events (overriding of ice-sheet fragments one upon the other), and recent studies of winter ice growth in the central Weddell Sea now indicate that rafting of frazil-rich pancake ice is an important if not major mechanism of frazil ice production at the advancing ice edge (Lange et al. 1988). However, Gow et al. (1987a) observed frazil ice occurring in a variety of textures and at depths of up to 5 m in the thickest floes, indicating that other mechanisms in addition to surface turbulence and rafting may also contribute to frazil generation in the Weddell Sea. For example, because of its buoyancy, surface-derived frazil is not likely to be transported to depths of 3 m or more, as was observed in some Weddell Sea floes.

Weeks and Ackley (1982), in an attempt to assess the conditions leading to widespread occurrence of frazil ice in the Weddell Sea, described four processes by which frazil may form in polar oceans:

1. *Wind- and wave-induced turbulence.* This well-known mechanism accounts for substantial frazil growth in leads, polynyas, and the open areas of marginal ice zones. As noted above (Lange et al. 1988), rafting of frazil-rich pancake ice may lead to enhanced thicknesses of frazil ice. In fact, based on their wintertime observations, Lange et al. (1988) now believe that it is the rafting of frazil-rich pancake ice that accounts for the dominance of frazil ice in the Weddell Sea ice pack. In addition, Lange et al. (1988) obtained frazil/congelation percentages of 57/43, values in almost exact agreement with those found by Gow et al. (1987a) at the end of the summer.

2. *Adiabatic expansion of seawater as it ascends from beneath thick ice shelves.* The Weddell Sea is backed by large ice shelves, including the Filchner and Ronne, and higher frazil contents might be expected close to these ice shelves.

3. *Contact between two water masses of significantly different salinities.* One such case would involve the interaction of seawater with freshwater derived from surface melting. This occurs in limited situations in Antarctica, e.g., beneath an ice shelf in McMurdo Sound (Gow et al. 1965, Gow and Epstein 1972). A similar process was proposed by Untersteiner and Badgley (1958) to explain the formation of frazil beneath Arctic ice floes. However, this mechanism is not likely to be an important source of frazil in the Weddell Sea because of the lack of surface melting.

Recently, Lange et al. (1988) have reported the widespread occurrence of platelet-like ice in layers up to 5 m thick in ice formed along the ice shelf front in the eastern Weddell Sea. They suggest that such ice, as distinct from frazil, originates as a result of the supercooling of meltwater from the bottom of the Filchner Ice Shelf. Similar platelet ice was also reported by Dieckmann et al. (1986) to form in water 200 to 270 m deep off the Filchner Ice Shelf. They attribute this growth to freezing from supercooled water streaming out from beneath the shelf. Lewis and Perkin (1985, 1987) have postulated a similar situation existing off the front of the Ross Ice Shelf.

4. *Thermohaline convection related to surface freezing.* Such freezing results in the formation of cold brine plumes, which, as they descend, could cause frazil to crystallize in the water column underlying the growing ice sheet. This process, given the depth characteristics, textures, and exceptional thicknesses of frazil ice observed by Gow et al. (1982, 1987a) in Weddell Sea pack ice, seems attractive because it is not constrained by the problem of crystals having to overcome the buoyancy forces encountered during downward advection of surface-derived crystals.

Large platelike crystals measuring several centimeters long and even larger, loosely bonded, wafer-like crystals were also observed in bottom ice of several multiyear floes examined by Gow et al. (1987a) in the Weddell Sea. Such platy, wafer-like crystal texture appears transitional between those of frazil and congelation ice and is probably equivalent structurally to the so-called underwater ice of the east Antarctic coast described by Serikov (1963) and by Paige (1966) and Gow et al. (1982) in the bottom of sea ice in McMurdo Sound. In McMurdo Sound this kind of platelet ice appeared to be growing in place, unlike that forming at depth in the Weddell Sea as discussed above (Dieckmann et al. 1986, Lange et al. 1988).

In Weddell Sea floes, congelation ice was most prevalent in first-year ice, averaging 58% of the ice thickness of 49 floes examined by Gow et al. (1987a). It was structurally similar to Arctic congelation ice, with c-axes often showing a preferred alignment (Fig. 29).

Virtually nothing is known of the structural characteristics of pack ice in seas bordering other parts of the Antarctic coastline (e.g., the Ross Sea), and observations of shorefast ice have been confined to a few coastal areas where there are established scientific bases, including McMurdo Sound, where the winter ice cover is composed largely of congelation ice that frequently exhibits aligned c-axes. As in the Arctic, these alignments appear controlled by the direction of the current at the ice/water interface. Much of the bottom ice in McMurdo Sound is also modified by platelet growth extending several tens of centimeters below normal congelation ice (Gow et al. 1982). The formation of platelet crystals would appear to be confined to late

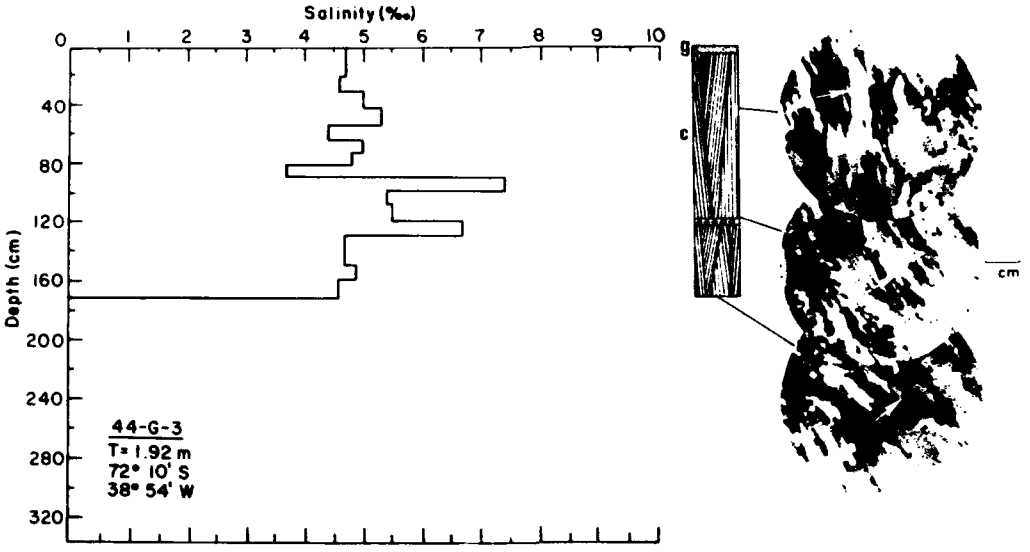

Figure 29. Salinity and structure profiles of a 1.92-m-thick first-year floe from the Weddell Sea. The floe is composed of 94% columnar ice exhibiting a near-constant direction of alignment of its c-axes (arrowed), consistent with growth under nearshore or shelf-fast conditions. The average salinity of the floe was 5.1‰ (after Gow et al. 1987a).

winter or early spring, indicating that the onset of platelet ice growth is related in some way to changes in the composition or circulation patterns of sea water in McMurdo Sound at that particular time of the year.

LARGE-SCALE ICE PROPERTIES

The mass balance of ice within a region is governed by the amounts of ice growth, ice ablation, and ice that drifts into or out of the area. In this section we discuss large-scale ice growth, decay, and dynamic characteristics of ice as they apply to the Arctic and Antarctic. Characteristic features of sea ice resulting from deformation will be touched upon. Finally, large-scale features of the variations in ice extent and zonation in both areas are discussed.

Ice growth and decay

General considerations and Arctic implications

Once an initial ice sheet has formed, further ice growth or ablation is controlled by the energy balances at the upper and lower surfaces of the sheet. The balance at the upper surface, where the ice is in contact with the atmosphere, is approximated by:

$$(1-\alpha)\,S - I + L_i - L_e + T_s + T_L + C_u - M = 0 \quad (4)$$

where S = incoming shortwave (solar) radiation
α = the albedo of the ice surface
I = flux of shortwave radiation that passes through the thin surface layer into the ice interior
L_i = incoming longwave radiation
L_e = longwave radiation emitted by the ice surface
T_s = sensible heat flux
T_L = latent heat flux
C_u = the conducted heat flux at the upper surface
M = amount of heat loss due to melting or sublimation at the surface.

In eq 4, the signs of individual terms are positive if they represent a gain in energy by the ice surface and negative if they represent a loss.

On the underside of the ice, the energy balance can be represented by

$$Q_f + C_L + F_W = 0 \quad (5)$$

where Q_f = heat gain or loss due to freezing or melting on the bottom of the ice
C_L = conduction of heat away from the bottom toward the ice surface
F_w = turbulent heat transfer between the ice and the ocean.

In numerical simulations of thermodynamic processes, eq 4 and 5 are coupled by the heat conduction terms C_u and C_L. These terms are considerably more complex than represented here, with the primary complexity being introduced by the vertical temperature

profile within the ice. If the temperature profile is nonlinear, a thermal diffusion equation must be implemented to calculate further changes in internal ice temperature. Most large-scale models simplify the problem by using simpler estimates (often linear) of the temperature profile, thus reducing the numerical complexity.

Because major energy gains and losses occur at the ice surface, this balance will be considered first. Figure 30 shows average monthly values of the radiative fluxes (S, L_i, and L_e) over ice for the central Arctic Basin (Maykut 1985). In addition to the original estimates of the fluxes, we have shown the net solar radiation [$(1-\alpha)S$], the net incoming and outgoing longwave radiation ($L_i + L_e$), and the total net radiation (R_{net}). Of the three basic radiative fluxes, the solar radiation clearly shows the largest seasonal variations. It varies from zero during winter months of total darkness to about 300 W m^{-2} around the summer solstice when the sun is continuously above the horizon. The pronounced effect of ice and snow albedo can be seen in the $(1-\alpha)S$ curve. The peak absorption lags that of the incoming shortwave by about a month because the albedo is steadily decreasing as a result of surface melting. The largest influences on the albedo reduction are caused by the loss of the highly reflective snow cover and the increase in the number of surface melt ponds, creating a puddled ice surface.

The incoming longwave radiation (L_i) is produced by the emission of radiation from clouds and atmospheric water vapor. A significant increase during summer is caused by an increase in Arctic cloudiness during summer and a corresponding increase in cloud temperatures, with L_i being proportional to the 4th power of the temperature of the radiating matter (i.e., cloud droplets and water vapor). The longwave radiation emitted by the ice (L_e) is proportional to the 4th power of the surface temperature, and is the only radiative flux by which the ice loses energy. A significantly larger loss occurs during summer in response to warming of the ice. It should be noted that aS is also considered to be a flux but is contained within the $(1-\alpha)S$ term.

As Figure 30 indicates, the net longwave radiation components ($L_i + L_e$) represent a small loss of energy from the ice surface. Inclusion of the solar radiation component shows that the net radiative flux, R_{net}, is substantially positive in summer and slightly negative during winter. The importance of the radiative fluxes is further emphasized in Figure 31, where R_{net} is contrasted to estimates of the sensible and latent heat fluxes. The sensible heat flux, T_s, is driven by temperature differences between ice and atmosphere while the latent heat flux, T_L, arises from humidity differences. In addition, both depend upon surface roughness, wind speed,

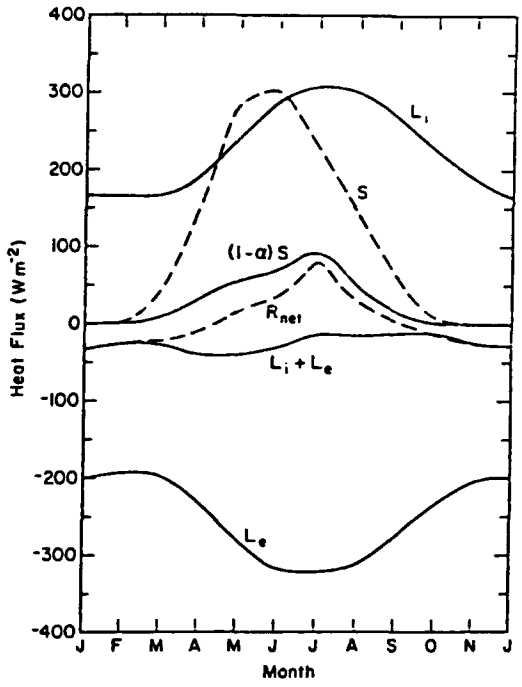

Figure 30. Average monthly values of radiative heat fluxes. L_i *is incoming longwave,* L_e *is outgoing longwave,* S *is shortwave,* $(1-\alpha)S$ *is the net shortwave input at the surface (taking into account ice and snow albedo),* $L_i + L_e$ *is the net longwave, and* R_{net} *is the net radiative flux. Positive indicates a heat gain by the ice and negative indicates loss (from data of Maykut 1985).*

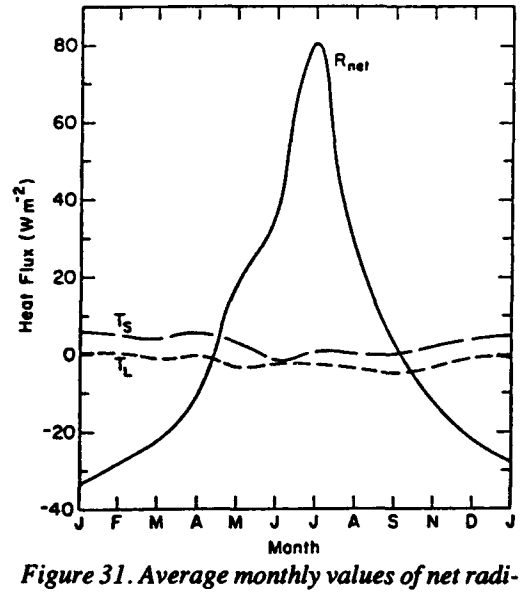

Figure 31. Average monthly values of net radiative heat flux R_{net} *and sensible,* T_s, *and latent,* T_L, *heat fluxes observed over perennial ice (would be different for thin ice). Positive indicates heat gain by the ice and negative indicates loss. (from data of Maykut 1985 and Leavitt et al. 1978).*

and the stability of the atmospheric boundary layer. The latent heat flux is negligible in winter and slightly negative in summer when the wet ice surface allows vapor transfer into the atmosphere. The sensible heat exchange is positive during winter, when there is usually a strong temperature inversion in the lower atmosphere over the central Arctic.

On a monthly basis the turbulent heat fluxes are small compared to the radiative fluxes. Daily values, particularly of the sensible heat flux, can be large (Maykut 1985), but frequent reversals of flux direction tend to keep the cumulative totals small. The fluxes are important on an annual basis, however, because the sum of the two turbulent exchanges is 20 to 50% of the annual net radiation balance (Maykut 1985). Model simulations by Maykut and Untersteiner (1969) indicate that, without the turbulent heat losses, the surface ablation during summer would be 20 to 100% larger, resulting in a reduction in the equilibrium ice thickness (the thickness of undeformed perennial ice reached after several annual cycles) of about 50%. There is little doubt, however, that shortwave radiation is primarily responsible for the advanced decay of the ice during summer (Langleben 1972).

The remaining fluxes in the surface energy balance are the solar radiation passing into the ice interior, I, conductive heat flux C_u, and the loss due to melting or sublimation, M. The melting term specifies that excess energy will be used to ablate the ice, and it is this term that is calculated in thermodynamic ice models. The term I is generally a small percentage of the incident solar radiation. As Maykut (1985) explains, however, this term can be more significant for "blue ice," which is characteristic of refrozen melt ponds. The other significant effect of I is that it allows for solar radiation to be directly absorbed by brine pockets in the ice interior, which is a means of internal energy storage that can alter the ice temperature profile and increase the brine volume.

As mentioned earlier, the conduction of heat in sea ice (represented by C_u) is complicated because the thermal conductivity of sea ice is not a constant. Instead, it is a function of temperature and salinity and, as such, it typically varies with depth. The conductivity is affected by the presence of brine and air pockets and channels. The brine in these pockets exists in a unique phase equilibrium that depends upon its temperature and salinity. If the temperature of the ice decreases, brine in the pockets begins to freeze, releasing latent heat that in turn acts to warm the ice. The net effect is to retard the cooling of the ice (Maykut 1985). The opposite occurs when the ice warms. That is, warming causes melting first around the walls of the brine pockets, which requires additional heat, hindering the overall warming of the sheet. The net effect of the brine inclusions is to act as thermal buffers that dampen the transport of heat through the ice.

Equation 5 describes the energy balance at the ice/water interface. Q_f, the growth term, is again a residual term indicating that if the sum of the oceanic heat flux, F_w, and the lower boundary conduction term, C_L, are positive, the ice will melt. If the sum is negative, the ice will grow, which in turn releases latent heat to be conducted toward the surface. There is generally an upward conduction of heat in the ice, except during the summer (Maykut 1985). Thus, C_L supplies much of the

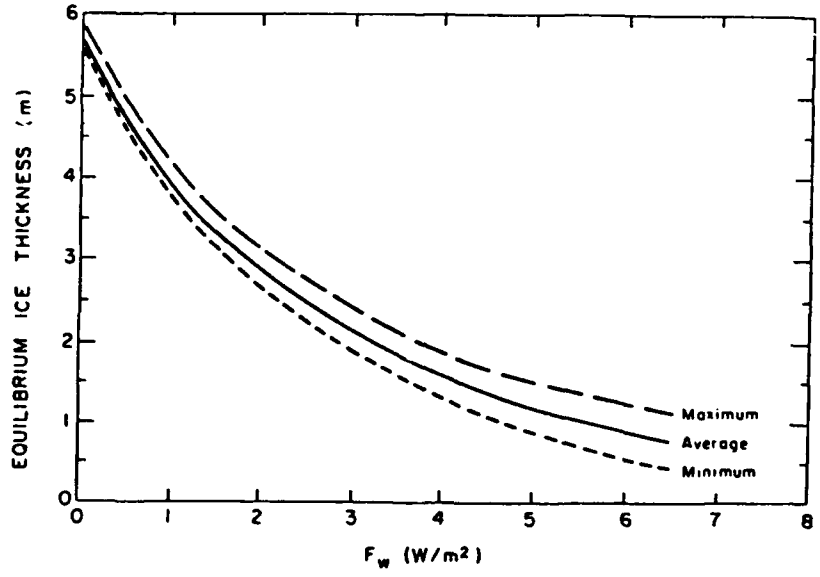

Figure 32. Equilibrium thickness of Arctic sea ice as a function of average annual oceanic heat flux (after Maykut 1985).

energy required to balance the substantial longwave radiation loss at the surface. It should be noted that C_u is equal to the sum of C_L and the latent heat associated with mass changes in the ice surrounding brine pockets. The conductivity flux at the surface (C_u) couples the lower and upper surface energy balances and is the sum of the heat input from the ocean, the net annual latent heat released by ice growth, and stored solar energy. Maykut (1985) estimates C_u to be about 8.8 W m^{-2} in perennial ice on an annual basis. In thin ice the heat conducted to the surface is 2 to 3 times that in perennial ice.

The oceanic heat flux, F_w, is a very important component of the energy exchange. This flux is estimated to be 2 W m^{-2} in the central Arctic on an annual basis (Maykut 1985). The primary source of this heat in the central Arctic Basin is primarily the input of solar radiation directly into the upper layer of the ocean through leads and very thin ice. In the marginal ice zone of the Fram Strait where warmer Atlantic waters make up a major component of the surface layer, the oceanic heat flux can be as high as 40 W m^{-2}. It is this northerly influx of oceanic heat that keeps the Norwegian coast ice free, for example. Maykut and Untersteiner (1971) carried out detailed numerical simulations of the growth and decay of sea ice over many seasonal cycles, examining in particular the effects of the various energy fluxes on the equilibrium thickness of perennial ice, which is reached after several annual cycles. Figure 32 shows the effects of average annual oceanic heat flux on the equilibrium thickness. The implication is that the radiative and turbulent heat exchanges are balanced so that small changes in the oceanic heat flux can make major differences in the ice thickness. For example, at average annual oceanic heat flux values exceeding 7 W m^{-2}, the simulations indicate that the Arctic ice cover would disappear in summer. A much more rigorous and detailed discussion of the energy fluxes and thermodynamic modeling is presented in Maykut (1986).

Thus far, the discussion on the thermodynamics of sea ice growth and decay has omitted discussion of a snow cover, except with regard to albedo changes. The existence of a snow cover on sea ice provides additional insulation from the atmosphere. Changes in the thickness of the snow layer can alter not only the growth rate of the ice but the energy exchanges over it as well. Maykut (1978) shows that the effects of snow cover on energy exchanges are particularly pronounced for young ice. The simulations of Maykut and Untersteiner (1971) showed, however, that the equilibrium ice thickness in the Arctic is not significantly affected until snow depths reach about 80 cm (Fig. 33). Snow, therefore, has two contrasting effects on thick ice: it delays summer ablation by restricting solar radiation input to the ice, and it retards winter growth by insulating the ice from the atmosphere. At snow depths ranging from 30 to 70 cm, the simulations showed that the net effect of snow was to hinder ice growth rather than retard ablation, thus slightly reducing equilibrium thickness. More than 80 cm of snow, however, acts to delay surface ice ablation until late summer when all snow has finally melted. At this late date in the annual cycle, however, the shortwave flux has been reduced to the point that minimal ice ablation occurs.

Snow thicknesses on Arctic sea ice appear highly variable. Thicknesses measured on floes in the Fram Strait (Tucker et al. 1987) ranged from 3 to 65 cm on multiyear ice and from 0 to 20 cm on first-year floes. While these thickness differences furnished a provisional means of distinguishing between first- and multiyear ice, the thicker snow covers on multiyear ice are not enough to significantly alter the equilibrium ice thicknesses according to the simulations.

In certain areas of the Arctic, however, ice reaches very great thicknesses. Walker and Wadhams (1979) believe that the combination of large snow depths and little or no oceanic heat flux accounts for floes over 6 m thick that may originate in restricted bays and channels of high-latitude islands in the Canadian Archipelago,

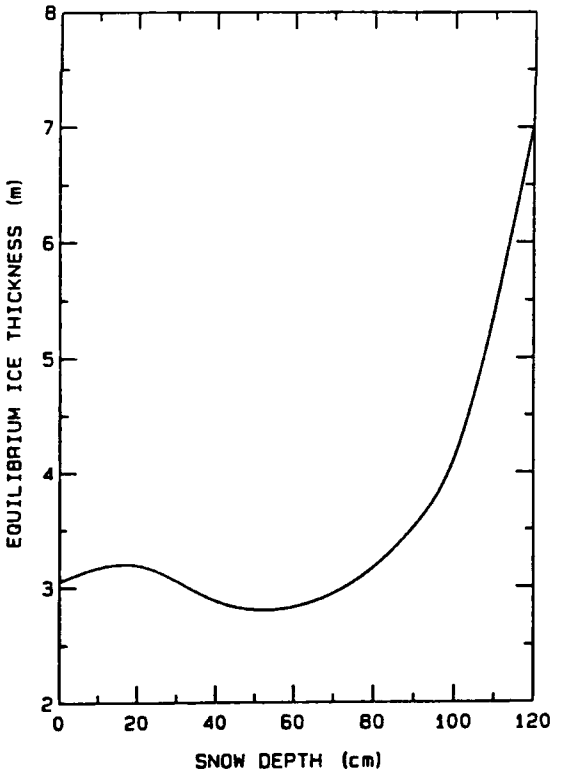

Figure 33. Average equilibrium thickness of perennial Arctic sea ice as a function of annual snow depth (after Maykut 1985).

for example. Using the Maykut and Untersteiner (1971) model, Walker and Wadhams (1979) demonstrated that ice grown under climatic conditions typical of the high Arctic but with zero oceanic heat flux and 1 m annual snowfall would eventually reach a thickness of at least 12 m.

The thermodynamic model calculations of Maykut and Untersteiner (1971) yield many other interesting results. The equilibrium thickness is most affected by parameters that influence the summer melting process. Besides the snow depth and oceanic heat flux, other critical factors include the air temperature, the surface albedo, the incoming radiation, and the turbulent exchanges that are manifested by surface roughness, temperature differences, and wind speed. The simulations indicate that the Arctic ice cover would completely disappear in summer if there were a 3–5°C increase in air temperature, a 25–30% increase in incident solar radiation, or a 15–20% decrease in albedo. A natural occurrence that would increase the incident shortwave radiation seems unlikely because it would almost certainly have to be caused by a dramatic decrease in cloudiness. The increased amounts of open water would, in turn, cause clouds and reduce the incident radiation. The possibility of an air temperature increase or a decrease in albedo is plausible, however. These could possibly be stimulated by large atmospheric CO_2 increases or large volcanic eruptions. These events would also be accompanied by ice–ocean–atmosphere feedback effects such as increased cloudiness, which must be carefully considered before speculating on the demise of the ice cover.

The simulations of Maykut and Untersteiner (1971) showed that the equilibrium thickness of undeformed Arctic sea ice is between 3 and 4 m. This predicted thickness is in general agreement with field observations of older undeformed multiyear ice. Once the equilibrium thickness is reached, the annual cycle shows that about 40 to 50 cm of ice ablates from the upper surface each summer and a similar amount accretes on the bottom side each winter. A newly accreted ice particle then, moves upward through the ice sheet at a rate of about 40–50 cm per year until it reaches the surface and melts. In reality, the surface of undeformed multiyear ice during summer also includes pools of meltwater that, early in the summer, may cover 60% of the ice surface (Maykut 1985). As the snow melts and melt ponds deepen, they occasionally penetrate completely through the ice. Eventually, the melt-pond coverage is reduced to 10-30%. Melt-pond coverage on smooth first-year ice may be much greater than on multiyear ice. With the onset of winter the ice surface exhibits an undulating appearance consisting of low level areas created by the frozen melt ponds and small rounded hummocks. Typical standard deviations in the thickness of undeformed multiyear ice have been found to be about 0.6 m (Ackley et al. 1976, Hibler et al. 1972a).

An important aspect of the energy exchange that has not been discussed is the solar radiation that passes through the ice into the underlying ocean. This energy is critical to biological activity beneath the ice and contributes to the heat balance of the upper ocean. In terms of the surface energy balance (eq 4), it is some portion of I that travels completely through the ice into the ocean. I is strongly affected by albedo in that the lower the albedo, the more shortwave energy is available to pass into and through the ice. As the energy passes through the ice, however, it is reduced by scattering and absorption. These processes are parameterized by an extinction coefficient. Theory and measurements indicate that the amount of shortwave radiation passing through the ice decays exponentially with depth. Perovich et al. (1986) indicated that lower albedos and reduced scattering occur as the ice warms, so more energy passes into the ocean. The converse is true during the ice growth season. For more complete treatment of the optical properties of snow and ice, the reader is referred to Grenfell and Maykut (1977) and Perovich et al. (1986).

Antarctic contrasts

Ice growth and ablation in the southern ocean is governed by the same energy fluxes as in the Arctic, but there are several factors that make for considerable differences in the nature of the sea ice in the Antarctic. Whereas the Arctic Ocean lies within a basin nearly surrounded by land masses, Antarctic sea ice occurs in an open sea that surrounds a continent. Close to the continent, cold katabatic winds can rapidly thicken ice, but at the open ocean boundary, marginal ice zone conditions exist, including any warmer air and ocean temperatures and wave action that tends to break up the ice cover into small floes. It appears that the largely unconstrained nature of the ice edge in the Antarctic allows far more vigorous wave action within the ice than occurs in the Arctic.

In general, most of the energy fluxes in the 60–70°S latitude band, where the majority of Antarctic sea ice is found, are similar to those fluxes found in the Arctic. Small differences occur in the shortwave radiation component due to latitude differences, and the turbulent exchanges may be larger because of generally higher wind speeds in the region. The most notable difference is in the oceanic heat flux. While it is generally accepted that the oceanic heat flux in the central Arctic is about 2 W m^{-2}, the average annual flux in many parts of the southern ocean (e.g., the Weddell Sea) may be as large

as 12 W m^{-2} (Gordon et al. 1984). The heat flux is much larger for specific periods. For example, values approaching 60 W m^{-2} are estimated to be required to account for the massive melt of ice that occurs from mid-November to mid-January (Gordon 1981). Allison (1981) reports values ranging from 0 to over 50 W m^{-2} depending on location and time of year for shorefast ice adjacent to coastal stations. It is believed that for offshore locations much of this heat originates from the flux into the surface layer of warmer water from below the pycnocline (Gordon 1981). A large amount of heat also results from the absorption of solar radiation in the mixed layer in leads and in the open ocean beyond the ice edge. In dynamic–thermodynamic model simulations of the Weddell Sea ice cover, Hibler and Ackley (1982) obtained generally reasonable agreement with observed ice extent, using only 2 W m^{-2} for the oceanic heat flux. The simulations demonstrated that much of the overall seasonal cycle of ice extent could be accounted for by a wind-driven dynamic–thermodynamic model. However, specific features in some regions of the Weddell Sea, such as the Weddell Polynya, were not well accounted for and these can likely be attributed to the large oceanic heat fluxes.

Antarctic sea ice is relatively free of surface melting, as evidenced by the obvious lack of surface melt ponds during summer (Andreas and Ackley 1982, Gow et al. 1987). This is believed to be due to increased latent heat losses from the ice to the atmosphere induced by lower relative humidities and higher wind speeds. The result is that, unlike the Arctic, surface-layer air temperatures must be significantly above 0°C for melting to begin. Air temperatures are normally less than 0°C over Antarctic sea ice. An important secondary effect is that the surface albedo remains high due to the lack of melt ponds and the persistence of the snow cover. Internal ice warming is retarded because most of the incident shortwave radiation is reflected. Recent data reported by Wadhams et al. (1987) indicate snowfall amounts over Antarctic sea ice that are comparable to those for the Arctic.

Model simulations to determine the thermodynamic equilibrium thickness of Antarctic sea ice have not been conducted. Whereas the ice drift patterns (discussed in the next section) prevent most Antarctic sea ice from reaching ages greater than 1–2 yr, it is fruitful to speculate on the "potential" equilibrium thickness. At certain locations adjacent to the continent where the oceanic heat flux is negligible, air temperatures are lower, and winds are stronger, first-year ice can reach thicknesses approaching 3 m, substantially exceeding the 2-m first-year thicknesses seen in the Arctic. In a recent midwinter research cruise that crossed a large part of the Weddell Sea, however, Wadhams et al. (1987) found the mean thicknesses of undeformed sea ice floes to be about 50–60 cm. Examination of ice cores revealed that many of these floes were composed of rafted pancakes and showed little evidence of new ice growth on the bottom side of the ice (Lange et al. 1988, Ackley*). The implication is that the equilibrium thickness of Antarctic pack ice would be less than that of the Arctic. Congelation growth at significant distances from the coast appears to be substantially retarded by the large oceanic heat flux.

A major component of ice sampled in the Antarctic has proven to be frazil. Recent observations by Clarke and Ackley (1982), Gow et al. (1987a), and Lange et al. (1988) have shown that 50–60% of all first-year and multiyear ice floes sampled in the Weddell Sea consisted of frazil. Similar studies of Arctic sea ice (Martin 1981, Tucker et al. 1987) have found only 5–20% frazil ice. As discussed previously, processes dominating frazil ice production are different from those that control the congelation growth of a stable ice sheet. The result is that, by whatever mechanism frazil is generated, it apparently accumulates and consolidates rapidly, thus making up for the ostensible reduction in congelation growth in the southern oceans. Gow et al. (1987a) report occasionally finding undeformed first-year floes more than 2 m thick that were composed substantially of frazil ice. Thus it is possible that reasonable thicknesses may accumulate very rapidly through the consolidation of frazil ice. Lange et al. (1988) believe that a most important mechanism may be the rapid thickening of the ice cover due to the rafting and consolidation of pancake ice. The rafted pancakes composed of frazil permit a reasonably thick ice cover to be established despite the large oceanic heat flux. A similar situation was observed in the Arctic during April 1987 in the southern Barents Sea (Gow and Tucker, unpublished), which has an open sea boundary on its southern periphery. It is not known whether this phenomenon is common in other seas bounding the Arctic Ocean.

Ice dynamics and drift

The momentum balance

In neither the polar oceans nor the peripheral seas is the pack ice stationary. Except for areas of landfast ice, the ice is in a state of nearly continuous motion and deformation that causes the formation of individual ice floes, leads, ridges, and rubbled ice as opposed to a continuous, unbroken ice sheet. The movement of ice and its subsequent deformation are caused by atmospheric and oceanic stresses acting upon the relatively

* S.F. Ackley, USACRREL, personal communication, 1989.

thin ice cover. The force balance for sea ice can be written as:

$$m \frac{d\vec{u}}{dt} = \vec{C} + \vec{\tau}_w + \vec{\tau}_a + \vec{F} + \vec{G} + \vec{T} \qquad (6)$$

where $\vec{u}$ is the ice velocity, m the ice mass per unit area, $\vec{C}$ the Coriolis force, $\vec{\tau}_w$ the water stress, $\vec{\tau}_a$ the air stress, $\vec{F}$ the force due to the variation of internal ice stress, $\vec{G}$ the force due to geostrophic currents, and $\vec{T}$ is the force attributed to the tilt of the ocean surface. The implementation of eq 4, 5, and 6 into numerical ice models has been discussed extensively by Hibler (1979, 1980, 1986) and Parkinson and Washington (1979). Here we will discuss aspects of the major components of the ice momentum balance.

Theoretical treatment and observations have verified that the dominant components of the force balance are the air and water stresses, the Coriolis force, and the ice interaction (internal ice stress variation). Hibler (1986) estimates that the air and water stresses typically vary about a value of 0.1 N m^{-2}, whereas the Coriolis force is about half this value. In an analysis of ice station and automatic data buoy drifts in the Arctic Basin, Thorndike and Colony (1982) were able to account for 70% of the variance of the ice velocity using the geostrophic wind alone. It has been well known for many years that much of the ice drift far from shore could be explained solely from winds (Nansen 1902, Zubov 1943).

The ice interaction, $\vec{F}$, is the result of the ability of the ice pack to transmit stresses over considerable distances. The effect of internal ice stresses is made readily apparent to an observer by the fact that in enclosed areas such as bays and fiords the ice does not move under high wind or current forcing. This indicates that F is at least as large as the wind and water stress terms. Having knowledge of the other terms in eq 6, F can be calculated as a residual of the force balance. One such example (Fig. 34), with the ice interaction calculated as a residual of other components, was measured by Hunkins (1975). It is easily ascertained that F may not be ignored except in cases where the ice concentration is so low that the large-scale (covering many floes) ice strength approaches zero and the ice is unable to transmit stress. Much effort has been invested in properly accounting for F in numerical models of sea ice. Hibler (1986) provides a comprehensive review of the incorporation of the ice interaction into numerical models.

The total derivative of ice velocity, $d\vec{u}/dt$, is composed of a local time derivative of velocity plus a momentum advection term. The local ice acceleration is usually very small and can generally be ignored in numerical simulations of ice drift. The term can be

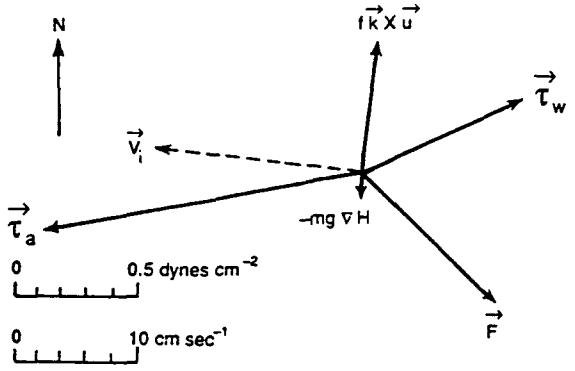

Figure 34. Estimate of the force balance on sea ice for winter conditions based on wind and water stress measurements. $\vec{V}_i$ is the ice velocity, $\vec{\tau}_a$ the air stress, $\vec{\tau}_w$ the water stress, fk × u the Coriolis force, $-mg\nabla H$ the force due to ocean tilt and geostrophic currents, and $\vec{F}$ the internal ice stress, which is determined as a residual (after Hunkins 1975).

significant during periods of low ice concentration when the ice interaction is minimal, however. McPhee (1980) showed that inertial oscillations that result from changing directions of the ice motion are a significant part of summer sea-ice motion. The momentum advection term is almost always negligible because relatively large velocity changes would be required to generate a substantial force (Hibler 1986).

The force balance diagram (Fig. 34) indicates that the geostrophic current and ocean tilt terms (combined as $mg\nabla H$) are relatively small. This is a result of generally small currents beneath the polar pack ice. Hibler and Tucker (1979) demonstrated that the effects of currents in the central Arctic Basin are small over time periods of a few days, but that long-term effects are important because some of the long-term effects of winds average out the short-term fluctuations. Very recently, Moritz and Colony (1988) pointed out that currents actually dominate the ice drift in the Fram Strait, and Pritchard (1988) has found similar results in the Bering Sea. Currents are particularly important in shallow areas where barotropic effects may be significant.

Ice circulation in the Arctic and the Antarctic

As mentioned previously, the motion of sea ice at some distance from shore is primarily wind-driven. This tends to be the general case in both the Arctic and Antarctic. Until recently, techniques for predicting the drift of ice used the forecast geostrophic wind as the sole external parameter. Zubov (1943) established the well-known rule-of-thumb that ice drifts parallel to the sea-level pressure isobars (usually about 20° to the right of the surface wind in the Northern Hemisphere) at about

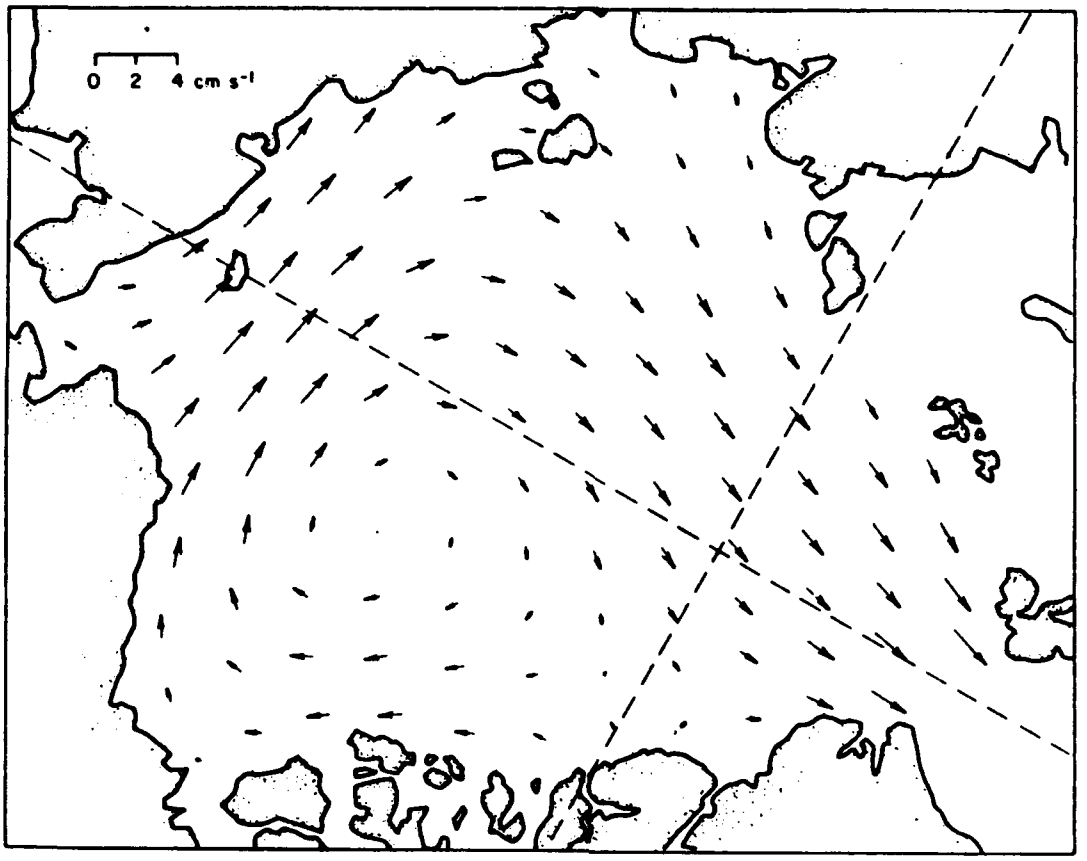

Figure 35. Mean field of ice motion interpolated spatially and temporally from manned ice stations and automatic data buoys (after Colony and Thorndike 1984).

2% of the geostrophic wind speed.

Two dominant features of the ice circulation in the Arctic Basin were first described by Gordienko (1958). These are the Beaufort Sea Gyre, a clockwise circulation pattern in the Beaufort Sea, and the Transpolar Drift Stream, a basin-wide feature that transports ice from the western to the eastern side of the basin. Both are manifestations of the mean sea-level pressure field, which indicates a large high pressure area over the Beaufort Sea and with isobars over the remainder of the basin generally running west to east. Recently, Colony and Thorndike (1984), using an analysis of ice station and drifting buoys spanning many years to estimate the mean field of sea-ice drift (Fig. 35), found that the Beaufort Gyre is much less pronounced than previously thought. The gyre covers the entire western portion of the basin, including not only the Beaufort but substantial parts of the Chukchi and East Siberian seas. Further, the Transpolar Drift is not well established although, as Figure 35 shows, there is still a trend of the ice to drift towards Fram Strait. It must be emphasized that the figure shows the mean motion and that large excursions from this motion frequently occur. Mean velocities are about 2 km day^{-1}, but the standard deviations, which describe the fluctuating component of the velocities, are much larger (ca. 7 km day^{-1}, according to Colony and Thorndike 1984). The ice can also remain motionless for weeks at a time, and McLaren et al. (1987) have suggested that gyre reversals may be common in the summer.

As a result of this circulation pattern, individual ice floes can remain in the basin for many years. For example, manned ice-island stations have circulated around the basin for decades. Stochastic model calculations by Colony and Thorndike (1985), where short-term drift observations from buoys were used to predict statistics of drift over long time periods, indicate that ice floe residence times of 5–7 years in the Arctic Basin are common. These long residence times result from the fact that there is only one major outflow area for the Arctic Basin (Fram Strait). Relatively little ice leaves the basin through other exits such as the Bering Strait or the Canadian Archipelago. On an annual basis about 10% of the ice cover in the basin flows out through the Fram Strait (Maykut 1985). Upon entering the Fram Strait and the Greenland Sea, southward-flowing drift

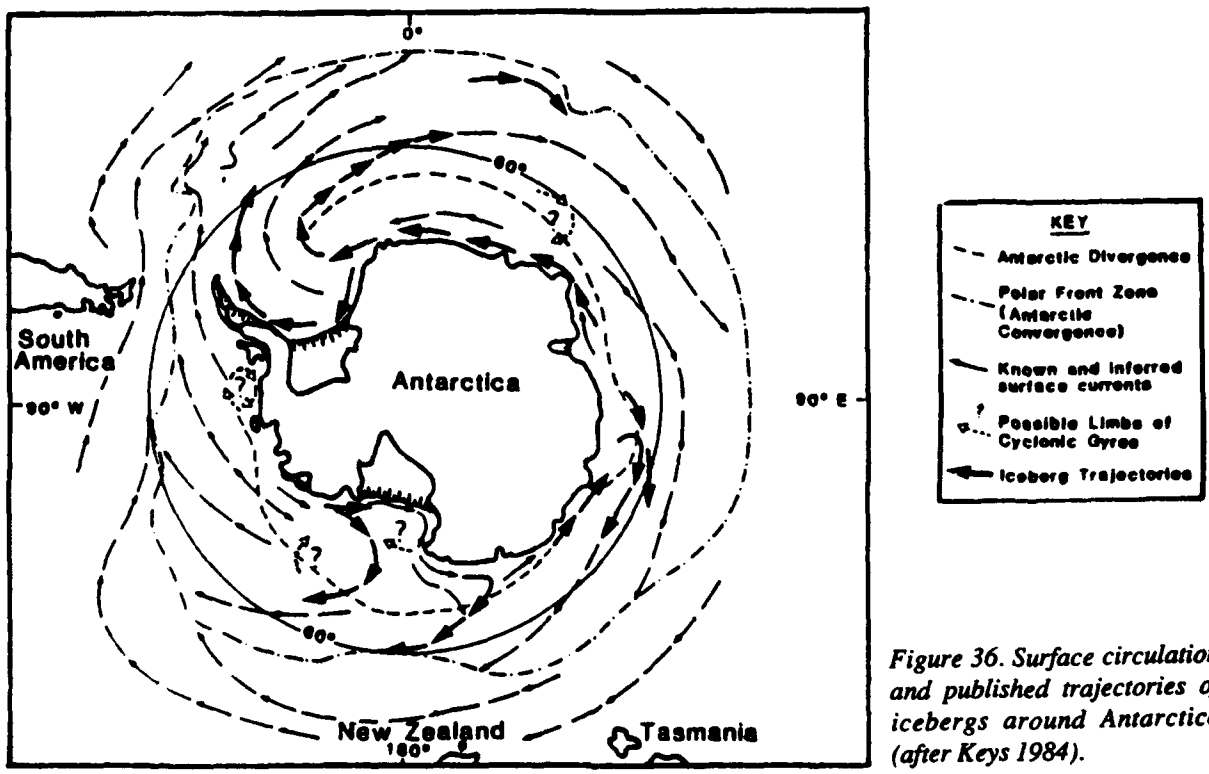

Figure 36. Surface circulation and published trajectories of icebergs around Antarctica (after Keys 1984).

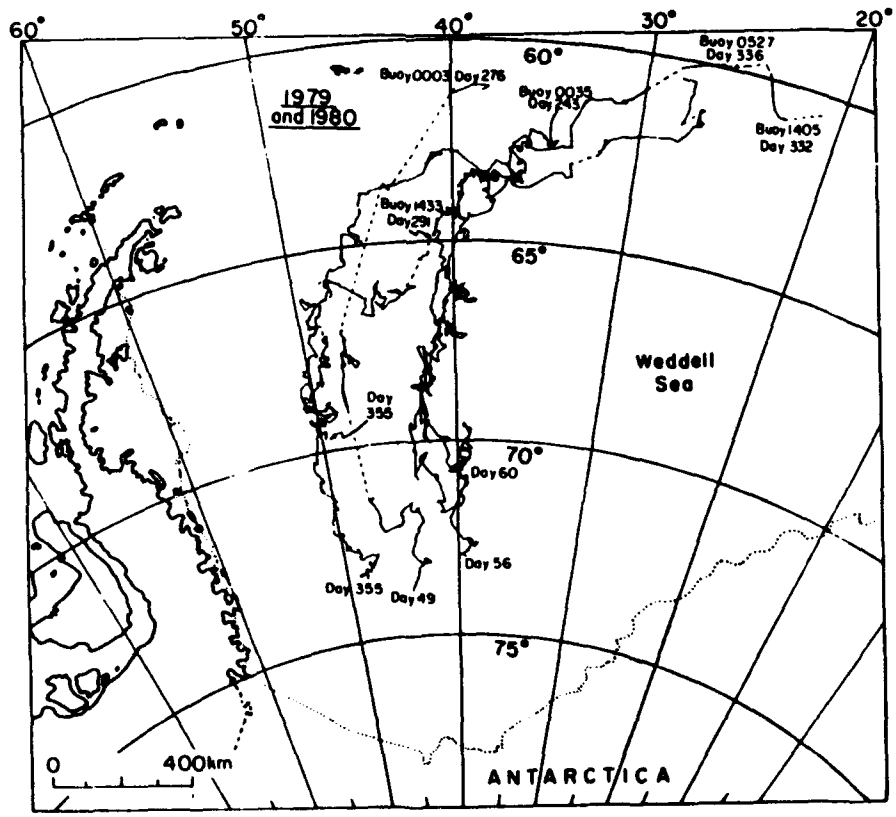

Figure 37. Drift tracks of automatic data buoys in the Weddell Sea during 1979 and 1980 (after Ackley and Holt 1984).

velocities increase to about 15 km day^{-1}. Similar drift rates have been observed in the Bering Sea as the first-year ice is "conveyored" southward to the ice edge, where it melts (Pease 1980, Reynolds et al. 1985).

Much less is known about the movement of ice in the Southern Ocean (Fig. 36). Major features of the drift are the Antarctic Circumpolar Current, which transports ice clockwise around the continent, and the East Wind Drift, which flows in the opposite direction immediately adjacent to the continent. This coastal flow is directed north by protrusions of the continent in the Weddell and Ross seas. The ice contained within the northward flow joins the Circumpolar Current, which transports it into warmer water that eventually melts it.

Figure 37, showing tracks of drift buoys that were placed deep in the southern Weddell Sea (Ackley and Holt 1984), demonstrates the characteristic northward flow along the Antarctic Peninsula. These tracks imply that residence times of sea ice in the Weddell Sea are short relative to those of ice in the central Arctic. All buoys completed their northward journeys in less than a year, emphasizing the extremely short residence times in the Antarctic.

Keys (1984) estimates that multiyear ice is limited to about 10–15% of the total area of Antarctic sea ice. This contrasts sharply with the 70–80% estimate of multiyear ice in the central Arctic basin by Koerner (1973) and the estimate of 75% multiyear ice exiting from the Fram Strait during June and July 1984 (Tucker et al. 1987). What is implied is that except for ice that remains in isolated bays and coves, sea ice in the Antarctic is rarely more than two years old. Because of the generally thinner ice cover in the Antarctic, along with generally higher wind speeds, drift rates could be expected to be somewhat larger than those for Arctic sea ice. Ackley (1981) found that drift rates exceeding 20 km day^{-1} were common in the Weddell Sea, and Keys (1984) reported similarly high rates for the Ross Sea. Mean ice velocities would, of course, be much less because of fluctuations in direction and speed of the wind.

Morphological ice features

Leads and polynyas

The continuous motion of sea ice combined with ongoing growth and ablation processes causes a variety of ice types to exist within areas on the scale of a few kilometers. Diverging motions cause the ice to pull apart and form leads, allowing the ocean to come into direct contact with the atmosphere. During winter, in the absence of further motion, the leads rapidly refreeze and thicknesses of up to 10 cm can be attained in less than one day.

Leads are relatively small linear features, usually tens to hundreds of meters wide and up to several kilometers long. Polynyas are large nonlinear openings in the ice that tend to recur at the same locations or become semipermanent features. Polynyas can occur adjacent to coastlines where shearing or divergence of the pack ice acts to move the ice away from the coast. For example, such features occur on the southern side of St. Lawrence Island in the Bering Sea and at locations along the east coast of Greenland. Other polynyas are the result of oceanographic influences such as upwelling. A particularly noteworthy polynya of this nature is the Weddell Polynya, a large area of open water occasionally observed in the eastern Weddell Sea. Leads and polynyas are significant because they are sources of very large heat losses to the atmosphere. During winter, leads and polynyas constitute the major source of new ice production and subsequent salt fluxes to the upper ocean. In summer, when new ice growth is not taking place, small leads often develop into major open water areas and allow shortwave radiation to be absorbed by the upper ocean, which further stimulates ice ablation. Under such conditions the concept of leads becomes increasingly vague. Leads generally refer to the linear features developing in compact ice, whereas during the melt season there is a changing mixture of floes and interconnected areas of open water rather than leads per se. For this reason we usually characterize a summer ice pack by its concentration, i.e., the fractional area covered by ice.

The amount of open water in the central Arctic during winter is estimated to be about 1% (Wittmann and Schule 1966, Maykut 1985). During summer the amount of open water increases to 10–20%. In marginal ice zones, where divergence and melting are taking place, the percentages of open water can be so large that defining the ice boundary becomes very difficult.

By virtue of its open ocean boundary, the ice-covered ocean surrounding Antarctica has significantly larger marginal ice zones than the Arctic and therefore is expected to have higher percentages of open water. Zwally et al. (1983), using satellite passive microwave observations, have estimated that the ice concentration over most of the year averages between 60 and 80%. This may be accurate for the outer regions of the pack, but recent field observations indicate that ice concentrations are higher in the interior regions, similar to those in the Arctic pack*. There is usually more open water in the Antarctic pack ice than in the Arctic because of the relatively larger area of marginal ice zone and greater divergence in the ice produced by a significant northward component in the wind and ice velocity fields.

* S.F. Ackley, USACRREL, personal communication, 1989.

Ice roughness

While this section deals primarily with large-scale roughness features such as ridges and rubble fields, smaller-scale features are worth pointing out because of their importance to the air and water stress. On the surface, scales of roughness on the order of centimeters result from variations in freeboard levels of contiguous ice floes of different thicknesses. In the MIZ, the exposed vertical sides of many broken floes, although exhibiting reliefs of only tens of centimeters, give rise to larger wind stress drag coefficients than are observed in the central Arctic, where larger ridges occur. Other small-scale roughness on the surface is caused by the formation of pancake ice with the raised edges surrounding each pancake, by the fracture and rafting of thin ice, and by the densely packed wind-blown snow features known as sastrugi.

On the bottom side of the ice, differences in floe thickness cause variations in ice draft from a few millimeters to several meters. One important small-scale roughness element is a consequence of ice growth. As described in the first section, the freezing of seawater causes brine to be rejected from the growing ice interface, which develops a dendritic structure consisting of platelets of pure ice protruding downward into the seawater. The individual platelets, spaced about a millimeter apart, create small roughness elements that contribute to the water stress and the amount of mechanical mixing in the water column. During the melt season, these platelets are completely ablated, leaving a much smoother surface.

The major roughness features of a sea ice pack are caused by deforming ice that is manifested in the form of rubble fields or individual ridges. These features are

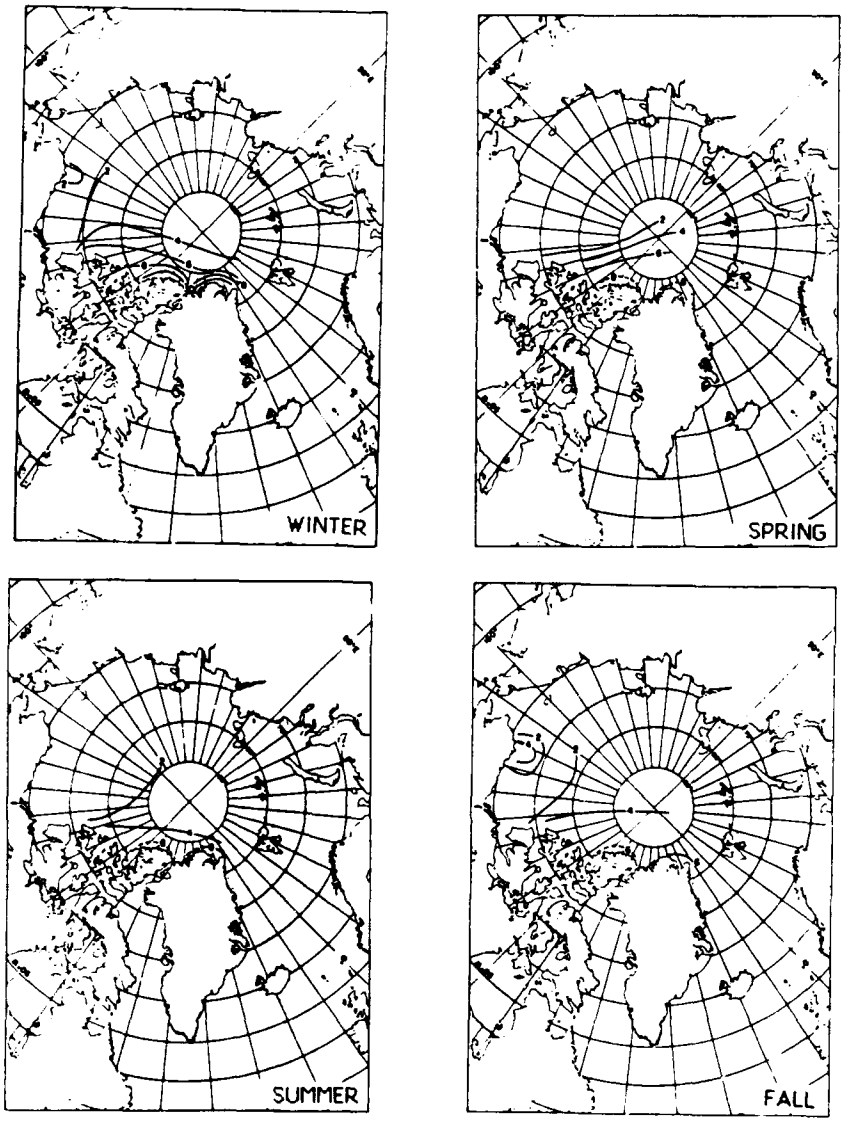

Figure 38. Contours of ridge sail frequency (number of ridges per km greater than 1.22 m high) for the four seasons (after Tucker and Westhall 1973).

formed by compression and shear that result from converging ice, in contrast to divergence, which creates leads. Many ridges are indeed long linear features sometimes several kilometers in length but only tens of meters wide. However, as Rothrock (1986) points out, ridges frequently overlap due to repeated ridging events, forming piles of rubble that are difficult to characterize quantitatively. Therefore, using only single ridges to define the volume of deformed ice may lead to substantial errors.

It is the thin ice that most often deforms, simply because it has considerably less strength than older first-year or multiyear ice. However, if no thin ice is present and the driving forces are sufficient, thick ice may also deform. This was shown by field investigations of Tucker et al. (1984b), who found many pressure ridges containing ice blocks more than 1 m thick. In addition, there have been numerous unpublished reports of ridges containing blocks 3 and 4 m thick.

When an ice sheet deforms under compression, the ice blocks, broken by bending and buckling, are piled above and below the surface. The above-surface portion is called the sail, and the below-surface portion is called the keel. Sail heights and thus keel depths appear to be limited by the thickness of the deforming ice (Tucker et al. 1984b). Pressure-ridge modeling by Parmerter and Coon (1972) shows that for ice of a given thickness, strength, and modulus, there is a limiting height to which a ridge can build; further compression of the ice results in a rubble field that stabilizes at the limiting height. The ridge mass as a whole should tend toward isostatic equilibrium, so we might expect a general relationship between sail heights and keel depths. Indeed, drillings through ridges indicate that the ratio of keel depth to sail height in first-year ridges is about 4.5:1 and in multiyear ridges is about 3.3:1 (Kovacs 1983). The consolidation of the ridge through the freezing of water-filled voids and subsequent isostatic adjustments is partly responsible for the reduction of the keel-to-sail ratio as the ridge ages. In addition, ablation during summer tends to round both the top and bottom surfaces of ridges.

Ridges and rubble fields are particularly important because they account for a large portion of the total ice mass. Williams et al. (1975) estimate that ridges account for about 25% of the total Arctic ice mass, and in heavily ridged regions this amount can reach 50%. Wadhams (1980a) found about 40% of the total ice cover in the central Beaufort Sea was composed of ridged ice.

Quantitative data on ice topography has evolved from two sources. Airborne laser profiles have provided thousands of kilometers of sea-ice surface topography, and upward-looking sonar mounted on submarines has provided the ice bottom relief. Because of the inherent aircraft motion, analysis of the laser data has been restricted to the counting of ridges. The sonar profiles, on the other hand, provide ice draft to a relatively high degree of accuracy. This is particularly useful because isostasy dictates that draft should be about 90% of the thickness, thereby allowing estimates of the total thickness to be made from draft measurements alone. Rothrock and Thorndike (1980), however, warn that using only ridge counts from sonar profiles to estimate amounts of deformed ice may lead to serious underestimates because much deformed ice is found at scales smaller than would fit the specification of a ridge as defined in a computer algorithm.

Studies using laser and submarine profiles have clearly delineated regional and seasonal variations in ice morphology (Fig. 38). Histograms of the mean keel depths for various seasons and regions in the Arctic (Fig. 39) indicate that ridging is significantly heavier in some regions. There is little doubt that more ridges are

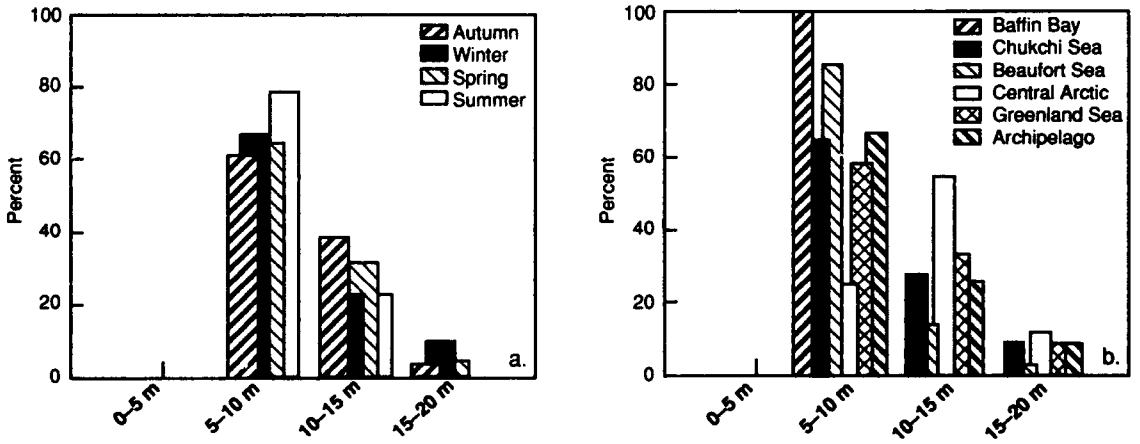

Figure 39. Distribution of mean ridge keel depths for (a) the four seasons, and (b) various Arctic Ocean subregions (after Bourke and Garrett 1987).

found in spring and winter, and that regionally heavier ridging occurs to the north and west of the Canadian Archipelago. The heavier ridging in this region is the result of ice motion toward the shore. Considerable year-to-year variations in ridging have also been observed. For example, Tucker et al. (1979) saw significant interannual variations in ridging intensity at Alaskan coastal locations. Similarly, McLaren (1989), in an analysis of two corresponding submarine tracks across the Arctic Basin, found more severe ice conditions in 1958 than in 1970. Year-to-year variations are not surprising in that we should expect variability in the environmental parameters that govern ice growth, drift, and decay.

There are very little data on deformational features in the Antarctic ice pack, although one recent study by Weeks et al. (1988) has made use of airborne laser profiles to contrast winter and spring ridging in the Ross Sea with selected Arctic locations. A brief synopsis of the ridging statistics is shown in Table 1. The mean ridge height in the Ross Sea is less than at all Arctic locations, and there are also less ridges in the offshore Ross Sea than for comparable Arctic locations. The less severe ridging statistics for the Ross Sea are clearly the manifestation of the open boundary conditions in the Antarctic and the fact that thinner ice is being ridged. Although no similar data are available for the Weddell Sea, it is suspected that more deformed ice may exist in that region.

Statistical models have been developed to describe the distributions of heights and spacings of ridges (Hibler et al. 1972b, 1974; Wadhams, 1980b, 1981; Wadhams and Horne 1980; Wadhams and Davy 1986). A comparison of the distributions is presented by Wadhams (1984). The distributions generally take the form of a negative exponential or log normal. All have coefficients that can be determined from the mean ridge height or spacing. The models indicate that the height and spacing distributions can be described adequately with only minimal input parameters.

Table 1. Ridging parameters from the Ross Sea compared to data from Arctic locations for winter and early spring. Parameters were obtained from laser profilometer data (data from Weeks et al. 1988).

Location	*Ridges (km)*	*Mean ridge height (m)*
Ross Sea		
Coastal	6.8	1.25
Offshore	1.9	1.21
Central Beaufort Sea	2.6	1.47
Beaufort/Chukchi shear zone	4.4	1.51
West Eurasian Basin	4.7	1.50
North Greenland	8.2	1.68

Ice thickness distribution

Once a sea ice cover is established, its most significant attribute is its thickness. We have discussed the deformation of the pack ice that causes the formation of very thick ridges as well as leads. Subsequent growth in leads produces new ice. Thus the combination of dynamic and thermodynamic processes causes a variety of ice thicknesses to coexist at any given time within relatively small areas (< 1 km). These same processes also cause the thickness within that area to change constantly.

The distribution of ice thicknesses profoundly affects the atmosphere–ocean exchanges of heat, moisture, and momentum. The thickness distribution determines the regional ice strength, thereby affecting the future role of ice dynamics within the region. Knowing the distribution of ice thicknesses within a region allows us to couple dynamic and thermodynamic processes, and so to estimate regional scale quantities such as the heat and moisture exchanges and salt and solar input to the upper ocean (Maykut 1982). At present, there are no means by which the thickness distribution within a region can be continuously monitored. A theoretical framework for estimating the thickness distribution from available data has been developed (Thorndike et al. 1975). This formulation and a two-thickness-level approach developed by Hibler (1979) are especially suited for inclusion into dynamic–thermodynamic sea ice models.

The essence of the preceding discussion has been to point out the importance of the ice thickness distribution and to make note of the fact that for any area the thickness distribution is constantly changing. However, there are large-scale regional differences in mean thicknesses due to such effects as proximity to a coastline or near-continuous divergence. The following discussion briefly examines available data concerning aspects of large-scale ice thickness of the Arctic and Antarctic.

The few submarine sonar profiles that have been analyzed provide information on the variability of thicknesses in the Arctic Basin. Thickness can be inferred reasonably well from these profiles of ice draft because, as mentioned earlier, about 90% of the thickness is below sea level. Figure 40 shows a probability density function (PDF) plot of ice drafts collected along 400 km of submarine track in April 1976. The ice draft distribution of this transect is bimodal. The small, distinct peak evident in the 0–1.0 m range is indicative of young first-

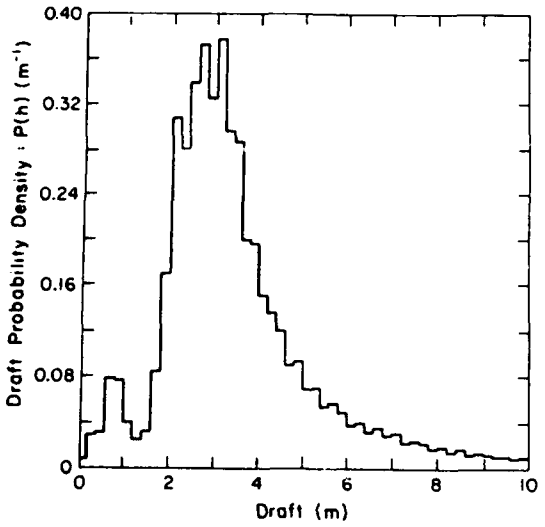

Figure 40. Probability density function of ice draft from 400 km of submarine track in the Beaufort Sea (after Hibler 1980; data from Wadhams and Horne 1980).

year ice evident in winter and spring, whereas the larger peak centered at about 3.0 m would indicate undeformed multiyear ice, with a potential contribution from deformed first-year ice. The tail of the distribution is due to deformed multiyear and first-year ice. It is clear that deformed ice constitutes a large portion of the total ice mass represented by this PDF.

Estimates of the mean thickness and standard deviation of the ice within the Arctic Basin have also been derived from the submarine data (Hibler 1979, LeShack 1983, Bourke and Garrett 1987). Figure 41 shows mean drafts for the summer and winter seasons as compiled from data analyzed by Bourke and Garrett (1987). Clearly delineated in these figures are the extremely thick ice areas to the north of Greenland and west of the Canadian Archipelago. Obviously, it is the severe deformation that occurs in these areas that produces such large mean drafts. An artifact in the analysis, caused by the fact that only ice-covered areas were used in the mean draft calculations (i.e., areas containing open water were deleted), is that the mean draft in the area near the North Pole is larger in summer than winter. Thus in summer, when little thin ice is present, the mean drafts are biased by the surviving deformed and thick ice. Clearly, estimates of mean draft or thickness should be used with caution.

As with other data regarding ice conditions in the Antarctic, there is a dearth of information on the thickness distribution. The most comprehensive information has evolved from a recent midwinter cruise across the eastern Weddell Sea (Wadhams et al. 1987). The PDF for the entire cruise, consisting of over 4400 individual drill holes (Fig. 42), has a single mode between 50 and 60 cm as the dominant thickness. Wadhams et al. (1987) stated that the PDF seriously underestimates the contribution of ridges and deformed ice to the distribution because they were not often sampled. However, the undeformed ice thicknesses are much less than thicknesses of undeformed ice in the Arctic (see, for example, Fig. 40). With less ridging and relatively little multiyear ice, it is safe to assume that ice thickness in the Antarctic will be considerably less than in the Arctic even when the deformed ice contribution is included. Other thickness data from the Weddell Sea obtained from ice-coring investigations (Gow et al. 1987a) indicate that thicknesses of some undeformed floes exceeded 4 m. Keys (1984) states that thicker first-year ice is present in the Ross Sea, occasionally reaching thicknesses exceeding 2 m, but time- and space-averaged thicknesses are probably 1–2 m. He also states that multiyear ice is uncommon in the Ross Sea.

Ice extent and zonation

The most important aspect of the sea-ice cover in both the northern and southern hemispheres is the seasonal variability in ice extent. The ice cover experiences large variations in extent because it is an extremely thin layer in comparison to the large area that it covers. Thus, small changes in climate (including seasonal changes) and oceanic heat transport can cause major changes in the extent of the ice cover. Such changes can significantly alter heat and momentum exchanges between the ocean and atmosphere over large areas.

The extent of ice in the Arctic reaches a minimum of about 7×10^6 km^2 in late August or early September (Fig. 43). At its maximum in late February or March, the area is doubled, covering about $14–16 \times 10^6$ km^2 (Walsh and Johnson 1979, Parkinson et al. 1987). During summer, the ice is essentially confined to the Arctic basin with small extensions reaching into the Greenland and Barents seas and the Canadian Archipelago. At its maximum, the ice extends far to the south along continental boundaries in many of the adjacent seas. The most southerly extensions of the ice pack occur in the Labrador Sea and the Sea of Okhotsk, where the ice reaches as far south as 45°N in both seas. As might be reasoned, these areas (as well as the Bering Sea, Baffin Bay, and Davis Strait) contain primarily first-year ice.

In an analysis of the fluctuations of Arctic sea ice extent, Walsh and Johnson (1979) detected a slight asymmetry in the average rate of advance and retreat of the ice edge. Their findings showed that the growth period proceeded slightly more rapidly than the decay period. In contrast, though using a less extensive data

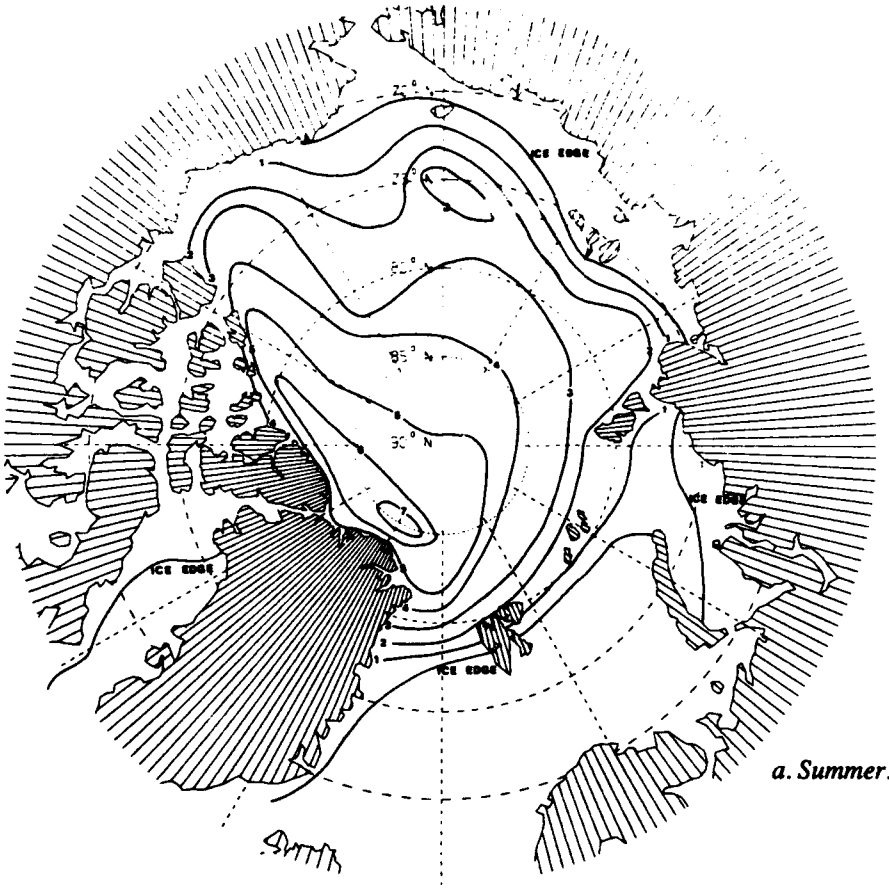

a. Summer.

Figure 41. Mean ice draft derived from submarine tracks (after Bourke and Garrett 1987).

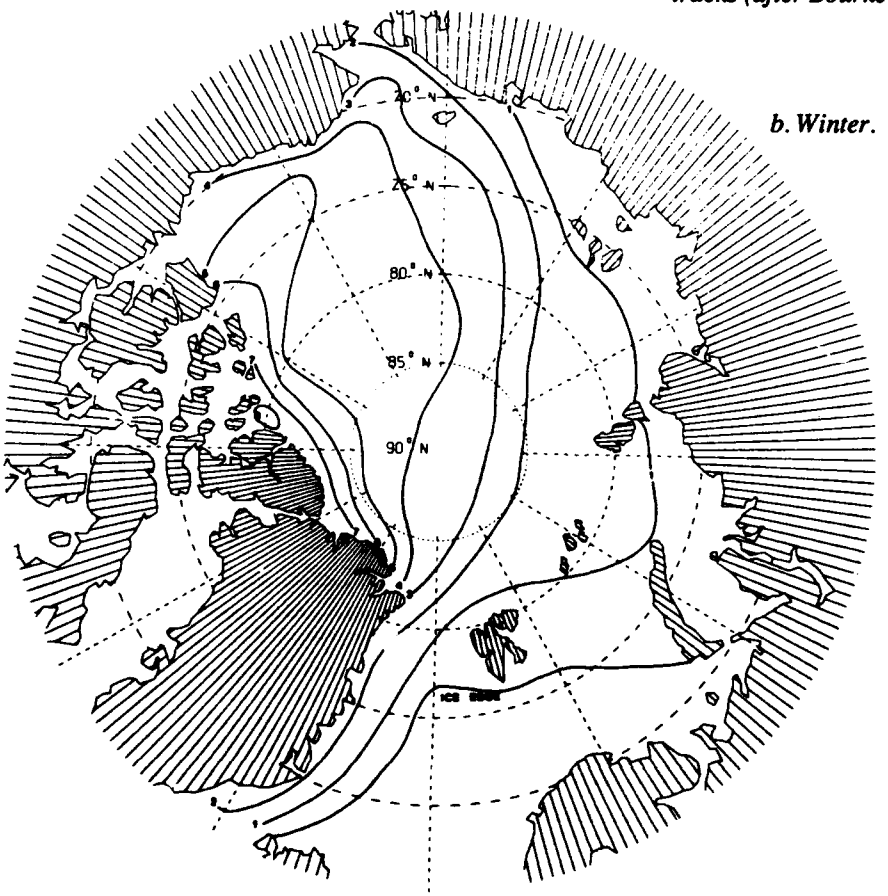

b. Winter.

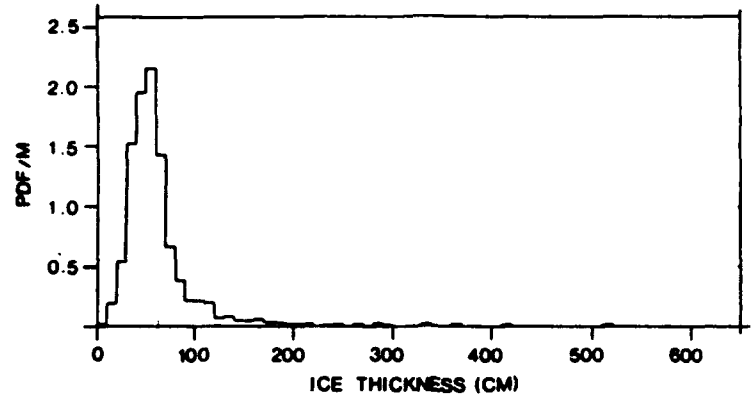

Figure 42. Probability density function of ice thickness derived from 4400 drill-hole measurements made during winter in the Weddell Sea (after Wadhams et al. 1987).

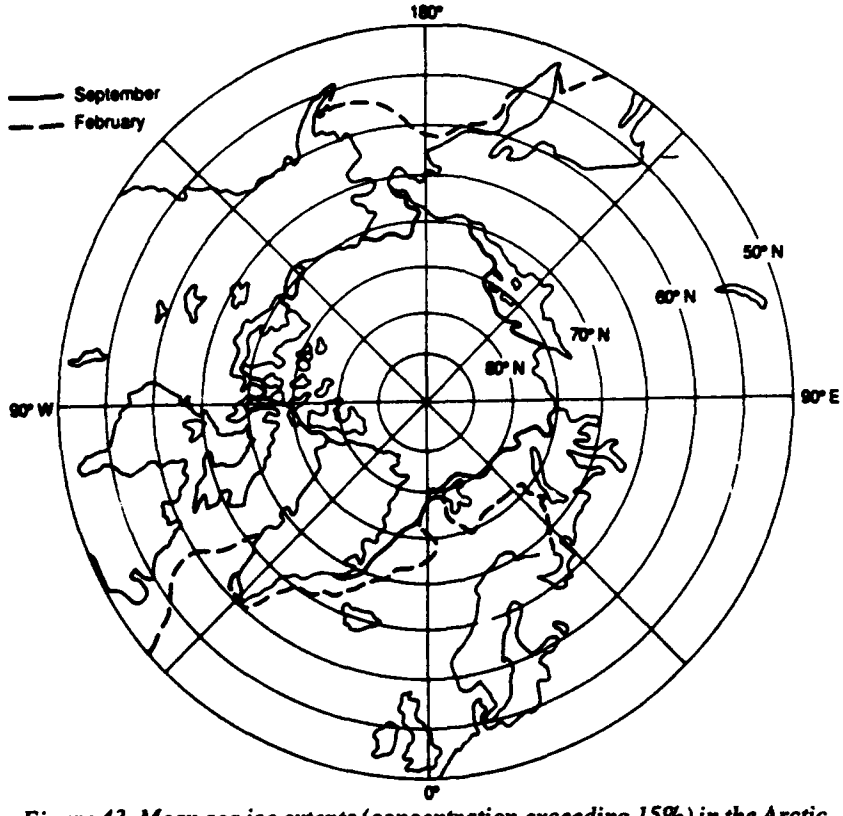

Figure 43. Mean sea ice extents (concentration exceeding 15%) in the Arctic for the months of February and September averaged for the years 1973–1976. Extents were determined from the Electrically Scanning Microwave Radiometer (ESMR) on the NIMBUS 5 satellite (adapted from data presented by Parkinson et al. 1987).

set, Parkinson et al. (1987) determined that the growth and decay cycles were nearly symmetrical. Walsh and Johnson (1979) and Parkinson et al. (1987) both found substantial departures from normal of both monthly and yearly Arctic sea ice extent. These fluctuations indicate the extreme sensitivity of the ice cover to external forcing.

The seasonal variation of ice extent in the Antarctic is far greater than that of the Arctic (Fig. 44). Minimum extent is reached in February, when the total coverage is approximately 4×10^6 km^2, about half of the minimum coverage of Arctic ice. Maximum coverage of about 20×10^6 km^2 occurs in September. The ice cover at maximum extent represents a five-fold increase over

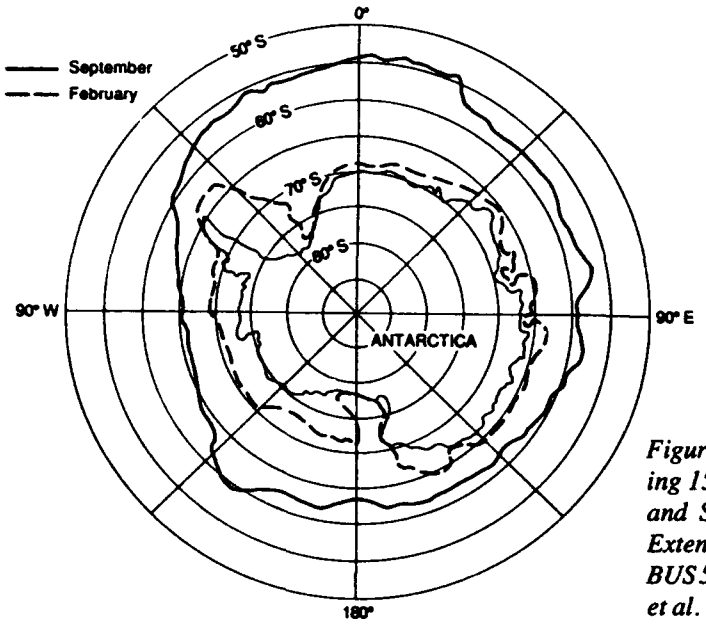

Figure 44. Mean sea ice extents (concentration exceeding 15%) in the Antarctic for the months of February and September averaged for the years 1973–1976. Extents were determined from the ESMR on the NIMBUS 5 satellite (adapted from data presented by Zwally et al. 1983).

the minimum extent and is about 25% larger than the Arctic ice extent maximum. In contrast to the relatively symmetric ice advance and retreat in the northern hemisphere, the spring and summer decay of the Antarctic ice cover occurs much more rapidly than the fall and winter expansion (Zwally et al. 1983). Gordon (1981) suggests that atmospheric heating is not sufficient to account for the rapid decay and implies that the upwelling of warmer deep water may provide a large contribution to the decay process. As with the Arctic, significant monthly and annual departures from normal ice extent have been observed (Zwally et al. 1983).

The differences in seasonal ice extent between the Arctic and Antarctic are due, in large part, to the distribution of the polar land masses. The Antarctic continent is generally contained poleward of 70°S, and the sea ice cover forms in the ocean surrounding the continent. The northernmost ice extent occurs in the Weddell Sea, with the maximum extent in other Antarctic oceans generally being confined poleward of 60°S (Fig. 44). The seasonal sea ice zone (SSIZ), that area between the minimum and maximum extent, is very large. However, even at maximum extent, the ice cover is confined to a relatively narrow annulus around the continent; its northward progression is hindered by the warmer ocean and atmosphere. The perennial ice zones where the limited amounts of multiyear ice exist are located in the Weddell Sea and adjacent to the continent in other Antarctic seas.

In the Arctic, the area north of 70°N is a landlocked ocean basin that essentially remains ice-covered throughout the year. Thus, there are large amounts of multiyear ice in the Arctic Basin. During winter, cold air flowing from the adjacent continents allows the ice cover to extend far to the south in some locations, particularly in the Sea of Okhotsk, the Labrador Sea, and the Greenland Sea. In contrast, warm Atlantic water flowing north keeps the southern Barents and Norwegian seas ice-free throughout the year. Therefore the land masses serve to direct the atmospheric and oceanic heat flow, which in turn controls ice extent in the SSIZ of the Arctic. In the marginal ice zones (MIZ), ice conditions and concentrations can vary dramatically as a result of complex interactions between the atmosphere, ice, and ocean. The role of ocean waves in floe breakup is significant for tens of kilometers inside the ice edge. This mechanical breakup greatly expedites the decay of the ice cover in the MIZ.

Shorefast ice zones are located against coastal boundaries. Fast ice is made relatively stable by anchoring itself to the shoreline and to the sea bottom in shallow areas. Pressure ridge keels and multiyear floes that have become grounded in the shallow water also act to stabilize the fast ice. It is in these stable, shallow areas that the largest thicknesses of undeformed first-year ice can accumulate because the shallow water cools to the freezing point early in the growth season. Widths of the fast ice zone vary, e.g., from a few kilometers as off Pt. Barrow, Alaska, to over 100 km on the shallow Siberian shelf. The maximum extent of fast ice in the Antarctic is about 100 km (Keys 1984). Where rivers are present, the fast ice decays rapidly in the spring once flooding of the ice begins. In some areas of the Canadian Archipelago and in fiords of northern Greenland, fast ice can

remain for years and grow to large thicknesses (Walker and Wadhams 1979). Similarly, fast ice can persist for many years in some bays and coastal indentations of Antarctica, such as McMurdo Sound, where Gow and Epstein (1972) have reported congelation sea ice measuring 15 m thick in an active state of growth.

A shear zone generally is evident between the fast ice and the moving pack ice. This zone consists of extremely deformed ice resulting from shear and pressure of the moving pack against the relatively stable fast ice. The newly created areas of deformed ice tend to become somewhat stable themselves, effectively acting to extend the shear zone tens of kilometers seaward. The coast of Alaska and the western coast of the Canadian Archipelago have very pronounced shear zones, but little is known about the occurrence and extent of shear zones in the Antarctic.

While we generally think of sea ice in terms of the freezing of surface seawater, it is now believed that large amounts of sea ice are also accreting to the bottoms of Antarctic ice shelves. For example, at Camp J-9, located on the Ross Ice Shelf approximately 200 km seaward of the grounding line (the boundary separating land ice from the floating ice shelf), Zotikov et al. (1980) measured 6 m of coarse-grained congelation ice still actively accreting to the ice shelf bottom located more than 350 m below sea level. Zotikov et al. (1980) estimate that 1–2 cm of sea ice is accreting annually in the vicinity of Camp J-9 and that freezing is occurring over more than 50% of the underside of the Ross Ice Shelf. They infer from additional oceanographic evidence that some distance north of Camp J-9, toward the seaward edge of the Ross Ice Shelf, freezing gives way to bottom melting. Similar situations probably exist under other Antarctic ice shelves, e.g., Filchner-Ronne and Amery, but the areal extent over which freezing is occurring is not known.

SUMMARY

In comparing the crystalline structure and salinity characteristics of ice forming in polar oceans it has been shown that major differences exist between the Arctic and the Antarctic that derive directly from differences in land/sea relationships and their effect on ocean/atmosphere interaction and oceanic circulation. Whereas congelation ice, formed by direct freezing of seawater to the bottom of an existing ice sheet, is the dominant crystalline form in Arctic shorefast ice and in most multiyear floes of Arctic pack ice, it is superseded by frazil and platelet ice in the Weddell Sea, a major region of pack ice formation in Antarctica. Frazil, formed by free nucleation and growth of crystals in a turbulent water column, constitutes at least 50% of the ice production in the Weddell Sea. Such a process is consistent with the existence around Antarctica of a broad, substantially unrestricted marginal ice zone. In the Arctic Basin, however, where the land-locked nature of the ocean greatly restricts surface turbulence effects, frazil represents less than 20% of the total ice production. A number of mechanisms to explain the diverse nature of frazil in Weddell Sea pack ice have been suggested; the most recent observations point to a frazil-rich pancake-rafting process as an important if not major generator of frazil. However, the relative importance of this and other mechanisms of frazil ice generation in Antarctic waters still needs further evaluation.

Arctic and Antarctic sea ice also differ significantly in terms of their entrapped salt content or salinity, that of Antarctic sea ice generally exceeding that measured in ice of comparable age and thickness in the Arctic. These differences, which apply to both first- and multiyear ice, reflect significant differences in seasonal weather patterns in the Arctic and Antarctic. This is especially true of multiyear ice in the Weddell Sea where, because of the absence of top surface melting during the summer, the ice is able to retain brine that in Arctic sea ice is flushed out by the percolation downwards of surface meltwater, the major cause of desalination of Arctic summer ice. The desalinating of Arctic sea ice during the summer also leads to significant increases in the hardness and transparency of the ice, which allow floes exhibiting these characteristics in freshly drilled cores to be immediately identified as multiyear. By using a combination of structural and salinity characteristics it has also proven possible to estimate ages of Arctic floes.

In our examination of the dynamic and thermodynamic balances of floating sea ice covers, we pointed out the contributions made by individual components of the balance. The heat and momentum balance equations for the ice are the same for both the northern and southern hemispheres, but the magnitudes of the terms are different and this gives rise to major differences in the sea ice environments. For instance, the lack of surface melt features on Antarctic sea ice occurs because high wind speeds and low relative humidities have enhanced the turbulent heat losses from the ice, significantly raising the melting temperature. The oceanic heat flux in Antarctic seas is considerably larger than in the Arctic Ocean. Regarding ice dynamics, higher wind speeds and an unconstrained ice edge cause ice velocities to be several times larger than those within the Arctic Basin. Within the Arctic Basin, residence times of ice floes are estimated to be 5 to 7 years, while Antarctic sea ice rarely survives more than two years before it is advected to the ice edge, where it melts. The thickness of Antarctic sea ice appears to be considerably

less than its Arctic counterpart because of the larger oceanic heat flux and the low survival time of the ice. The most significant contrast, however, is between the extent of the ice covers in the northern and southern hemispheres. Whereas the Arctic ice cover nearly doubles its extent in winter, the Antarctic ice cover experiences a five-fold increase in size. At its minimum, the areal extent of Antarctic sea ice is about half that of the Arctic but at maximum extent it expands to roughly 25% more than the maximum Arctic extent.

The differences in the sea ice environments between the two hemispheres are ultimately a result of the distribution of the polar land masses. The Arctic Ocean is a closed basin surrounded by land, effectively restricting the southward expansion of the ice during winter. With only one major point of egress (Fram Strait), ice that survives the summer may be held captive in the Arctic Basin for a number of years. In contrast, Antarctic sea ice occurs in oceans that surround a continent. Under the influence of generally higher winds, the ice is advected away from the continent toward the open edge where large oceanic heat fluxes and enhanced wave action ablates the ice. The free exchange of the oceans results in larger oceanic heat fluxes.

The past two decade have seen reasonable progress made in advancing our base of knowledge of sea ice. However, compared to other disciplines, this progress has been relatively slow. This is particularly true of Antarctica where, with the notable exception of the Weddell Sea, very large gaps in our knowledge of the nature and behavior of the sea ice still exist, for example, in the Ross Sea. In the United States, this situation can be attributed largely to the lack of a suitable ice-breaking vessel dedicated to this kind of research. New initiatives in the National Science Foundation and the Department of Defense may provide for more solid funding and logistical support for such research. This support is sorely needed if our knowledge of sea ice is to reach acceptable levels. This is especially true in light of current conceptions of the importance of polar sea ice on climate and human interaction.

LITERATURE CITED

Ackley, S.F. (1979a) Drifting buoy measurements in Weddell Sea pack ice. *Antarctic Journal of the U.S.*, **16:** 1 08.

Ackley, S.F. (1979b) Mass balance aspects of Weddell Sea pack ice. *Journal of Glaciology*, **24:** 391–405.

Ackley, S.F. (1981) Sea-ice atmosphere interactions in the Weddell Sea using drifting buoys. In *Sea Level, Ice and Climatic Change* (I. Allison, Ed.). International Association of Hydrological Sciences Publication No. 131. Washington, D.C.: IAHS, p. 177–191.

Ackley, S.F. and E.T. Holt (1984) Sea ice data buoys in the Weddell Sea. USA Cold Regions Research and Engineering Laboratory, CRREL Report 84-11.

Ackley, S.F., A.J. Gow, K.R. Buck and K.M. Golden (1980) Sea ice studies in the Weddell Sea aboard USCGS *Polar Sea*. *Antarctic Journal of the U.S.*, **15:** 84–86.

Ackley, S.F., W.D. Hibler III, F.K. Kugzruk, A. Kovacs and W.F. Weeks (1976) Thickness and roughness variations of Arctic multi-year sea ice. USA Cold Regions Research and Engineering Laboratory, CRREL Report 76-18.

Ackley, S.F., S. Taguchi and K.R. Buck (1978) Primary productivity in sea ice of the Weddell Sea region. USA Cold Regions Research and Engineering Laboratory, CRREL Report 78-19.

Allison, I. (1981) Antarctic sea ice growth and oceanic heat flux. In *Sea Level, Ice and Climatic Change* (I. Allison, Ed.). International Association of Hydrological Sciences Publication No. 131. Washington, D.C.: IAHS, p. 161–170.

Andreas, E.L. and S.F. Ackley (1982) On the differences in ablation seasons of the Arctic and Antarctic sea ice. *Journal of Atmospheric Science*, **39:** 440–447.

Bourke, R.H. and R.P. Garrett (1987) Sea ice thickness distribution in the Arctic Ocean. *Cold Regions Science and Technology*, **13:** 259–280.

Campbell, K.J. and A.J. Orange (1974) The electrical anisotropy of sea ice in the horizontal plane. *Journal of Geophysical Research*, **79:** 5059–5063.

Cherepanov, N.V. (1964) Structure of sea ice of great thickness. *Trudy Arktiki i Antarktiki Nauchno-Issled. Institute*, **367:** 13–18.

Cherepanov, N.V. (1971) Spatial arrangement of sea ice crystal structure. *Problemy Arktiki i Antarktiki*, **38:** 176–181.

Clarke, D.B. and S.F. Ackley (1982) Physical, chemical and biological properties of winter sea ice in the Weddell Sea. *Antarctic Journal of the U.S.*, **17:** 107–109.

Colony, R. and A.S. Thorndike (1984) An estimate of the mean field of Arctic sea ice motion. *Journal of Geophysical Research*, **89:** 10623–10629.

Colony, R. and A.S. Thorndike (1985) Sea ice motion as a drunkard's walk. *Journal of Geophysical Research*, **90:** 965–974.

Cox, G.F.N. and W.F. Weeks (1974) Salinity variations in sea ice. *Journal of Glaciology*, **13:** 109–120.

Cox, G.F.N. and W.F. Weeks (1975) Brine drainage and initial salt entrapment in sodium chloride ice. USA Cold Regions Research and Engineering Laboratory, Research Report 345.

Cox, G.F.N. and W.F. Weeks (1983) Equations for determining the gas and brine volumes in sea ice samples. *Journal of Glaciology*, **29:** 306–316.

Cox, G.F.N. and W.F. Weeks (1988) Numerical simulations of the profile properties of undeformed first-year sea ice during the growth season. *Journal of Geophysical Research*, **87:** 1971–1984.

Dayton, P.K. and S. Martin (1971) Observations of ice stalactites in McMurdo Sound, Antarctica. *Journal of Geophysical Research*, **18:** 445–463.

Dieckmann, G., G. Rohardt, H. Hellimer and J. Kipfstul (1986) The occurrence of ice platelets at 250-m depth near the Filchner Ice Shelf and its significance for sea ice biology. *Deep Sea Research*, **33:** 141–148.

Frankenstein, G. and R. Garner (1967) Equations for determining the brine volume of sea ice from –0.5° to –22.9°C. *Journal of Glaciology*, **6:** 943–944.

Gordienko, P. (1958) Arctic ice drift. *Arctic Sea Ice*, National Academy of Sciences Publication 598. Washington, D.C.: National Academy of Sciences, p. 210–222.

Gordon, A.L. (1981) Seasonality of southern ocean sea ice. *Journal of Geophysical Research*, **86:** 4193–4197.

Gordon, A.L., C.T.A. Chen and W.G. Metcalf (1984) Winter mixed layer entrainment of Weddell deep water. *Journal of Geophysical Research*, **86:** 4193–4197.

Gow, A.J. and S. Epstein (1972) On the use of stable isotopes to trace the origin of ice in a floating ice tongue. *Journal of Geophysical Research*, **77:** 6552–6557.

Gow, A.J. and W.F. Weeks (1977) The internal structure of fast ice near Narwhal Island, Beaufort Sea, Alaska. USA Cold Regions Research and Engineering Laboratory, CRREL Report 77-29

Gow, A.J., W.F. Weeks, G. Hendrickson and R. Rowland (1965) New light on the mode of uplift of the fish and fossiliferous moraines of the McMurdo Ice Shelf, Antarctica. *Journal of Glaciology*, **5:** 813–828.

Gow, A.J., W.F. Weeks, J.W. Govoni and S.F. Ackley (1981) Physical and structural characteristics of sea ice in McMurdo Sound. *Antarctic Journal of the U.S.*, **16:** 94–95.

Gow, A.J., S.F. Ackley, W.F. Weeks and J.W. Govoni (1982) Physical and structural characteristics of Antarctic sea ice. *Annals of Glaciology*, **3:** 113–117.

Gow, A.J., S.F. Ackley, K.R. Buck and K.M. Golden (1987a) Physical and structural characteristics of Weddell Sea pack ice. USA Cold Regions Research and Engineering Laboratory, CRREL Report 87-14.

Gow, A.J., W.B. Tucker and W.F. Weeks (1987b) Physical properties of summer sea ice in the Fram Strait, June–July 1984. USA Cold Regions Research and Engineering Laboratory, CRREL Report 87-16.

Grenfell, T.C. and G.A. Maykut (1977) The optical properties of ice and snow in the Arctic basin. *Journal of Glaciology*, **18:** 445–463.

Harrison, J.D. and W.A. Tiller (1963) Controlled freezing of water. In *Ice and Snow: Processes, Properties and Applications* (W.D. Kingery, Ed.). Cambridge, Massachusetts: MIT Press, p. 8–27.

Hendrickson, G. and R. Rowland (1965) Strength studies of Antarctic sea ice. USA Cold Regions Research and Engineering Laboratory, Technical Report 157.

Hibler, W.D. III (1979) A dynamic thermodynamic sea ice model. *Journal of Physical Oceanography*, **9:** 815–846.

Hibler, W.D. III (1980) Sea ice growth, drift and decay. In *Dynamics of Snow and Ice* (S. Colbeck, Ed.). New York: Academic Press, p. 141–209.

Hibler, W.D. III (1986) Ice dynamics. In *The Geophysics of Sea Ice* (N. Untersteiner, Ed.). New York: Plenum Press, p. 577–640.

Hibler, W.D. III and S.F. Ackley (1982) On modeling the Weddell Sea pack ice. *Annals of Glaciology*, **3:** 125–130.

Hibler, W.D. III and W.B. Tucker (1979) Some results from a linear viscous model of the Arctic ice cover. *Journal of Glaciology*, **22:** 293–304.

Hibler, W.D. III, S.F. Ackley, W.F. Weeks and A. Kovacs (1972a) Top and bottom roughness of a multiyear ice floe. *AIDJEX Bulletin*, **13**: 77–91.

Hibler, W.D. III, S.J. Mock and W.B. Tucker (1974) Classification and variation of sea ice ridging in the western Arctic basin. *Journal of Geophysical Research*, **79:** 2735–2743

Hibler, W.D. III, W.F. Weeks and S.J. Mock (1972b) Statistical aspects of sea-ice ridge distributions. *Journal of Geophysical Research*, **77:** 5954–5970.

Horner, R.A (1985) History of ice algal investigations. In *Sea Ice Biota* (R.A. Horner, Ed.). Boca Raton, Florida: CRC Press, p. 1–19.

Hunkins, K. (1975) The oceanic boundary layer and stress beneath a drifting ice floe. *Journal of Geophysical Research*, **80:** 3425–3433.

Keys, J.R. (1984) *Antarctic Marine Environments and Offshore Oil*. Wellington, New Zealand: Commission for the Environment, p. 1–168.

Koerner, R.M. (1973) The mass balance of the sea ice of the Arctic Ocean. *Journal of Glaciology*, **12:** 173–185.

Kovacs, A. (1983) Characteristics of multi-year pressure ridges. In *Proceedings of the 7th International Conference on Port and Ocean Engineering under Arctic Conditions*. VTT Symposium 37, Helsinki, Finland. p. 173–182.

Kovacs, A. and R. Morey (1978) Radar anisotropy of sea ice due to preferred azimuthal orientation of the horizontal c-axes of ice crystals. *Journal of Geophysical Research*, **83:** 6037–6046.

Lange, M.A., S.F. Ackley, P. Wadhams, G.S. Dieckmann, and H. Eicken (1988) Development of sea ice in the Weddell Sea, Antarctica. *Annals of Glaciology*, **12:** 92–96.

Langhorne, P.J. (1983) Laboratory experiments on crystal orientation in NaCl ice. *Annals of Glaciology*, **4:** 163–169.

Langhorne, P.J. and W.H. Robinson (1986) Alignment of crystals in sea ice due to fluid motion. *Cold Regions Science and Technology*, **12**(2): 197–214.

Langleben, M.P. (1972) The decay of an annual ice cover. *Journal of Glaciology*, **11:** 337–344.

Leavitt, E., M. Albright and F. Carsey (1978) Report on the AIDJEX meteorological experiment. *AIDJEX Bulletin*, **29:** 121–148.

LeShack, L.A. (1983) Arctic Ocean ice deformation chart using sonar data recorded from nuclear submarines. In *Proceedings of the 7th International Conference on Port and Ocean Engineering under Arctic Conditions*. VTT Symposium 37, Helsinki, Finland. p. 148–157.

Lewis, E.L. and R.G. Perkin (1985) The winter oceanography of McMurdo Sound, Antarctica. In *Oceanology of the Antarctic Continental Shelf*. Antarctic Research Ser. 43. Washington, D.C.: American Geophysical Union, p. 145–165.

Lewis, E.L. and R.G. Perkin (1987) Ice pumps and their rates. *Journal of Geophysical Research*, **91:** 756–762.

Lofgren, G. and W.F. Weeks (1967) Effect of growth parameters on substructure spacing in NaCl ice crystals. USA Cold Regions Research and Engineering Laboratory, CRREL Report 195.

Martin, S. (1981) Frazil ice in rivers and oceans. *Annual Review of Fluid Mechanics*, **13:** 374–397.

Maykut, G.A. (1978) Energy exchange over young sea ice in the Central Arctic. *Journal of Geophysical Research*, **83:** 3646–3658.

Maykut, G.A. (1982) Large scale heat exchange and ice production in the central Arctic. *Journal of Geophysical Research*, **87:** 7971–7984.

Maykut, G.A. (1985) The ice environment. In *Sea Ice Biota* (R.A. Horner, Ed.). Boca Raton, Florida: CRC Press, p. 21–82.

Maykut, G.A. (1986) The surface heat and mass balance. In *The Geophysics of Sea Ice* (N. Untersteiner, Ed.). New York: Plenum Press, p. 385–463.

Maykut, G.A. and N. Untersteiner (1969) Numerical prediction of the thermodynamic response of Arctic sea ice to environmental changes. Memorandum RM-6093-PR. Santa Monica, California: Rand Corporation, p. 1–173.

Maykut, G.A. and N. Untersteiner (1971) Some results from a time-dependent thermodynamic model of sea ice. *Journal of Geophysical Research*, **76**(6): 1550–1575.

McLaren, A.S. (1989) The under-ice thickness distribution of the Arctic basin as recorded in 1958 and 1970. *Journal of Geophysical Research*, **94:** 4971–4983.

McLaren, A.S., M.C. Serreze and R.G. Barry (1987) Seasonal variations of sea ice motion in the Canada Basin and their implications. *Geophysical Research Letters*, **14:** 1123–1126.

McPhee, M.G. (1980) Analysis of pack ice drift in summer. In *Sea Ice Processes and Models* (R.S. Pritchard, Ed.). Seattle: University of Washington Press, p. 62–75.

Moritz, R.E. and R. Colony (1988) Statistics of sea ice motion, Fram Strait to North Pole. In *Proceedings of the 7th International Conference on Offshore Mechanics and Arctic Engineering*, Vol. IV (D.S. Sodhi, C.H. Luk, and N.K. Sinha, Ed.). New York: American Society of Mechanical Engineers, p. 75–82.

Nakawo, M. and N.K. Sinha (1981) Growth rate and salinity profile of first-year sea ice in the high Arctic. *Journal of Glaciology*, **27:** 315–330.

Nansen, F. (1902) The oceanography of the North Polar Basin, the Norwegian North Polar Expedition, 1893–1896. *Science Research*, **3:** 1–427.

Osterkamp, T.E. and J.P. Gosink (1984) Observations and analyses of sediment-laden sea ice. In *The Alaskan Beaufort Sea: Ecosystems and Environments* (P.W. Barnes, D.M. Schell and E. Reimnitz, Ed.). New York: Academic Press, p. 73–93.

Overgaard, S., P. Wadhams and M. Lepparanta (1983) Ice properties in the Greenland and Barents Sea during summer. *Journal of Glaciology*, **29**(101): 142–164.

Paige, R.A. (1966) Crystallographic studies of sea ice in McMurdo Sound, Antarctica. Technical Report R494. Port Hueneme, California: Naval Civil Engineering Laboratory, p. 31.

Parkinson, C.L. and W.M. Washington (1979) A large-scale numerical model of sea ice. *Journal of Geophysical Research*, **84:** 311–337.

Parkinson, C.L., J.C. Comiso, H.J. Zwally, D.J. Cavalieri, P. Gloersen and W.J. Campbell (1987) Arctic sea ice, 1973–1976: Satellite passive-microwave observations. NASA SP-489. Washington, D.C., p. 1–296.

Parmerter, R.R. and M.D. Coon (1972) Model of pressure ridge formation in sea ice. *Journal of Geophysical Research*, **77:** 6565–6575.

Pease, C.H. (1980) Eastern Bering Sea ice processes. *Monthly Weather Review*, **108:** 2015–2023.

Perovich, D.K., G. A. Maykut and T.C. Grenfell (1986) Optical properties of ice and snow in the polar oceans. 1: Observations. In *Proceedings of the International Society for Optical Engineering. Ocean Optics VIII.* (M. Blizard, Ed.). SPIE 637. p. 232–241.

Perovich, D.K., A.J. Gow and W.B. Tucker (1988) Physical properties of snow and ice in the winter marginal ice zone of Fram Strait. In *Proceedings of 1988 International Geoscience and Remote Sensing Symposium (IGARSS '88)*, University of Edinburgh, Edinburgh, Scotland. p. 1119–1123.

Peyton, H.R. (1966) Sea ice strength. Geophysical Institute, University of Alaska Rept. UAG-182, p. 1–187.

Pritchard, R.S. (1988) Norton Sound and northeastern Bering Sea ice behavior: 1981–1982. In *Proceedings of the 7th International Conference on Offshore Mechanics and Arctic Engineering*, Vol. IV (D.S. Sodhi, C.H. Luk, and N.K. Sinha, Ed.). New York: American Society of Mechanical Engineers, p. 69–74.

Reimnitz, E., E.W. Kempema, and P.W. Barnes (1987) Anchor ice, seabed freezing, and sediment dynamics in shallow Arctic seas. *Journal of Geophysical Research*, **92:** 14671–14678.

Reynolds, M., C.H. Pease and J.E. Overland (1985) Ice drift and regional meteorology in the southern Bering Sea: results from MIZEX West. *Journal of Geophysical Research*, **90:** 11967–11981.

Richter-Menge, J.A. and G.F.N. Cox (1985a) Effect of sample orientation on the compressive strength of multi-year pressure ridge ice samples. In *Proceedings of the Conference Arctic '85, Civil Engineering in the Arctic Offshore*. San Francisco, Calif.: American Society of Civil Engineers, p. 465–475.

Richter-Menge, J.A. and G.F.N. Cox (1985b) Structure, salinity and density of multi-year ice pressure ridges. In *Proceedings of the 4th International Offshore Mechanics and Arctic Engineering Symposium* (J. Chung, Ed.). New York: American Society of Mechanical Engineers, p. 194–198.

Rothrock, D.A. (1986) Ice thickness distribution—measurement and theory. In *The Geophysics of Sea Ice* (N. Untersteiner, Ed.). New York: Plenum Press, p. 551–575.

Rothrock, D.A. and A.S. Thorndike (1980) Geometric properties of the underside of sea ice. *Journal of Geophysical Research*, **85:** 3955–3963.

Schwarz, J. and W.F. Weeks (1977) Engineering properties of sea ice. *Journal of Glaciology*, **19:** 499–530.

Serikov, M.I. (1963) Structure of Antarctic sea ice. *Information Bulletin of Soviet Antarctic Expeditions*, **4:** 265–266.

Smith, D.D. (1964) Ice lithologies and structure of ice island Arlis II. *Journal of Glaciology*, **5:** 17–38.

Stander, E. and G.A. Gidney (1980) The measurement of finite strain in sea ice by impulse radar techniques. In *Proceedings of Workshop on Sea Ice Field Experiments*. C-Core Publ. 80-21. St. Johns, Newfoundland: Memorial University, p. 127–164.

Stander, E. and B. Michel (1989) The effect of fluid flow on the preferred orientations in sea ice: Laboratory experiments. *Cold Regions Science and Technology*, **17**(2): 153–161.

Thorndike, A.S. and R. Colony (1982) Sea ice motion in response to geostrophic winds. *Journal of Geophysical Research*, **87:** 5845–5852.

Thorndike, A.S., D.A. Rothrock, G.A. Maykut and R. Colony (1975) The thickness distribution of sea ice. *Journal of Geophysical Research*, **80:** 4501–4513.

Tiller, W.A., K.A. Jackson, J.W. Rutter, and B. Chalmers (1953) The redistribution of solute atoms during the solidification of metals. *Acta Metallurgica*, **1:** 428–437.

Tucker, W.B. and V.H. Westhall (1973) Arctic sea ice ridge frequency distributions derived from laser profiles. *AIDJEX Bulletin*, **21:** 171–180.

Tucker, W.B., A.J. Gow and J.A. Richter (1984a) On small-scale horizontal variations of salinity in first-year ice. *Journal of Geophysical Research*, **89:** 6505–6514.

Tucker, W.B., A.J. Gow and W.F. Weeks (1987) Physical properties of summer sea ice in Fram Strait. *Journal of Geophysical Research*, **92:** 6787–6803.

Tucker, W.B., D.S. Sodhi and J.W. Govoni (1984b) Structure of first-year pressure ridge sails in the Alaskan Beaufort Sea. In *The Alaskan Beaufort Sea: Ecosystems and Environments* (P.W. Barnes, D.M. Schell and E. Reimnitz, Ed.). New York: Academic Press, p. 115–135.

Tucker, W.B., W.F. Weeks and M. Frank (1979) Sea ice ridging over the Alaskan Continental Shelf. *Journal of Geophysical Research*, **84:** 4885–4897.

Untersteiner, N. (1968) Natural desalination and equilibrium salinity profile of perennial sea ice. *Journal of Geophysical Research*, **73:** 1251–1257.

Untersteiner, N. and F. Badgley (1958) Preliminary results of thermal budget studies on Arctic pack ice during summer and autumn. *Arctic Sea Ice*, National Academy of Sciences Publication 598. Washington, D.C.: National Academy of Sciences, p. 85–89.

Wadhams, P. (1980a) A comparison of sonar and laser profiles along corresponding tracks in the Arctic Ocean. In *Sea Ice Processes and Models* (R.S. Pritchard, Ed.). Seattle: University of Washington Press, p. 283–299.

Wadhams, P. (1980b) Ice characteristics in the seasonal sea ice zone. *Cold Regions Science and Technology*, **2:** 37–87.

Wadhams, P. (1981) Sea-ice topography of the Arctic Ocean in the region 70°W to 25°E. *Philosophical Transactions of the Royal Society of London*, **302:** 45–85.

Wadhams, P. (1984) Arctic sea ice morphology and its measurement. In *Arctic Technology and Policy* (I. Dyer and C. Chrysostomidis, Ed.). Washington, D.C.: Hemisphere Publishing Corporation, p. 179–195.

Wadhams, P. and R.J. Horne (1980) An analysis of ice profiles obtained by submarine sonar in the Beaufort Sea. *Journal of Glaciology*, **25:** 401–424.

Wadhams, P. and T. Davy (1986) On the spacing and draft distribution for pressure ridge keels. *Journal of Geophysical Research*, **91:** 10697–10708.

Wadhams, P., M.A. Lange and S.F. Ackley (1987) The ice

thickness distribution across the Atlantic sector of the Antarctic Ocean in midwinter. *Journal of Geophysical Research*, **92:** 14535–14552.

Walker, E.R. and P. Wadhams (1979) Thick sea-ice floes. *Arctic*, **32:** 140–147.

Walsh, J.E. and C.M. Johnson (1979) An analysis of Arctic sea ice fluctuations, 1957–77. *Journal of Physical Oceanography*, **9:** 580–591.

Weeks, W.F. and S.F. Ackley (1982) The growth, structure and properties of sea ice. USA Cold Regions Research and Engineering Laboratory, Monograph 82-1.

Weeks, W.F. and A.J. Gow (1978) Preferred crystal orientations in the fast ice along the margins of the Arctic Ocean. *Journal of Geophysical Research*, **83:** 5105–5121.

Weeks, W.F. and A.J. Gow (1980) Crystal alignments in the fast ice of arctic Alaska. *Journal of Geophysical Research*, **85:** 1137–1146.

Weeks, W.F., S.F. Ackley and J. Govoni (1988) Sea ice ridging in the Ross Sea, Antarctica as compared with sites in the Arctic. *Journal of Geophysical Research*, **94:** 4984–4988.

Williams, E., C.W.M. Swithinbank and G. de Q. Robin (1975) A submarine study of Arctic pack ice. *Journal of Glaciology*, **15:** 349–362.

Wittmann, W. and J.J. Schule (1966) Comments on the mass budget of Arctic pack ice. In *Proceedings of the Symposium on Arctic Heat Budget and Atmospheric Circulation, Lake Arrowhead, California* (J.O. Fletcher, Ed.). Memorandum RM-5233-NSF. Santa Monica, California: Rand Corporation, p. 215–246.

WMO (1956) *Abridged Ice Nomenclature*. World Meteorological Organization, Executive Committee Report, **8:** 107–116.

Zotikov, I.A., V.S. Zagorodnov and J.V. Raikovsky (1980) Drilling through the Ross Ice Shelf (Antarctica) confirmed basal freezing. *Science*, **207:** 1463–1465.

Zubov, N.N. (1943) L'dy Arktiki (Arctic Ice). Izdatel'stvo Glavsevmorputi, Moscow. (U.S. Navy Hydrographic Office, Translation 217, 1963; available as AD426972 from NTIS, Springfield, Virginia.) p. 1–491.

Zwally, H.J., J.C. Comiso, C.L. Parkinson, W.J. Campbell, F.D. Carsey and P. Gloersen (1983) Antarctic sea ice, 1973–1976: Satellite passive-microwave observations. NASA SP-459. Washington, D.C.

☆U.S. GOVERNMENT PRINTING OFFICE: 1992-600-063/60017

REPORT DOCUMENTATION PAGE

Form Approved
OMB No. 0704-0188

1. AGENCY USE ONLY (Leave blank)	2. REPORT DATE	3. REPORT TYPE AND DATES COVERED
	September 1991	

4. TITLE AND SUBTITLE

Physical and Dynamic Properties of Sea Ice in the Polar Oceans

5. FUNDING NUMBERS

PR: 4A161102AT24
PE: 6.11.02A
WU: SS/001, SS/006

6. AUTHORS

Anthony J. Gow and Walter B. Tucker III

7. PERFORMING ORGANIZATION NAME(S) AND ADDRESS(ES)

U.S. Army Cold Regions Research and Engineering Laboratory
72 Lyme Road
Hanover, New Hampshire 03755-1290

8. PERFORMING ORGANIZATION REPORT NUMBER

Monograph 91-1

9. SPONSORING/MONITORING AGENCY NAME(S) AND ADDRESS(ES)

Office of Naval Research
Arlington, Virginia 22217
and
Office of the Chief of Engineers
Washington, D.C. 20314-1000

10. SPONSORING/MONITORING AGENCY REPORT NUMBER

11. SUPPLEMENTARY NOTES

ONR Contracts N0001488WM24013, N0001489WM24004

12a. DISTRIBUTION/AVAILABILITY STATEMENT

Approved for public release; distribution is unlimited.

Available from NTIS, Springfield, Virginia 22161.

12b. DISTRIBUTION CODE

13. ABSTRACT (*Maximum 200 words*)

This monograph provides a current review of the state of knowledge of the growth, properties, and small- and large-scale behavior of sea ice found in the polar oceans of the northern and southern hemispheres. A major focus of the report is to contrast and compare the physical and dynamic properties of ice found in the Arctic seas with those found in the seas surrounding the Antarctic continent. Very significant differences in the physical and dynamic properties of the ice are shown to exist that derive directly from differences in land–sea relationships between the two polar regions and their effect on ocean–atmosphere interaction and oceanic circulation. The same factors also determine, to a large degree, major differences in the seasonal distribution and extent of sea ice in the Arctic and Antarctic oceans.

14. SUBJECT TERMS

Energy balance	Ice growth	Ridging
Ice dynamics	Ice structure	Salinity
Ice extent	Polar oceans	Sea ice

15. NUMBER OF PAGES
63

16. PRICE CODE

17. SECURITY CLASSIFICATION OF REPORT	18. SECURITY CLASSIFICATION OF THIS PAGE	19. SECURITY CLASSIFICATION OF ABSTRACT	20. LIMITATION OF ABSTRACT
UNCLASSIFIED	UNCLASSIFIED	UNCLASSIFIED	UL